

FLUID SIMULATION OF ELECTRON BEAM DRIVEN WAKEFIELD IN A COLD PLASMA

By

Ratan Kumar Bera

PHYS06201204009

INSTITUTE FOR PLASMA RESEARCH, GANDHINAGAR

A thesis submitted to the
Board of Studies in Physical Sciences

In partial fulfillment of the requirements

For the Degree of

DOCTOR OF PHILOSOPHY

of

HOMI BHABHA NATIONAL INSTITUTE



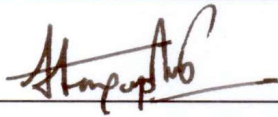
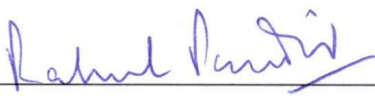
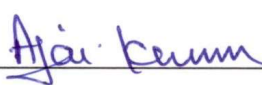



Aug 2018

Homi Bhabha National Institute

Recommendations of the Viva Voce Committee

As members of the Viva Voce Committee, we certify that we have read the dissertation prepared by **Ratan Kumar Bera** entitled "**Fluid Simulation of Electron Beam Driven Wakefield in a Cold Plasma**" and recommend that it may be accepted as fulfilling the thesis requirement for the award of Degree of Doctor of Philosophy.

	9/8/18
Chairman – Dr. R. Srinivasan	Date:
	9-8-18
Guide / Convener – Prof. Amita Das	Date:
	09/8/2018
Co-guide - Prof. Sudip Sengupta	Date:
	9/8/18
Examiner – Prof. Rahul Pandit	Date:
	9/8/18
Member 1- Prof. Ajai Kumar	Date:
	9/8/18
Member 2- Dr. Devendra Sharma	Date:

Final approval and acceptance of this thesis is contingent upon the candidate's submission of the final copies of the thesis to HBNI.

I/We hereby certify that I/we have read this thesis prepared under my/our direction and recommend that it may be accepted as fulfilling the thesis requirement.

Date: 9th August 2018

Place: Gandhinagar

Prof. Sudip Sengupta

Co-guide

Prof. Amita Das

Guide

STATEMENT BY AUTHOR

This dissertation has been submitted in partial fulfillment of requirements for an advanced degree at Homi Bhabha National Institute (HBNI) and is deposited in the Library to be made available to borrowers under rules of the HBNI.

Brief quotations from this dissertation are allowable without special permission, provided that accurate acknowledgement of source is made. Requests for permission for extended quotation from or reproduction of this manuscript in whole or in part may be granted by the Competent Authority of HBNI when in his or her judgment the proposed use of the material is in the interests of scholarship. In all other instances, however, permission must be obtained from the author.

Ratan Kumar Bera

DECLARATION

I, hereby declare that the investigation presented in the thesis has been carried out by me. The work is original and the work has not been submitted earlier as a whole or in part for a degree/diploma at this or any other Institution or University.

Ratan Kumar Bera

List of Publications arising from the thesis

Journals:

- **Fluid simulation of relativistic electron beam driven wakefield excitation in a cold Plasma.,**
[Ratan Kumar Bera](#), Sudip Sengupta, and Amita Das
Physics of Plasmas (22), 073109 (2015)
- **Relativistic electron beam driven longitudinal wake-wave breaking in a cold plasma,**
[Ratan Kumar Bera](#), Arghya Mukherjee, Sudip Sengupta, and Amita Das
Physics of Plasmas (23), 083113 (2016)
- **Accessibility and stability of an electron-ion mode in plasma wake-field acceleration,**
[Ratan Kumar Bera](#), Sudip Sengupta, and Amita Das
(Ready for submission)
- **2-D fluid simulation of relativistic electron beam driven wakefield in a cold plasma.,**
[Ratan Kumar Bera](#), Amita Das, and Sudip Sengupta
(Ready for submission)

Other publications:

- **The stability of 1-D soliton in transverse direction,**
Deepa Verma, [Ratan Kumar Bera](#), Amita Das, and Predhiman Kaw
Physics of Plasmas (23), 123102 (2016)
- **Observation of 1-D time dependent non-propagating laser plasma structures using fluid and PIC codes,**
Deepa Verma, [Ratan Kumar Bera](#), Atul Kumar, Bhavesh Patel and Amita Das, Physics of Plasmas 24, 123111 (2017)
- **Observation of 1-D time dependent propagating laser plasma structures using fluid and PIC codes,**

Deepa Verma, [Ratan Kumar Bera](#), Atul Kumar, Bhavesh Patel and Amita Das, (To be submitted)

- **Evidence of new finite beam plasma instability for magnetic field generation,**

Amita Das, Atul Kumar, Chandrasekhar Shukla, [Ratan Kumar Bera](#), Deepa Verma, Bhavesh Patel, Y. Hayashi, K. A. Tanaka, Amit D. Lad, G. R. Kumar, Predhiman Kaw, (To be submitted)

Conferences:

International Participation

- Relativistic electron beam driven longitudinal wake-wave breaking in a cold plasma. (**Poster presentation**)
[Ratan Kumar Bera](#), Arghya Mukherjee, Sudip Sengupta, and Amita Das
Asia Plasma And Fusion Association (APFA), 14-18 DEC 2015, Gandhinagar, India.
- Study of relativistic electron beam driven wakefield in a cold plasma. (**Oral presentation**)
[Ratan Kumar Bera](#), Sudip Sengupta, and Amita Das
ASHULA-2015, 20-21 January, 2015 Lonavala, Maharashtra, India.
- 2-D fluid simulation of relativistic electron beam driven wakefield in the blow-out regime. (**Poster presentation**)
[Ratan Kumar Bera](#), Amita Das, and Sudip Sengupta
59th Annual Meeting of the APS Division of Plasma Physics, Milwaukee, Wisconsin, USA.

National Participation

- Fluid simulation of relativistic electron beam driven wakefield in a cold plasma (**Poster presentation**)
[Ratan Kumar Bera](#), Sudip Sengupta, and Amita Das
PSSI-2014, 8-11 Dec 2014, Kottayam, Kerala, India.
- Relativistic electron beam driven longitudinal wake-wave breaking in a cold plasma (**Oral presentation**)
[Ratan Kumar Bera](#), Arghya Mukherjee, Sudip Sengupta, and Amita Das
PSSI-plasma scholars' colloquium, 6-17 Aug 2015, Jadavpur University, Kolkata, India.

-
- Effect of ion motion on relativistic electron beam driven wakefield in a cold plasma (**Poster presentation**)

[Ratan Kumar Bera](#), Sudip Sengupta, and Amita Das

PSSI-2015, SINP, Kolkata, India, 1-4 December 2015.

- 2-D fluid simulation of electron beam driven wakefield in a cold plasma (**Oral presentation**)

[Ratan Kumar Bera](#), Amita Das, and Sudip Sengupta

PSSI-2017, IPR, Gandhinagar, India, 7-10 November 2017.

Schools:

- DST SERC school on Tokamaks and Magnetized plasma fusion (**school**)
[Ratan Kumar Bera](#)
25 Feb-15 Mar, 2013, Institute for Plasma Research, India.
- Fluid simulation of relativistic electron beam driven wakefield in a cold plasma (**Poster presentation**)
[Ratan Kumar Bera](#), Sudip Sengupta, and Amita Das
CERN Accelerator School, 23-29 Nov, 2014, Switzerland.
- Study of relativistic electron beam driven wakefield in a cold plasma (**Poster presentation**)
[Ratan Kumar Bera](#), Sudip Sengupta, and Amita Das
International School on Ultra-Intense lasers (ISUIL), 4-9 October, 2015, Russia.
- LPA workshop at ICTS, Bangalore (**workshop**)
[Ratan Kumar Bera](#)
6-17 March, 2017, Bangalore.

Ratan Kumar Bera

Dedicated to

my beloved wife, Sayanti...

ACKNOWLEDGEMENTS

First and foremost, I would like to express my great gratitude to my thesis supervisor(s) Prof. Amita Das and Prof. Sudip Sengupta for guiding me all the way in my research. Without their support, understanding, and instruction, it would not have been possible for me to conduct all the work in this dissertation. I would really like to acknowledge them for the time they have spent discussing with me during this entire tenure. I have always received a constant encouragement and motivation to pursue my work implementing new, independent thoughts and ideas. Their deep insight into research problems, approach to tackle the problems, marvelous skills in computational physics, and amount of patience to pursue it, have always been a great source of inspiration to me. I could not have imagined having better advisors and mentors for my Ph.D.

I would also like to thank my doctoral committee members Prof. Predhiman Kaw, Prof. Ajay Kumar, Dr. R. Srinivasan, and Dr. Devendra Sharma, for their careful monitoring of my progress during the Ph.D. tenure and giving their crucial comments on the work. Their appreciations and suggestions have always induced and boosted me to give my best in the work.

I am also indebted to Dr. Prabal Chattopadhyay, Dr. Joydeep Ghosh, Dr. Subrato Mukharji, Dr. Mrityunjay Kundu, Dr. Shantanu Kumar Karkari, Dr. R. Ganesh, Dr. Devendra Sharma, Dr. G. Ravi, Dr. Mainak Bandyopadhyaya and Dr. Pintu Bandyopadhyay for their excellent teaching and support during my first-year course-work at IPR.

I would also like acknowledge the computer center staff, library staff and the administration staff at the IPR for always being cooperative. I would also like to thank to all my seniors Ritu, Maya, Vikrant, Shekhar, Sharad, Jugal, Satya, Sita, Gurudatt, Vikram, Ujjwal, Ashwin, Kshitish, Deepak, Prabal, Sanat, Sushil, Rameswar, Pravesh, Sayak, Manjeet, Soumen, Aditya, Vikram, Rana, Akanksha, Vidhi, Vara, Neeraj, Roopendra, Bibhu, Mangilal, Harish, Megharaj, Sameer, Chandrasekhar, Deepa, Veda, Sandeep, Dushyant and my juniors for their wonderful company in the hostel and their co-operation whenever I needed.

I really feel grateful to my batch-mates, Sonu, Debraj, Rajnarayan, Anup, Amit, Umesh, Narayan, Arhya, Modhu, Surbhi, and Bhumika for their love and unconditional support throughout. I also wish a special thank Dr. Bhavesh Patel, Dr. Sanat Kumar Tiwari (we use to call him “Bhaiya”), Dr. Vikram Singh Darodhi, Dr. Chandrasekhar Shukla, Dr. Deepa Verma, Atul Kumar and Sandeep Shukla, Srimanta, for their support and patience while discussing, teaching and debating on many cutting-edge research problems, numerical techniques, and current affairs. I really would like to thank Avadhesh for his technical and other official support throughout my Ph.D. tenure.

I would also like to convey my heartiest thank to my dearest wife Sayanti, whose love and confidence on me, took a great load off my shoulder. In spite of her own course-work and domestic work, she has always been supported my goals. Truly, without her constant concerns about my work, it would have been definitely very harder for me to complete the Ph.D. I would also like to express my heartiest regards to my parents whose blessings and moral support helped me a lot achieving my goal.

Contents

List of Figures	xviii
List of Tables	xxiv
1 Introduction	3
1.1 Introduction	3
1.2 Motivation	4
1.2.1 Plasma Based Acceleration	7
1.2.2 Laser Wakefield Acceleration (LWFA)	8
1.2.3 Plasma Wakefield Acceleration (PWFA)	11
1.3 Review of Earlier Works on PWFA	16
1.4 Plan of the Thesis	22
2 Excitation of relativistic electron beam driven wakefield in a cold plasma in 1-D	29
2.1 Introduction	29
2.2 Governing Equations	31
2.3 1-D Fluid Simulation of electron beam driven wakefield excitation	33
2.4 Numerical Observations	37
2.4.1 Wake field excited by a rigid beam driver	37
2.4.2 Excitation of wake field including beam evolution	39
2.5 Analytical Description of Beam driven wakefield	42
2.5.1 Solution inside the beam	47
2.5.2 Solution behind the beam	49
2.6 Summary	53
3 Breaking of relativistic electron beam driven longitudinal wake wave in a cold plasma	55
3.1 Introduction	56
3.2 Governing Equations and Fluid simulation techniques	57
3.3 Numerical Observations and Discussions	58
3.4 Analysis of wake wave breaking	63
3.5 Summary	72

4	Accessibility and stability of an electron-ion mode in plasma wake-field acceleration	73
4.1	Introduction	74
4.2	Governing Equations	76
4.3	Fluid simulation of the relativistic electron beam driven wakefield .	78
4.4	Numerical observations and discussion	80
4.5	Breaking of electron-ion wake waves in a cold plasma	84
4.6	Summary	89
5	2-D fluid simulation of relativistic electron beam driven wakefield in a cold plasma	91
5.1	Introduction	92
5.2	Governing Equations	95
5.3	2-D fluid simulation techniques	97
5.4	Simulation results	98
5.4.1	Effect of finite transverse beam size	99
5.4.2	Fluid simulation in the blowout regime	111
5.5	Test particle simulation	117
5.6	Summary	120
6	Conclusion and Future Scope	123
6.1	Salient features of this thesis	123
6.2	Future scope	130
A	Appendix	135
A.1	2-D fully relativistic electromagnetic fluid simulation techniques . .	135
A.2	Derivation of wave breaking limit for a relativistic electron-ion mode (Khachtryan) in a cold plasma	141
A.3	Analytical formalism for 2-D linear relativistic electron beam wake-fields	148
A.4	Method of Green's function for solving ODE's	152
A.4.1	Solution of forced SHO like equation	152
A.4.2	Solution of Poisson like equation in cylindrical geometry . .	155
A.5	Test particle simulation techniques	157

SYNOPSIS

In their quest to test the standard model and search for new physics beyond it, particle physicists have sought increasingly larger and more powerful facilities for accelerating and colliding charge particles. In conventional radio frequency linear accelerators (RF linacs), the accelerating gradients are limited to about $100\text{MV}/m$, partly due to material breakdown which occurs on the walls of the structure. With accelerating gradient limited by this constraint, high energy experiments required a distance of many kilometers to accelerate the particles to ~ 100 GeV energies for Higgs Boson detection (the energy of Higgs boson being of this order).

Another issue pertaining to the acceleration of particles is that while protons or heavier particles can be accelerated in circular paths, lighter mass particles such as electrons and positrons have to be accelerated in linear devices. This is to ensure that the copious energy loss by the synchrotron radiation in the case of lighter particles gets eliminated. The 3-km linear accelerator at Stanford Linear Accelerator (SLAC) is currently the worlds longest machine which can accelerate electrons to ~ 50 GeV energies. Clearly, for higher energies the size of the conventional electron accelerator would become increasingly unwieldy and costlier. New techniques which can reduce the dimension are, therefore welcome. The accelerator based on plasma medium offers such a cheaper technological alternative. Being an ionized medium, plasma is not constrained by the material breakdown limit of voltage and hence can support electric fields several orders of magnitude higher than that of the conventional RF-based accelerators [1, 2]. For example, a plasma having density $n_0 = 10^{18}\text{cm}^{-3}$ can sustain an electric field of the order of non-relativistic wave breaking limit, $E_0 \sim \frac{m_e c \omega_{pe}}{e} \approx 100\text{GV}/m$, which is approximately three orders of magnitude higher than that obtained from conventional RF linacs; where c and ω_{pe} represent the speed of light in vacuum and the plasma frequency of electron having mass m , charge e respectively. This distinct feature of plasma offers a way to build an affordable high-performance particle accelerator of much smaller size than the conventional devices.

In plasma-based accelerators, charge particles get accelerated by the electric field associated with electron plasma wave or other high-gradient electric field structures (like shock and sheath fields) in plasma medium. An intense plasma wave is excited either using an intense laser pulse or ultra-relativistic electron beam. When a laser beam is used, it is called laser wakefield acceleration (LWFA),

and when a particle beam is used, it is called plasma wakefield acceleration (PWFA) [3–5]. The charge particles ride suitably on this relativistically intense plasma wave and get accelerated to higher energies. In LWFA, the wave can accelerate the charge particles almost from rest. Therefore, this scheme offers a way to design a “free-standing” tabletop accelerator. On the other hand, in PWFA, both the bunches (driver and witness) must start out at relativistic energies. This scheme is most suitable to boost the energy of the existing linacs. The success of LWFA scheme has been demonstrated in a number of experiments by accelerating charge particles to GeV energies [6–12]. A series of experiments have also been executed at different national and international laboratories for demonstrating the success of PWFA scheme [13–18]. The most promising PWFA results were published by Blumenfeld et al. [19] where a 42 GeV electron bunch efficiently accelerates the electrons up to maximum energies of 85 GeV in a meter long plasma (known as “energy-doubling experiment”). Recently, Litos et al. [20] designed an experiment using a discrete trailing bunch about 74 pico-coulombs of charge in an accelerating gradient of 4.4GV/m and minimized the energy spread hardly 2%, and obtained the energy-transfer efficiency from the wake to the bunch that can exceed 30 per cent (17.7 per cent on average). In terms of theoretical work, till date, both linear and nonlinear theory has been well established to examine LWFA and PWFA scheme for several driver configurations [21–28]. The theoretical work, under several approximations, provides for reasonable empirical guidance for experiments.

The present thesis covers an extensive theoretical and numerical study of relativistic electron beam driven wakefield by proposing fluid depiction of the plasma wave excitation in a cold plasma. The numerical study has been carried out using fluid simulation techniques (fluid code) both in 1-D and 2-D. Till to date, most of the simulations in this field have been carried out using extensive particle-in-cell (PIC) simulations (e.g. OSIRIS, QUICKPIC, EPOCH, XOOPIC and many more) [19, 29, 30]. These PIC simulations are computationally heavy and hence require powerful computational facilities. Here we present that the fluid simulations which are simpler than any sophisticated PIC simulations have been found to be pretty adequate at representing the potential structure of the ultra-relativistic electron beam driven wake. Further, injecting test particles (test particle simulations) in the fluid simulations, we have examined the energy gain and focusing of the accelerated particles. The extensively used fluid code has been benchmarked against the widely used PIC code OSIRIS. The technique used to develop the fluid code

will be discussed in detail in my thesis. First, we have studied the excitation of relativistic electron beam driven wakefield using 1-D fluid simulation techniques for both rigid and non-rigid driver over a wide range of beam parameters (density, length and velocity). Rigid beam defines such a bunch which can penetrate an infinite length in plasma without significant deformation, whereas a non-rigid beam loses its identity after propagating some distance. The criteria required for a beam to be rigid has also been checked in this thesis. Further, an earlier 1-D nonlinear analytical work given by Rosenzweig et al. [24] only for a rigid, homogeneous beam having density less than or equal to half of the plasma density, has been extended for an arbitrary value of beam density. The numerical and analytical results have been compared for several plasma periods.

At later times in the simulation, it is found that the excited wake wave breaks via phase mixing process. This is an obvious feature which arises due to the relativistic mass variation effect [31–33]. In all earlier theoretical works [24–27], the contribution of phase mixing on the wake wave has been ignored. In this thesis, a characteristic study on the longitudinal wake wave breaking is presented in detail. It is identified that the excited wake wave is nothing but an identical Akhiezer-Polovin mode [34]. The breaking of the wake wave has been understood in terms of phase mixing of Akhiezer-Polovin (AP) mode. It is also worth noting that, in earlier works, the effect of ion motion has been neglected because of their heavy mass. Including the effect of ion motion, the excitation of relativistic electron beam driven wakefield has also been studied in 1-D here. It is observed that the transformer ratio that measures the efficiency of the acceleration saturates to unity for over-dense beam in both the electron-positron and hydrogen plasmas. Therefore, there will be no gain for an over dense beam in 1-D. It is also seen that the excited wake wave breaks at later times in simulation due to phase mixing process. For the sake of understanding the wake wave breaking, it is observed that the excited wake wave is an equivalent Khachatryan mode [35]. We have identified that the wave breaking limit lies much below the analytical limit derived by Khachatryan et al. [35]. This is so as they have not considered the possibility of the phase mixing process.

Next, two-dimensional fluid simulation has been employed to study the multi-dimensional behavior of the relativistic electron beam driven wakefield in a cold plasma. This study shows a limit in the transverse extension of the beam when 2-D effect must be incorporated. In the recent experiments [16, 17, 36], the wakefield

is typically excited by a short, intense beam to create a “Blow-out” (a pure ion channel free from cold plasma electrons) region. In the blow-out regime, the head of a short driver ejects all the plasma electrons from its propagation channel and most part of the beam propagates in the electron-free region (termed the cavern or bubble henceforth). Our 2-D fluid simulation also excites blow-out structure for a sufficiently intense beam which matches with the analytical form predicted by Lu et al. [28], before phase mixing occurs. As phase mixing steps in, the blow-out structure gets destroyed in the fluid simulations. However, for low beam density ($n_b/n_0 < 5$), the blow-out remains intact for several hundred of plasma periods; where n_b and n_0 are the beam density and plasma density respectively. Whereas it immediately gets destroyed after the formation, for the high-density beam ($n_b/n_0 > 5$) in the fluid simulation. Further, injecting the test particles in the simulation, we have studied the energy acquired by the test electrons and focusing of the accelerated particles. A maximum energy gain of $\sim 2.8\text{GeV}$ by the electrons from the back of the driver beam of energy $\sim 28.5\text{GeV}$ in a 10 cm long plasma is shown to be achieved. This is in conformity with the experimental result of ref. [37]. This shows that a fluid simulation which is much simpler than Particle-in-Cell simulations is good enough at representing the wakefield structure and also providing a good estimate of the acceleration. It is also observed in our simulation that the maximum energy gain can get doubled to $\sim 5.7\text{GeV}$ when the bunch of test particles was placed near the axial edge of the first blowout structure.

The thesis is composed of six chapters based on above discussion and detailed studies on the relativistic electron beam driven wakefield. Below we briefly give a point-wise summary of these chapters.

- **Chapter - I** provides an introduction to plasma based acceleration schemes and physical mechanisms behind the excitation of wakefield. It also covers the experimental achievements and the recent challenges to build a next generation plasma based accelerator. The introduction is geared along following points:

1. In recent years, plasma based acceleration schemes have made amazing progress because of their wide applications ranging from medical, industry to high energy physics. The concept of plasma based accelerator was first proposed by Tajima and Dawson [22]. The authors proposed a useful mechanism and suggested the generation of a high longitudi-

nal electric field (\sim hundreds of GV/m) by injecting an ultra-intense laser pulse in plasma, known as LWFA. This electric field is set up by expelling nearby plasma electrons due to the ponderomotive force of the laser pulse. Ions only provide a stationary neutralizing background because of their heavy masses. As the laser propagates further inside the plasma, the repelled electrons come back to their individual original positions and over-shoot because of their inertia. Finally, a wave, so-called wakefield, will be excited just behind the laser pulse, which propagates with the group velocity of the laser pulse[5]. However, the axial ponderomotive force from the laser pulse can not be used directly to accelerate electrons to high energies. The ponderomotive force on the accelerated electrons ($\gamma \gg 1$) is smaller than that on the plasma electrons by the factor $1/\gamma$, where γ is the relativistic factor associated with the accelerated electrons. Thus the laser pulse must first excite the plasma wave which, in turn, can be used for acceleration. There are two more schemes, laser beat-wave acceleration (LBWA) and self-modulated laser wakefield acceleration (SMLWFA), are also used to accelerate the charge particles using laser pulses [10, 21, 38]. Regardless of how, using these above schemes, near GeV quasi-mono-energetic electron beam was generated by Mangles et al. [39], Geddes et al. [38], Kneip et al. [10] and Faure et al. [6].

2. Recently, another exciting scheme, known as plasma wakefield accelerator (PWFA), shows promising results on the topic of the plasma-based accelerations which was originally proposed by Chen, huff and Dawson [40] in 1985 as a means of coupling between plasma wave to the electron beam velocity. In plasma wakefield accelerator, the relativistically intense wake wave is excited using a ultra-relativistic electron or proton beam propagating inside the plasma near the speed of light. The beam expels the nearby plasma electrons due to its space-charge force, whereas ions remain intact. As beam propagates, the expelled electrons will then come back to their individual equilibrium positions and overshoot because of their inertia. As a results, a wake wave will be excited just behind the beam having phase velocity equal to the velocity of the beam [40]. Basically, in PWFA, one bunch of first particles drives the wake wave that accelerates another bunch separated closely from the driver beam [41]. This scheme, however, behaves as an elec-

trical transformer which converts a large bunch (driver) of moderate energy electrons into a small bunch (witness) at higher energy.. This capability would be useful for particle-physics experiments, in which high collision energies are critical. On the other hand, this scheme has a potential to reduce the size and cost of x-ray free-electron lasers. The first experimental demonstration of plasma wakefield acceleration was reported by a research group at Argonne National Laboratory in 1988 [13]. After that, many experimental tests have been reported in this way [14, 15, 18]. The most exciting result was outlined by Blumenfeld et al. [19] in 2007. Below I directly quote the abstract from their report.

“Here we show that an energy gain of more than 42 GeV is achieved in a plasma wakefield accelerator of 85 cm length, driven by a 42 GeV electron beam at the Stanford Linear Accelerator Center (SLAC). The results are in excellent agreement with the predictions of three-dimensional particle-in-cell simulations. Most of the beam electrons lose energy to the plasma wave, but some electrons in the back of the same beam pulse are accelerated with a field of $\sim 52\text{GVm}^{-1}$. This effectively doubles their energy, producing the energy gain of the 3-km-long SLAC accelerator in less than a meter for a small fraction of the electrons in the injected bunch.”

In 2014, Litos et al. [20] designed their experiment using a discrete trailing bunch surfing in an accelerating gradient of 4.4GV/m and minimized the energy spread of the accelerated beam to $\sim 2\%$. These results successfully demonstrate the viability of plasma accelerators and illuminate a path towards its high-energy applications.

3. Although plasma based acceleration schemes made a strong headline in the field of particle accelerators, it has several drawbacks for an efficient acceleration. Among the several laser-plasma based acceleration schemes, the method which has received the most attention is the plasma beat wave acceleration (PBWA), in which a large amplitude plasma wave resonantly excited by the beating of two relatively low power, long laser beams having a frequency difference equal to the plasma frequency. In plasma wakefield accelerator (PWFA), the wake wave is excited by a high-current, relativistic particle beam whose current profile of the beam is tailored to have a slow, rise and a sudden termination. Therefore the precession engineering is required either for

tuning these laser pulses precisely or maintaining the current profiles in PWFA. On the other hand, for a successful operation, among the several constraints of either the PWFA or PBWA is that the driver must be capable of propagating a sufficiently long distance to avoid multiple acceleration stages. As all the stages needed to be sequentially synchronized, multi-staging would be impossible for an efficient acceleration from the practical point of view. One more challenge in the wakefield acceleration schemes is to keep the witness beam in a right spot for a long distance in such a high field. Accelerated beam undergoes many instabilities [16, 17] in this high field and, as a whole, the process of acceleration fails. Therefore, a strong R&D needed to be developed in this field for producing a high-quality energetic beam.

However, in this particular field, the design of experimental set up is extremely guided by the simulations. As stated above, most of the simulations in this field are performed using PIC techniques, which are computationally heavy and time consuming. The purpose of this thesis is to investigate the relativistic electron beam driven wakefield excitation, using fluid simulation techniques which is computationally much simpler and faster than any sophisticated PIC. We have studied the excitation of wakefield for several beam configurations both in 1-D and 2-D. A brief summary of our research work is covered in the next four chapters. The last (sixth) chapter summarizes the thesis work and provides some future scope of this work.

- **Chapter - II** presents a 1-D study of the excitation of wakefield driven by an ultra-relativistic electron beam in a cold plasma. In 1987, Rosenzweig et. al. [24] reported a 1-D analytical expression of electron beam driven wakefield only for a rigid, homogeneous electron beam having the density (n_b) less or equal to half the plasma density. Relaxing the restriction on beam parameters (density and velocity) used in the earlier analytical work, an extensive numerical study for the excitation of relativistic electron beam driven wakefield is performed here for arbitrary beam parameters, using 1-D fluid simulation techniques [42]. The simulation results are found to be in good agreement with the analytical work of Rosenzweig for a beam having the density less or equal to half the plasma density. Besides, Rosenzweig's work has been analytically extended to regimes where the ratio of beam density to plasma density is greater than half and results have been verified using simulations. Further, in contrast to Rosenzweig's work, if the beam

is allowed to evolve in a self-consistent manner, several interesting features have been observed in the simulation viz. splitting of the beam into beamlets (for $l_b > \lambda_p$) and compression of the beam (for $l_b < \lambda_p$); l_b and λ_p are the physical length of the beam and plasma wavelength respectively. It is also seen that beam can propagate a long distance without any significant deformation if the velocity of the beam is larger than $0.99c$. Therefore beam can be considered to be rigid in such limit.

- **Chapter - III** covers a complete study on the space-time evolution of relativistic electron beam driven wake wave in a cold plasma. It is observed that the wake wave gradually modifies with time and eventually breaks, exhibiting sharp spikes in the density profile and sawtooth-like features in the electric field profile after several plasma periods. This is a clear indication of wake wave breaking [31, 33] of relativistic electron beam driven wake-field in a cold, homogeneous plasma. This study is also carried out using fluid simulation techniques. In the simulation, it is observed that the structure of wake wave gradually modifies. The simulation has been performed for a long enough time for the excited wave to break. The wave breaking process, however, helps to self-inject the plasma electrons into acceleration phase, a complete knowledge on the wake wave breaking is therefore required for controlling and stabilizing the acceleration process [12]. In this chapter, a detailed characteristic study on the breaking of longitudinal wakefield has been investigated. It has been found here that the excited wakefield before it breaks is identical to longitudinal Akhiezer-Polovin (AP) mode excited using the same value of β_{ph} (phase velocity) and u_m (maximum fluid velocity) of the wake wave [34]. However, the steepening (breaking) of this wake has been understood in terms of phase mixing of the AP mode, which arises because of relativistic mass variation effects. The phase mixing time (breaking time) is studied as a function of beam density and beam velocity and, interestingly, is found to follow the well known scaling presented in ref. [43]
- **Chapter - IV** addresses the role of ion motion on the relativistic electron beam driven wakefield in a cold plasma. In plasma-based accelerators, the charge particles get accelerated using the huge electric field ($\sim GeV/cm$) associated with the wake wave. In 1998, Khachatryan et al. [35] reported in the study of strong plasma waves (i.e. $\gamma \gg 1$) that plasma ions (even for heavy ions) make an essential contribution to the process of charge separation under the influence of such a strong field where maximum relativis-

tic wavelength and amplitude of the wave grow in proportion to γ . Here, $\gamma = (1 - v^2/c^2)^{-1/2}$ is the Lorentz factor associated with the velocity of the electrons v . The study of relativistic plasma waves, including ion motion, is also important for some astrophysical scenarios. In the polar region of the pulsars, it is considered to be filled with electron-positron plasma and energetic charged particles are being generated from the plasma waves. Therefore it is important to incorporate the dynamics of ion in these studies replicating the structure of the wakefield in such applications. In this thesis, with the help of the fluid simulation, the excitation of relativistic electron beam driven wakefield is studied where the effect of the ion motion is included. Including ion motion, Rosenzweig et al. [44] presented a semi-analytical form of the electron beam driven wakefield and estimated the approximate value of transformer ratio (for mass ratio $\mu = m_e/m_i \ll 1$) only for beam density equal to half the plasma density using multiple-fluid (ion and electron fluid) model, where m_e and m_i are the mass of electrons and ions respectively. For further extension of Rosenzweig's work [30], fluid simulation has been executed for arbitrary mass ratios and beam densities using a rigid, homogeneous beam. As described in chapter II, the beam can be considered to be rigid if and only if the velocity of the beam exceeds $0.99c$. In all our simulations, the excitation is driven by the rigid beam to avoid the deformation in beam density. It is shown that simulation results match with the semi-analytical results given by Rosenzweig et al. [30] for different beam density and mass ratio. The transformer ratio, which determines the gain in the acceleration process, is also studied as a function of mass ratio and beam density. For overdense beam, the transformer ratio saturates to unity for both the electron-positron p (e.g. $\mu = 1$) and hydrogen (e.g. $\mu = 1/1836$) plasma. We have also seen that the excited wave also breaks via the gradual process of phase mixing after several plasma periods, exhibiting sharp spikes in the density profile. The corresponding electric field profile turns into the sawtooth form which is a clear signature of wave breaking. This particular feature observed in the present simulation has been found to be absent in the analytical calculations given in ref.[44]. However, it is shown that the wake wave, before it breaks, is an identical mode corresponding to the Khachatryan mode which is excited using the same parameter values of wake wave i.e. mass ratio, phase velocity and maximum value of electric field. The physical mechanism behind the wave breaking has been understood in terms of phase mixing process of the Khachatryan's mode. It is seen here that the

numerically obtained wave breaking limit lies much below the analytically estimated value given in ref. [35].

- **Chapter - V:** presents a study of 2-D wakefields driven by a rigid, ultra-relativistic electron beam in a cold homogeneous plasma using fluid simulation techniques. In our earlier work, the study of relativistic driven wakefield excitation was restricted to 1-D. However, in recent experiments, the wakefield is excited for a short, intense beam, which leads to “Blow-out” structure, which is an ion cavity totally free from cold plasma electrons [15, 16, 36]. Therefore a 2-D or even 3-D study is required for explaining the excitations in these regimes. For a short, ultra-intense bunch, the space charge force is large enough to expel all the nearby electrons, an ion channel just behind the beam is thereby formed. This ion channel so-called “Blow-out” structure is shielded by a narrow sheath of dense repelled electrons. For sufficiently intense beam the ion channel can have a spherical shape i.e. bubble or cavern. In recent experiments, bubble regime has been used for generating good quality beams. We have developed fluid code in 2-D geometry which solves fluid-Maxwell equations using flux corrected transport scheme [42, 45]. The numerical technique will be described in detail in the thesis. In simulation, it is observed that for both underdense and overdense rigid, bi-Gaussian beams, in the limit when transverse dimensions are greater than their longitudinal extension, the axial profile (integrated in the transverse directions) of the excited wakefield shows a good agreement with the 1-D results of Ratan et al. [27]. In the other limit i.e. when the transverse dimensions of the beam are smaller than the longitudinal extension, the 2-D simulation results deviate from 1-D results. Using a rigid, bi-parabolic beam profile, it is shown that simulation results also show a good agreement with 2-D linear theory only for $\frac{n_b}{n_0} \ll 1$. For a short, overdense beam, the excited wakefield exhibits blowout formation. The radius of the blowout structure matches with the analytical form given by Lu et al. [28], before phase mixing occurs. The phase mixing process is identified by steepening in the density profile which is accompanied by sawtooth structure in electric field profile. It is also seen that the total energy starts to decrease as soon as the wave breaks in the fluid simulation. Further, in our simulation, it is confirmed that, when the wake wave breaks the excursion length of the electrons in the wake exceeds the radius of curvature of the blow-out [46]. A detailed study on beam focusing, efficiency of acceleration is also analyzed in this chapter by injecting

the test particles in the simulations. It is observed in our simulation that the maximum energy gain of 2.8 GeV by the electrons from the back of the driver beam of energy 28.5 GeV in a 10 cm long plasma, matches with the experimental results given by Hogan et al. [37]. Our simulation shows that the maximum energy gain can be doubled to 5.7 GeV when the bunch of test particles was placed near the axial edge of the first blowout.

- **Chapter - VI** summarizes thesis work and recapitulate the salient points of this thesis. We then provide a over-view of the future research problems which can be carried out in continuation of the work described here.

The detailed investigations made in this thesis contribute significantly to the theoretical understanding of relativistic electron beam driven wakefield excitation in a cold plasma and the fluid code, which has been developed and used in this work extensively, sets a milestone in this particular field by giving satisfactory results.

-
- [1] C. B. Schroeder E. Esarey and W. P. Leemans. Physics of laser-driven plasma-based electron accelerators. *Rev. Mod. Phys.*, 81:1229, 2009.
- [2] V. Malka, S. Fritzler, E. Lefebvre, M.-M. Aleonard, F. Burgy, J.-P. Chambaret, J.-F. Chemin, K. Krushelnick, G. Malka, S. P. D. Mangles, Z. Najmudin, M. Pittman, J.-P. Rousseau, J.-N. Scheurer, B. Walton, and A. E. Dangor. Electron acceleration by a wake field forced by an intense ultrashort laser pulse. *Science*, 298(5598):1596–1600, 2002.
- [3] C. Joshi. The development of laser- and beam-driven plasma accelerators as an experimental field. *Physics of Plasmas*, 14(5):055501, 2007.
- [4] Chan Joshi and Victor Malka. Focus on laser- and beam-driven plasma accelerators. *New. J. Physics*, 12:045003, 2010.
- [5] T. Katsouleas. Physical mechanisms in the plasma wake-field accelerator. *Phys. Rev. A*, 33:2056–2064, Mar 1986.
- [6] J. Faure et al. A laser-plasma accelerator producing monoenergetic electron beams. *Nature*, 431:541–544, Sep2004.
- [7] A. Norlin A. Lifschitz Y. Glinec J. Faure, C. Rechatin and V. Malka. Controlled injection and acceleration of electrons in plasma wakefields by colliding laser pulses. *Nature*, 444:737, 2006.
- [8] G. Golovin, S. Chen, N. Powers, C. Liu, S. Banerjee, J. Zhang, M. Zeng, Z. Sheng, and D. Umstadter. Tunable monoenergetic electron beams from independently controllable laser-wakefield acceleration and injection. *Phys. Rev. ST Accel. Beams*, 18:011301, Jan 2015.
- [9] W. Lu, M. Tzoufras, C. Joshi, F. S. Tsung, W. B. Mori, J. Vieira, R. A. Fonseca, and L. O. Silva. Generating multi-gev electron bunches using single stage laser wakefield acceleration in a 3d nonlinear regime. *Phys. Rev. ST Accel. Beams*, 10:061301, Jun 2007.
- [10] S. Kneip, S. R. Nagel, S. F. Martins, S. P. D. Mangles, C. Bellei, O. Chekhlov, R. J. Clarke, N. Delerue, E. J. Divall, G. Doucas, K. Ertel, F. Fiuza, R. Fonseca, P. Foster, S. J. Hawkes, C. J. Hooker, K. Krushelnick, W. B. Mori, C. A. J. Palmer, K. Ta Phuoc, P. P. Rajeev, J. Schreiber, M. J. V. Streeter, D. Urner, J. Vieira, L. O. Silva, and Z. Najmudin. Near-gev acceleration of electrons by a nonlinear plasma wave driven by a self-guided laser pulse [phys. rev. lett. 103, 035002 (2009)]. *Phys. Rev. Lett.*, 103:049901, Jul 2009.

- [11] V. Malka. Laser plasma accelerators. *Physics of Plasmas*, 19(5):055501, 2012.
- [12] A. Modena. Electron acceleration from the breaking of relativistic plasma waves. *Nature*, 377, 1995.
- [13] J. B. Rosenzweig, D. B. Cline, B. Cole, H. Figueroa, W. Gai, R. Konecny, J. Norem, P. Schoessow, and J. Simpson. Experimental observation of plasma wake-field acceleration. *Phys. Rev. Lett.*, 61:98–101, Jul 1988.
- [14] P. Muggli and M. J. Hogan. Review of high-energy plasma wakefield experiments. *Comptes Rendus Physique*, 10:116–129, March 2009.
- [15] N. Vafaei-Najafabadi, K. A. Marsh, C. E. Clayton, W. An, W. B. Mori, C. Joshi, W. Lu, E. Adli, S. Corde, C. I. Clarke, M. Litos, S. Z. Green, S. Gessner, J. Frederico, A. S. Fisher, Z. Wu, D. Walz, and M. J. Hogan. Limitation on the accelerating gradient of a wakefield excited by an ultrarelativistic electron beam in rubidium plasma. *Phys. Rev. Accel. Beams*, 19:101303, Oct 2016.
- [16] E. S. Dodd, R. G. Hemker, C.-K. Huang, S. Wang, C. Ren, W. B. Mori, S. Lee, and T. Katsouleas. Hosing and sloshing of short-pulse gev-class wakefield drivers. *Phys. Rev. Lett.*, 88:125001, Mar 2002.
- [17] C. E. Clayton, B. E. Blue, E. S. Dodd, C. Joshi, K. A. Marsh, W. B. Mori, S. Wang, P. Catravas, S. Chattopadhyay, E. Esarey, W. P. Leemans, R. Assmann, F. J. Decker, M. J. Hogan, R. Iverson, P. Raimondi, R. H. Siemann, D. Walz, T. Katsouleas, S. Lee, and P. Muggli. Transverse envelope dynamics of a 28.5-gev electron beam in a long plasma. *Phys. Rev. Lett.*, 88:154801, Apr 2002.
- [18] J. B. Rosenzweig, D. B. Cline, B. Cole, H. Figueroa, W. Gai, R. Konecny, J. Norem, P. Schoessow, and J. Simpson. Experimental observation of plasma wake-field acceleration. *Phys. Rev. Lett.*, 61:98–101, Jul 1988.
- [19] Ian Blumenfeld, Christopher E. Clayton, Franz-Josef Decker, Mark J. Hogan, Chengkun Huang, Rasmus Ischebeck, Richard Iverson, Chandrashekhar Joshi, Thomas Katsouleas, Neil Kirby, Wei Lu, Kenneth A. Marsh, Warren B. Mori, Patric Muggli, Erdem Oz, Robert H. Siemann, Dieter Walz, and Miaomiao Zhou. Energy doubling of 42[thinsp]gev electrons in a metre-scale plasma wakefield accelerator. *Nature*, 445:741–744, 2007.
- [20] M. Litos, E. Adli, W. An, C. I. Clarke, C. E. Clayton, S. Corde, J. P. Delahaye, R. J. England, A. S. Fisher, J. Frederico, S. Gessner, S. Z. Green, M. J. Hogan, C. Joshi, W. Lu, K. A. Marsh, W. B. Mori, P. Muggli, N. Vafaei-Najafabadi, D. Walz, G. White, Z. Wu, V. Yakimenko, and G. Yocky. High-efficiency acceleration of an electron beam in a plasma wakefield accelerator. *Nature*, 515:92–95,

2014.

- [21] P. Sprangle, E. Esarey, A. Ting, and G. Joyce. Laser wakefield acceleration and relativistic optical guiding. *Applied Physics Letters*, 53(22):2146–2148, 1988.
- [22] T. Tajima and J.M. Dawson. Laser electron accelerator. *Phys. Rev. Lett.*, 43, 1979.
- [23] Han Sup Uhm and Glenn Joyce. Theory of wakefield effects of a relativistic electron beam propagating in a plasma. *Physics of Fluids B: Plasma Physics*, 3(7):1587–1598, 1991.
- [24] J. B. Rosenzweig. Nonlinear plasma dynamics in the plasma wake-field accelerator. *Phys. Rev. Lett.*, 58:555–558, Feb 1987.
- [25] S. Elbakram A. Ts. Amatuni and E. V. Sekhpessian. *Yerevan Physics Institute Report*, 85:832, 1985.
- [26] P. L. Morton R. D. Ruth, A. Chao and P. B. Wilson. *Particle Accelerator*, 17:171, 1985.
- [27] Ratan Kumar Bera, Sudip Sengupta, and Amita Das. Fluid simulation of relativistic electron beam driven wakefield in a cold plasma. *Physics of Plasmas*, 22(7):073109, 2015.
- [28] W. Lu, C. Huang, M. Zhou, W. B. Mori, and T. Katsouleas. Nonlinear theory for relativistic plasma wakefields in the blowout regime. *Phys. Rev. Lett.*, 96:165002, Apr 2006.
- [29] R. Fonseca et al. *Lecture Notes in Computer Science (Springer, Heidelberg)*, 2329:III–342, 2002.
- [30] K. V. Lotov, A. P. Sosedkin, A. V. Petrenko, L. D. Amorim, J. Vieira, R. A. Fonseca, L. O. Silva, E. Gschwendtner, and P. Muggli. Electron trapping and acceleration by the plasma wakefield of a self-modulating proton beam. *Physics of Plasmas*, 21(12):123116, 2014.
- [31] Sudip Sengupta, Predhiman Kaw, Vikrant Saxena, Abhijit Sen, and Amita Das. Phase mixing/wave breaking studies of large amplitude oscillations in a cold homogeneous unmagnetized plasma. *Plasma Physics and Controlled Fusion*, 53(7):074014, 2011.
- [32] E. Infeld and G. Rowlands. Relativistic bursts. *Phys. Rev. Lett.*, 62:1122–1125, Mar 1989.
- [33] Sudip Sengupta, Vikrant Saxena, Predhiman K. Kaw, Abhijit Sen, and Amita Das. Phase mixing of relativistically intense waves in a cold homogeneous plasma. *Phys. Rev. E*, 79:026404, Feb 2009.
- [34] A. I. Akhiezer and R. V. Polovin. Theory of wave motion of an electron plasma.

List of Figures

1.1	A schematic diagram of Laser wakefield Acceleration (LWFA).	9
1.2	A schematic diagram of a typical experimental set-up for LWFA which has been designed at the Center for ultra-fast Optical Science (CUOS), University of Michigan.	12
1.3	A schematic picture of electron beam driven PWFA.	13
1.4	A generic experimental set up for the PWFA experiment. Experimental parameters mentioned in this picture have been taken from SLAC National Accelerator Laboratory, USA.	15
2.1	Plot of numerical and analytical normalized perturbed plasma density (n_1) profiles for $n_b = 0.3$, $v_b = 0.99$, $l_b = 4/2\pi$ at different times.	35
2.2	Plot of numerical and analytical normalized electric field (E) profile for $n_b = 0.3$, $v_b = 0.99$, $l_b = 4/2\pi$ at different times.	36
2.3	Plot of Plot of numerical and analytical normalized perturbed plasma density (n_1) profiles for $n_b = 0.5$, $v_b = 0.99$, $l_b = 4/2\pi$ at different times.	38
2.4	Plot of numerical and analytical normalized electric field (E) profiles for $n_b = 0.5$, $v_b = 0.99$, $l_b = 4/2\pi$ at different times.	39
2.5	Plot of Plot of numerical and analytical normalized perturbed plasma density (n_1) profiles for $n_b = 0.7$, $v_b = 0.99$, $l_b = 4/2\pi$ at different times.	40
2.6	Plot of numerical and analytical normalized electric field (E) profiles for $n_b = 0.7$, $v_b = 0.99$, $l_b = 4/2\pi$ at different times.	41
2.7	Plot of transformer ratio (R) as a function of beam density (α) for $l_b/\lambda_p = 4/2\pi$ and $l_b/\lambda_p = 3$	41
2.8	Numerical and analytical normalized perturbed density (n_1) profiles for the normalized beam density (n_b) = 0.3 at different times, including beam evolution for $l_b/\lambda_p = 4/2\pi$ with $v_b \rightarrow 1$	43
2.9	Numerical and analytical normalized electric field (E) profiles for the normalized beam density (n_b) = 0.3 at different times, including beam evolution for $l_b/\lambda_p = 4/2\pi$ with $v_b \rightarrow 1$	45

2.10	Numerical and analytical normalized perturbed density (n_1) profiles for the normalized beam density (n_b) = 0.3 at different times, including beam evolution for $l_b/\lambda_p = 4/2\pi$ with $v_b = 0.99$	46
2.11	Numerical and analytical normalized perturbed plasma density (n_1) profiles for the normalized beam density (n_b) = 0.3 at different times, including beam evolution for $l_b/\lambda_p = 3$ with $v_b = 0.99$	50
2.12	Schematic diagram of the beam-plasma interaction in τ - frame.	52
3.1	Numerical and analytical normalized perturbed electron density (n_1) profile at different times for the normalized beam density (n_b) = 0.3, the beam velocity ($v = b$) = 0.99, and the beam length (l_b) = 4	58
3.2	Numerical and analytical normalized electric field (E) profile at different times for the normalized beam density (n_b) = 0.3, the beam velocity ($v = b$) = 0.99, and the beam length (l_b) = 4	59
3.3	Numerical and analytical normalized perturbed electron density (n_1) profile at different times for the normalized beam density (n_b) = 0.4, the beam velocity ($v = b$) = 0.99, and the beam length (l_b) = 4	60
3.4	Numerical and analytical normalized electric field (E) profile at different times for the normalized beam density (n_b) = 0.4, the beam velocity ($v = b$) = 0.99, and the beam length (l_b) = 4	61
3.5	Numerical and analytical normalized perturbed electron density (n_1) profile at different times for the normalized beam density (n_b) = 0.4, the beam velocity ($v = b$) = 0.8, and the beam length (l_b) = 4	62
3.6	Numerical and analytical normalized electric field (E) profile at different times for the normalized beam density (n_b) = 0.4, the beam velocity ($v = b$) = 0.8, and the beam length (l_b) = 4	65
3.7	Plot of perturbed density profile (n_1) of wake wave (magenta) and Akhiezer-Polovin mode (blue circles) for normalized beam density (n_b) = 0.3, beam velocity (v_b) = 0.99, and beam length (l_b) = 4 at $\omega_{pe}t = 25$	68
3.8	Plot for numerically obtained (circles) and fitted (solid) scaling of phase mixing time (τ_{mix}) with the phase velocity (β_{ph}) for the normalized beam density (n_b) = 0.3 and the beam length (l_b) = 4	69

3.9	Plot for numerically obtained (circles) and fitted (solid) scaling of phase mixing time (τ_{mix}) with the phase velocity (β_{ph}) for the normalized beam density (n_b)=0.4 and the beam length (l_b)= 4	70
3.10	Plot for analytical (solid) and numerical (circles) scaling of phase mixing time (τ_{mix}) as a function of maximum fluid velocity (u_m) for normalized beam velocity (v_b) = 0.99 and beam length (l_b) = 4. . .	71
4.1	Plot of normalized perturbed electron density (n_1) profile at different times for the normalized beam density (n_b)=0.1, $l_b = 4$ beam velocity (v_b) =0.99 and $\mu = 1$	78
4.2	Plot of normalized electric field (E) profile at different times for the normalized beam density (n_b)=0.1, beam velocity (v_b) =0.99, $l_b = 4$ and $\mu = 1$	80
4.3	Plot of normalized perturbed electron density (n_1) profile at different times for the normalized beam density (n_b)=0.2, beam velocity $v_b = 0.99$, $l_b = 4$ and $\mu = 1$	81
4.4	Plot of normalized electric field (E) profile at different time for the normalized beam density (n_b)=0.2, beam velocity $v_b = 0.99$, $l_b = 4$ and $\mu = 1$	82
4.5	Plot of normalized perturbed electron density (n_1) profile at different times for the normalized beam density (n_b)=0.3, beam velocity $v_b = 0.99$ and $l_b = 4$ and $\mu = 1/1836$	83
4.6	Plot of transformer ratio (R) vs. mass ratio (μ) for $n_b = 0.5$ and $n_b = 0.1$	84
4.7	Plot of semi-analytical and numerical values of transformer ratio (R) as a function of beam density (n_b) for $\mu = 1$ and $\mu = 1/1836$. The blue circles indicate the values of transformer ratio obtained from the analytical expression given by Ratan et. al. [<i>Physics of Plasmas</i> , 22, 073109 (2015)] for $\mu = 0$	85
4.8	Plot of plasma electron density (n_1) at different times $t = 123$ for $\mu = 1/1836$, $n_b = 0.3$, $v_b = 0.99$ and $l_b = 4$	86
4.9	Comparison of numerical electric field profile (E) with the analytical and Khachatryan mode for $n_b = 0.1$, $l_b = 4$, $v_b = 0.99$ and $\mu = 1$. . .	87

4.10	Plot of maximum amplitude of wave breaking electric field (E_{WB}) as a function of mass ratio (μ) for $n_b = 0.2$, $l_b = 4$ and $v_b = 0.99$ or $\gamma_{ph} = 7.08$	88
5.1	Plot of (a) normalized electron density (n), (b) contour of longitudinal electric field (E_x), (c) z - component of magnetic field (B_z) profile, (d) axial profile of analytical (solid black) and numerical (circle) longitudinal electric field at $\omega_{pe}t = 29$ for a bi-Gaussian beam of normalized peak density (n_{b0})=0.1, beam velocity (v_b)=0.9999, $\sigma_x = 0.5$ and $\sigma_y = \sqrt{15}$	100
5.2	Plot of (a) normalized electron density (n), (b) contour of longitudinal electric field (E_x), (c) z - component of magnetic field (B_z) profile, (d) axial profile of analytical (solid black) and numerical (circle) longitudinal electric field at $\omega_{pe}t = 28.28$ for a bi-Gaussian beam of normalized peak density (n_{b0})=0.1, beam velocity (v_b)=0.9999, $\sigma_x = \sqrt{5}$ and $\sigma_y = 0.5$	101
5.3	A schematic diagram of slab representation for cylindrical geometries.	102
5.4	A schematic diagram of beam dynamics in (ξ, r) -plane.	103
5.5	Plot of (a) normalized electron density (n), (b) longitudinal electric field (E_x), (c) beam profile, (d) profile of analytical (solid black) and numerical (circle) Axial profile of longitudinal electric field at $\omega_{pe}t = 23$ for a bi-parabolic beam of normalized peak density (n_{b0})=0.1, beam velocity (v_b)=0.9999, $b = 0.5$ and $a = \sqrt{15}$	104
5.6	Plot of (a) normalized electron density (n), (b) longitudinal electric field (E_x), (c) z - component of magnetic field (B_z) profile, (d) Axial profile of analytical (solid black) and numerical (circle) longitudinal electric field at $\omega_{pe}t = 17$ for a bi-parabolic beam of normalized peak density (n_{b0})=0.1, beam velocity (v_b)=0.9999, $b = \sqrt{5}$ and $a = 0.5$	105
5.7	Plot of (a) normalized plasma electron density (n) profile, (b) axial profile of density, electric longitudinal electric field (E_x) profile for a bi-Gaussian beam of normalized peak density (n_{b0})=1, beam velocity (v_b)=0.9999, $\sigma_x = \sqrt{1}$ and $\sigma_y = 0.4$ at $t = 21.21$	112

5.8	Plot of (a) normalized perturbed electron density (n_1) profile, (b) longitudinal electric field (c) axial profile of analytical and numerical longitudinal electric field profile (d) analytical obtained blowout curve (red line) for a bi-Gaussian beam of peak density (n_{b0})=1, beam velocity (v_b)=0.9999, $\sigma_x = \sqrt{2}$ and $\sigma_y = 1$ at $\omega_{pe}t = 6$	113
5.9	Plot of (a) normalized perturbed electron density (n_1) profile and (b) longitudinal electric field profile (c) analytically obtained blowout curve for a bi-Gaussian beam of peak density (n_{b0})=7, beam velocity (v_b)=0.9999, $\sigma_x = \sqrt{2}$ and $\sigma_y = 1$ at $\omega_{pe}t = 2.8$	114
5.10	Plot of normalized perturbed electron density (n_1) profile and analytical obtained blowout curve (solid green line) for a bi-Gaussian beam having peak density (n_{b0})=7, beam velocity (v_b)=0.9999, $\sigma_x = \sqrt{2}$ and $\sigma_y = 1$ at different times $\omega_{pe}t = 2.8$ and $\omega_{pe}t = 8$	115
5.11	Plot of normalized values of total energy, kinetic energy and field energy vs. time for the normalized beam density (n_b)=7.0, $\sigma_x = \sqrt{2}$ and $\sigma_y = 1$	116
5.12	Plot of (a) normalized values of perturbed plasma density (n_1), electron beam density ($n_{b0} = 3$, $\sigma_x = \sqrt{2}$, $\sigma_y = 1$, $v_b = 0.99999999$), and distribution of test electrons at $t = 0$, (b) normalized values of perturbed plasma density (n_1), electron beam density (n_b), and distribution of test electrons at $t = 50$, (c) the speed distribution function ($f(v)$) of test electrons at $t = 0$ and $t = 50$, (d) the energy (γ) distribution of test electrons at $t = 0$ and $t = 50$, (e) the distribution of test electrons at the blowout structure.	118
5.13	Plot of (a) normalized values of perturbed plasma density (n_1) and electron beam density (n_b) at $t = 0$, (b) normalized values of perturbed plasma density (n_1) and electron beam density (n_b) at $t = 77$, (c) the speed distribution function ($f(v)$) of test electrons at $t = 0$, (d) the distribution of test electrons at $t = 77$ (e) the energy distribution of test electrons at $t = 0$, (f) the energy distribution of test electrons at $t = 77$	119

5.14	Plot of (a) normalized values of perturbed plasma density (n_1), electron beam density (n_b), and the distribution of test electrons at $t = 0$, (b) normalized values of perturbed plasma density (n_1), electron beam density (n_b), and the distribution of test electrons at $t = 77$, (c) the energy distribution and the driver beam profile at $t = 0$, (c) the energy distribution and the driver beam profile at $t = 77$	120
A.1	A schematic diagram of test particle simulation techniques.	159
A.2	Flow chart of test particle simulation techniques.	161

List of Tables

2.1	Value of plasma parameters at the turning points inside the beam. .	47
2.2	Value of plasma parameters at the turning points outside the beam.	52

1

Introduction

*“God was invented to explain the mystery.
God is always invented to explain those things
that you do not understand.”*

-Richard P. Feynman

Introduction

This thesis is devoted to the studies of the relativistic electron beam driven wakefield excitation in a cold plasma. The wakefield structures are the basis for plasma based acceleration, which holds a great promise for high quality acceleration of charged particles over short distances. In this chapter we provide for the motivation, basic concepts and underlying principle of plasma wakefield acceleration. This chapter also includes the review of earlier works and a brief summary of the important results obtained in this thesis.

Motivation

High energy accelerators are one of the most versatile inventions in physics which produce a beam of energetic charge particles that can be used for various purposes ranging from medical, industry to high energy physics [1–5]. In the high energy physics studies the accelerated charge particle beam offers the possibility of an ultimate microscope as it can reveal fundamental forces and particles in the universe at the energy frontier. They also provide for powerful radiation sources (e.g. "X- rays" and beyond). These radiation sources have tremendous use in medical science. Millions of patients receive accelerator based diagnosis and therapy each year in hospitals and clinics around the world. In industries, particle accelerators are used in hundreds of industrial processes ranging from the manufacturing of computer chips to the cross-linking of plastic for shrink wrap and beyond. Particle accelerators also have a great impact in applications related to national security, including cargo inspection, stockpile stewardship, and material characterizations etc. Thus energetic charged particles created by accelerators touch nearly every part of our daily lives. Since the early days of the cathode ray tube in the 1890s, particle accelerators have made important contributions to scientific and technological innovation. Today, there are more than 30,000 particle accelerators in operation around the world.

High energy physicists use particle accelerators to answer most profound questions about the nature of the universe. They accelerate charged particles near the speed of light in particle accelerators and then smash them together, recreating the conditions that existed when our universe was cataclysmically born in the big

bang. By analyzing the debris of the collisions, physicists then understand how the seemingly disparate forces and particles can be connected by universal laws. Hence, with a deep understanding of the intrinsic nature of the forces and particles, they try to decipher the most fundamental building blocks (sub-atomic particles) of matter. The wavelength (λ_M) of matter-wave associated with the particle having energy E , momentum p and rest mass m_0 is related as, $\lambda_M = \frac{h}{p} = \frac{hc}{\sqrt{E^2 - m_0^2 c^4}}$ [6]. Therefore, as the energy of the particle increases the wave number associated with it decreases. Thus to resolve smaller dimensions we keep requiring increasingly higher energy particles. This implies that physicists need particle accelerators which can produce increasingly higher energy particles. This in turn increases the size as well as the cost of the accelerator, making it formidable. At present, the most powerful accelerator is the Large Hadron Collider (LHC) at CERN which is a circular tunnel of diameter 8.6 km. This giant accelerator is capable of producing a proton beam of energy $\sim 3.5 TeV$ [4, 7, 8]. However, the operation of this bulky machine is too costly and time-consuming. The total operating budget of Large Hadron Collider (LHC) at CERN runs about ~ 1 billion per year. One is, therefore, seeking newer techniques which can reduce the size and the cost of the machine.

Over two decades, high energy particle colliders including LHC, CERN have been using microwave cavities to propel the particle beams near the speed of light. In these cavities, electric fields spaced around the accelerator switch from positive to negative at a given frequency ($\sim MHz$), creating radio waves that accelerate particles in bunches. The approach has been applied by the 8.6-kilometer-diameter Large Hadron Collider (LHC), CERN, which reaches it's technological

and economic limits [8]. This is due to the fact that the accelerating gradient in conventional RF (microwave) based linear accelerators is presently limited to 100 MV/m , partly due to material breakdown limit which occurs on the wall of the acceleration tube. With the accelerating gradient limited by this constraint, high energy experiments required a distance of many kilometers to accelerate the particles to high energies ($\sim 100\text{ GeV}$) and beyond energies for Higgs Boson detection (the energy of Higgs boson being of this order). Therefore, physicists designed circular devices instead of linear machines to enlarge the effective acceleration path by turning the beam many times along the device until it reaches to the desired energy level. However, classically, any charged particle which moves in a curved path or is accelerated in a straight-line path will emit electromagnetic radiation. Particularly, in the circular particle accelerators where charged particles are accelerated to very high speeds, the radiation is referred to as synchrotron radiation. The classical formula for the radiated power (P) from a charge particle accelerated in a circular device of radius r is,

$$P \propto \frac{\gamma^4 v^4}{r^2} \tag{1.1}$$

where $\gamma = (\sqrt{1 - v^2/c^2})^{-1}$ is the Lorentz factor associated with the particle of velocity v [9]. Since the velocity becomes nearly constant for highly relativistic particles, the factor γ^4 becomes the dominating variable in determining loss rate. Therefore, the issue pertaining to the acceleration of particles is that while protons or heavier particles can be accelerated in circular paths, lighter mass particles such as electrons and positrons have to be accelerated in linear devices. The 3-km linear accelerator at Stanford Linear Accelerator (SLAC) is currently the world's longest machine which can accelerate electrons to $\sim 50\text{ GeV}$ energies. Clearly, for

higher energies the size of the conventional electron accelerators would become increasingly unwieldy and costlier. The major reason is the very large cost of building and maintaining particle accelerators due to their complicated structure and large sizes. New techniques which can shrink the size and hence expense of these new generation high energy colliders are, therefore welcome. The accelerators based on plasma offer such a cheaper technological alternative [10,11].

Plasma Based Acceleration

One important potential application of the physics of a short pulse laser or charged particle beam interacting with a plasma is plasma based acceleration. By definition, plasma is a collection of unbound charge particles having equal number of positively and negatively charged species, which exhibits quasi-neutrality and collective behavior [12]. Being an ionized medium, plasma is not constrained by the material breakdown limit of voltage and hence can support electric fields several orders of magnitude higher than that of the conventional RF-based accelerators [10,13–15]. For example, a plasma having density $n_0 = 10^{18} \text{cm}^3$ can sustain an electric field of the order of $E_0 \sim m_e c \omega_{pe} / e \approx 100 \text{GV/m}$. Here c and ω_{pe} represent the speed of light in vacuum and the plasma frequency of electron having mass m_e , charge e . The strength of the electric field is more than 1,000 times higher than the accelerating gradient of a typical conventional accelerator powered by microwaves. The remarkable point is that the wavelength of a plasma wave is typically of the order of 30 microns, whereas the typical microwave wavelength is 10 centimeters. This exceptional feature of plasma offers a way to build an affordable high-performance particle accelerator of much smaller size than the conventional devices [10,15,16].

In plasma-based accelerators, charge particles get accelerated by the electric field associated with the relativistically intense electron plasma wave or other high-gradient accelerating structures (like shock and sheath fields) [15,17–20]. Typically, these intense plasma waves are excited either using an intense laser pulse or ultra-relativistic electron beam propagating inside a plasma with a velocity close to the speed of light. When a laser beam is used, it is called Laser Wakefield Acceleration (LWFA) [15,17–24] and when a particle beam is used, it is referred to Plasma Wakefield Acceleration (PWFA) [16,17,25–33]. If the charge particles ride suitably on the plasma wave, they get accelerated to higher energies. The basic principle of acceleration is similar to “boat-wake-surfing”, in which a rider trails behind a boat and gets accelerated by the wake of the boat without being directly pulled by the boat. In plasma based accelerators, the charge particles gain energy by surfing on a plasma wave. We briefly discuss in the following subsections the two major mechanisms, LWFA and PWFA, for generating high energetic beams.

Laser Wakefield Acceleration (LWFA)

In laser wakefield acceleration technique, a short, ultra-intense laser pulse (TW scale) is injected into the plasma which creates a large electric field by separating the electrons and ions in a plasma. When a short, intense laser pulse is injected into the plasma, the pulse expels plasma electrons from its vicinity due to ponderomotive force [22,34–36]. Ions do not respond because of their heavy mass. They only provide neutralizing background. When the pulse moves ahead, the repelled electrons try to return back to their original location. However, they overshoot due to their inertia and continue their oscillations around the ions. Hence, a plasma wave gets established just behind the pulse. The phase velocity of the generated

plasma wave is found to match with the group velocity of the laser pulse. This is known as “wake wave”, and the electric field associated with the wake wave is called “wakefield”. Therefore, when the charge particles (either injected externally or trapped within) ride on such a wake field at an appropriate phase, they get accelerated to high energies. This scheme was first proposed by Tajima and Dawson [21] in 1979. A schematic diagram of LWFA scheme is shown in Fig. (1.1).

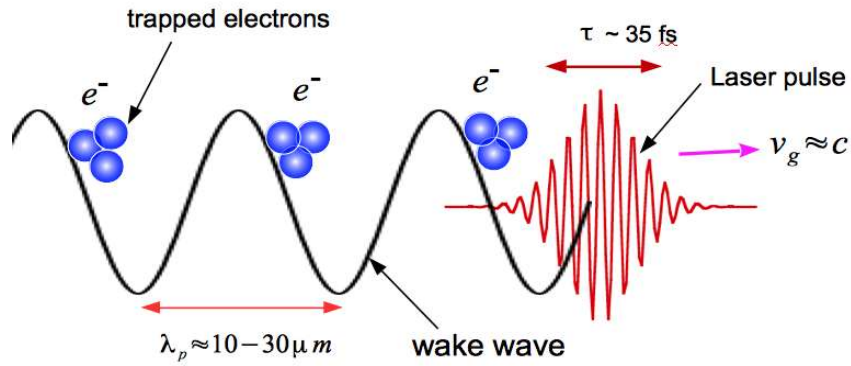


Figure 1.1: A schematic diagram of Laser wakefield Acceleration (LWFA).

It is to be noted that the axial ponderomotive force $F_{pond} = |e|\vec{\nabla}\phi_L$ exerted by the laser pulse on plasma cannot be used directly to accelerate electrons to high energies; where $\phi_L = -m_0c^2a_L^2/2|e|$ is the ponderomotive potential. The ponderomotive force on the accelerated electrons is smaller than that on the plasma electrons by the factor $1/\gamma$, where γ is the relativistic factor associated with the accelerated electrons [34]. Therefore, the laser pulses must first excite a plasma wave which, in turn, can be used for the acceleration process. However, in LWFA, the wakefield is driven most efficiently when the pulse length $L_b \sim \frac{\lambda_p}{2}$; where λ_p

is the plasma wavelength. Prior to 1998, due to the absence of the technologies for generating ultra-intense picosecond laser pulses, the electrons are accelerated using the concept of PBWA (Plasma Beat-Wave Accelerator), in which a large amplitude plasma wave is resonantly excited by the beating of two relatively low-power laser pulses having frequencies ω_1 and ω_2 [37–39]. The condition required for large amplitude excitations in PWBA is $\omega_1 - \omega_2 \approx \omega_{pe}$; where ω_{pe} is the plasma frequency. Clearly, this scheme requires a fine-tuning of frequencies in laser pulses to achieve the resonance condition for high-density plasmas. Another challenge is to hold the long driver for a sufficient time inside a plasma. The pulse undergoes many instabilities during the propagation inside the plasma [40, 41]. The successful demonstration of LWFA has been demonstrated in a late 90’s when chirped-pulse amplification was applied to compact solid-state laser and table-top tera-watt (TW) lasers. In LWFA, an ultra-intense, short laser pulse with a single frequency is injected into the plasma which utilizes the relativistic optical guiding [23, 34, 42] mechanism for the long distance propagation in the plasma. The pulse creates the charge separation and generates wake wave. In this scheme, the wake wave can accelerate particles almost from rest. Hence this scheme offers a way to design a self-contained tabletop accelerator for moderate-energy applications, such as medicine and materials science [2, 11, 33].

Recently, one more scheme known as self-modulated LWFA (SMLWFA) [43–45] has been received considerable interest in the filed of plasma based acceleration for accelerating electrons to the high energies ($\sim GeV$). The SMLWFA scheme uses a single short ($\sim 1ps$) ultrahigh intensity ($\sim 10^{18}W/cm^2$) laser pulse, as in the standard LWFA, but operates at higher densities than the standard LWFA

such that the laser pulse length becomes long compared to the plasma wavelength and the laser power is somewhat larger than the critical power for relativistic guiding. In this high-density regime, the laser pulse undergoes a self-modulation instability which causes the pulse to become axially modulated at the plasma period. Hence a large amplitude wake wave can be resonantly excited associated with the modulated pulse structure. The self-modulation instability resembles a highly 2-D version of a forward Raman instability [40, 41]. Forward Raman scattering occurs simultaneously, adding to the modulation, and in the 1-D limit, pulse modulation can occur via forward Raman scattering alone.

However, in terms of theoretical work, the nonlinear theory of the LWFA in one dimension was developed by Sprangle et al. [23], Ting et al. [46] and Berezhiani and Murusidze [35]. A fully two-dimensional nonlinear theory of the LWFA, including the self-consistent evolution of the laser pulse, was analyzed by Sprangle et al. [47]. In LWFA, the excitation of blow-out has also been well examined both theoretically [48] and numerically [49, 50] for self-generating high quality electron beam of high energies. In terms of experimental studies, the success of LWFA scheme was demonstrated by several authors by accelerating electrons to higher energies [22, 51–62]. There are now more than 20 active laboratories performing laser wakefield acceleration experiments. A typical experimental set-up of LWFA is shown in Fig. (1.2).

Plasma Wakefield Acceleration (PWFA)

Another scheme of wakefield accelerations is known as Plasma Wakefield Acceleration (PWFA) in which, instead of laser pulses, the energetic particle beam is used

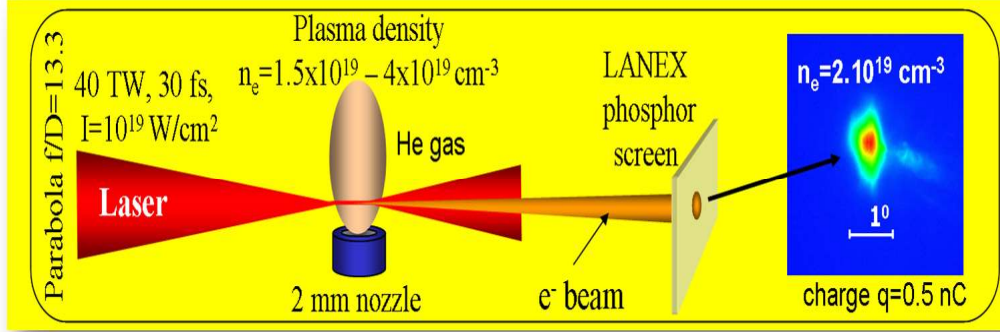


Figure 1.2: A schematic diagram of a typical experimental set-up for LWFA which has been designed at the Center for ultra-fast Optical Science (CUOS), University of Michigan.

to drive the wake wave inside the plasma. During the last two decades of research, the Plasma Wakefield Acceleration (PWFA) has achieved many significant milestones including the demonstration of ultra-high gradient acceleration of electrons over meter-scale plasma, efficient acceleration of a narrow energy spread electron bunch at high gradients, positron acceleration using wakes etc. PWFA uses an ultra-relativistic beam of charge particles (electrons or protons) terminated in a time shorter than the plasma period, ω_{pe}^{-1} for driving an extremely large electric field as a form of wake inside a plasma [13, 16, 17, 27, 29, 30, 32, 33, 63, 64]. The basic mechanism of PWFA was first proposed by Chen, Huff, and Dawson [26] as a means of coupling the relativistic electron beam to the phase velocity of the plasma wave. When an ultra-relativistic, short electron beam is injected into a plasma, the space charge force or Coulomb force displaces the nearby plasma electrons. Being heavy species, ions do not respond in the time scale of electron. They only provide a neutralizing background. For the beam driven plasma wake field or so-called plasma wakefield accelerator (PWFA), the electromagnetic force from

the beam charge and current plays a similar role as the ponderomotive force does in laser wakefield acceleration (LWFA) scheme. However, as the beam propagates further inside the plasma, the expelled plasma electrons try come back to their equilibrium positions. But, due to their inertia, they finally overshoot and thereby oscillate at a frequency close to the plasma frequency [27,30,31,64]. Hence, a wake wave will be established just behind the beam. It has to be remembered that the the phase velocity of the wake wave is equal to the velocity of the beam, and is independent of the plasma density. Therefore, if another bunch of electrons having velocity close the phase velocity of the wake rides the wave, it can be accelerated to high energies. A schematic picture of PWFA is shown in Fig. (1.3).

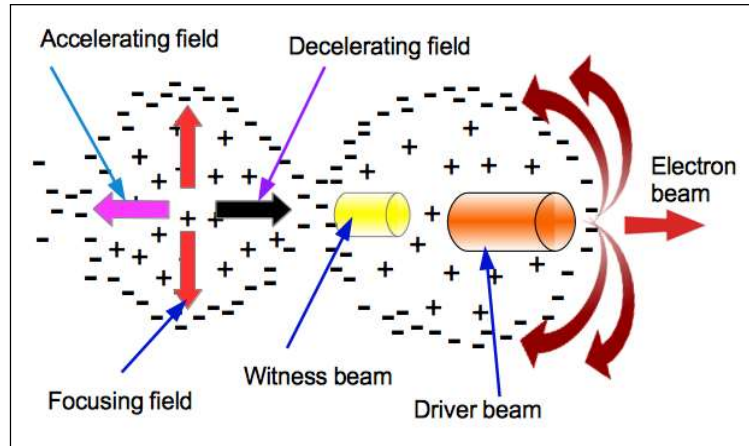


Figure 1.3: A schematic picture of electron beam driven PWFA.

In LWFA, the excited wake the wave can accelerate the charge particles almost from the rest. Therefore, this scheme offers a way to design self-contained tabletop accelerators which is much suited for moderate-energy applications such as medicine and materials sciences [65]. On the other hand, in plasma wakefield acceleration, one bunch of ultra-relativistic particles drive the plasma wave which

is then used to accelerate another late coming bunch placed at an appropriate location in the wake. However, both the bunches must start out at ultra-relativistic energies traveling so close to the speed of light that their separation does not change even as the first bunch loses energy and the second gains energy. The scheme is therefore not suitable for free-standing accelerators. It is most likened to an electrical transformer in which a large bunch of moderate energy can be converted into a smaller bunch at much higher energies. Hence this is most suitable to boost the energy of the existing linacs. The capability of PWFA would be more useful for particle-physics experiments, in which high collision energies are critical in the search for new particles and forces. It also has the potential applications in reducing the size and cost of x-ray free-electron lasers (XFEL).

The success of plasma wakefield acceleration was demonstrated by several groups by accelerating electrons to high energies [29, 63, 66–71]. In terms of experiments, there are far fewer PWFA experiments than LWFA experiments being performed worldwide. This is because there are far fewer facilities that can provide the high-current, highly relativistic charged particle beams that are needed for such experiments. However, there are now several laboratories world wide dedicated for demonstrating the success of PWFA scheme. A schematic diagram of a typical experimental design of PWFA is shown in Fig. (1.4).

Recently, a collaboration involving UCLA, USC and SLAC has achieved many milestones towards the demonstration of the key physics of a plasma afterburner [68–70]. The most striking result in PWFA was published by Blumenfeld et al. [72] in 2007, where an energy gain of more than 42GeV is achieved in a plasma wakefield accelerator of 85cm . Most of the beam electrons lose energy to the plasma wave, but some electrons in the back of the same beam pulse are accelerated with a field

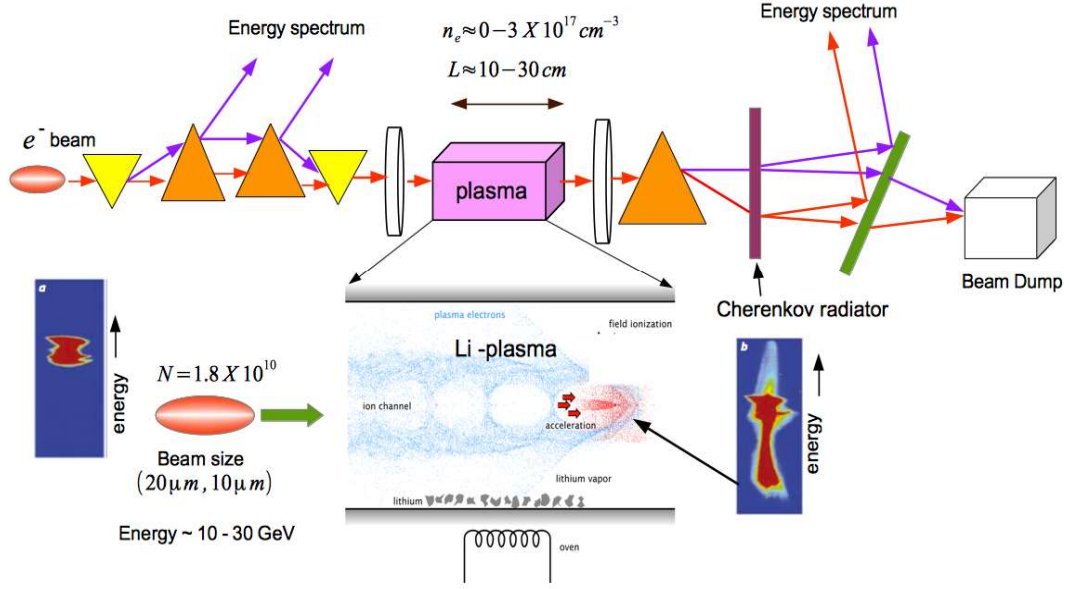


Figure 1.4: A generic experimental set up for the PWFA experiment. Experimental parameters mentioned in this picture have been taken from SLAC National Accelerator Laboratory, USA.

of $\sim 52 \text{ GV m}^{-1}$. This effectively doubles their energy, producing the energy gain of the 3-km-long SLAC accelerator in less than a meter for a small fraction of the electrons in the injected bunch. In 2014, Litos et al. [73] designed their experiment using a discrete trailing bunch surfing in an accelerating gradient of 4.4 GV/m . The idea of using discrete trailing bunch in the wake is to make the electric field profile flat inside the witness beam so that the witness electrons can be accelerated uniformly. Using a discrete trailing bunch, Litos et al. [73] minimized the energy spread of the accelerated beam to $\sim 2\%$. These exciting results are now pushing accelerator physicists to seriously consider the possible application of plasmas in high energy-physics.

Although plasma based acceleration schemes made amazing headlines in the

field of particle accelerators, there are several issues which have routinely been encountered for an efficient acceleration process. Particularly, in plasma wakefield accelerator (PWFA), the wake wave is excited by a high-current, relativistic particle beam whose current profile is tailored to have a slow-rise and a sudden termination. On the other hand, the driving beam must be terminated in a time shorter than the plasma period, ω_{pe}^{-1} , for an efficient acceleration process. Therefore a precision engineering is required either for profiling and maintaining the current profiles of the beam. Moreover, for a successful operation, among the several constraints of PWFA is that the driver must be capable of propagating a sufficiently long distance to avoid multiple acceleration stages. As all the stages needed to be sequentially synchronized, multi-staging would be impossible for an efficient acceleration from the practical point of view. In addition, another issue in the plasma wakefield acceleration is to keep the witness beam in a right spot for a long distance in such a high field. The accelerated beam undergoes many instabilities [74–77] in this high field and, hence, the process of acceleration fails. Therefore, a complete characterization of the electron beam driven wakefield excitation is needed to build a stable and efficient plasma based accelerator. This dissertation analyze through theory and simulation the excitation of relativistic electron beam driven wakefield in a cold plasma for several beam configurations over a wide range of beam parameters. In the following sections, we provide a brief review of earlier works in this area and scope of this dissertation.

Review of Earlier Works on PWFA

In this section, we provide a review of earlier investigations which are found to be relevant to the problems discussed in this thesis. The major topic of this disser-

tation is focused on the excitation of relativistic electron beam driven wakefield in a cold plasma. In past, the generation of wakefields using an ultra-relativistic electron beam propagating in a plasma has been extensively studied by several authors, both theoretically as well as numerically. Simultaneously, a large number of experimental effort has also been done in this direction demonstrating the viability of plasma based accelerators for high-energy physics applications.

Theoretically, the 1D excitation of wakefield has been well established both in the linear and non-linear regime for several driver configurations over a wide range of beam parameters [26,27,30,31,78–80]. First and foremost, the theoretical structure of the linear wakefields in 1-D for a series of relativistic bunch was given by Chen, Huff, and Dawson [26]. Later, many theoretical works have been reported in this way for several driver configurations in the linear regime in 1D [27,30,78,79]. In 1987, Rosenzweig et al. [31] presented an analytical solution of relativistic electron beam driven wakefield in a cold plasma in the non-linear regime for a beam having density smaller or equal to half the equilibrium background plasma density. Their analytical analysis was based on Akhiezer-Polovin [81] treatment. Later, many theoretical and numerical works have been reported in the non-linear regime for several driver configurations. However, these analytical works have been made in the quasi-static framework where the slow-evolution of physical quantities are ignored. In these analytical works, the self-consistent evolution of the beam has been ignored considering the velocity of the beam equal to the speed of light. The beam behaves as a rigid piston and propagates with a constant velocity. These theoretical treatments are also limited by a number of approximations on driver parameters and configurations. Therefore, a full nonlinear theory of PWFA tak-

ing account of the self-consistent evolution of the driver beam for arbitrary beam parameters is still largely an unexplored area of research even in 1-D. In this dissertation, we have studied through theory and simulation the excitation of relativistic electron beam driven wakefield in a cold plasma over a wide range of beam parameters. With the help of numerical techniques, we have also studied the excitation where the self-consistent evolution of the beam is included. We have expressed the exact analytical form of the wakefield for an arbitrary beam density. In addition, we have also analyzed many important aspects of electron beam driven wakefield including the complete characterization of the breaking of longitudinal wake wave which was not discussed in the earlier theoretical studies.

However, in all these earlier works, the excitation of relativistic electron beam driven wakefield has been studied where the ion motion was completely neglected. In 1998, Khachatryan et al. [82] reported in the study of strong plasma waves ($\gamma \gg 1$) that plasma ions (even heavy ions) can make an essential contribution to the process of charge separation under the influence of such a strong field; where $\gamma = (1 - v^2/c^2)^{-1/2}$ is the Lorentz factor associated with the velocity (v) of the electrons. Later in 2005, Rosenzweig et. al. [83] reported that the motion of ions plays an important role in PWFA which produces large perturbations in ion density, giving rise to transverse fields that in turn disrupt the motion of the beam. Recently, Vieira et al. [84] showed that ions can essentially affect the future proton driven plasma wakefield acceleration. Their motion can limit the energy transfer from the driver to the accelerated particles by reducing the accelerating gradient which is a result of early saturation in the self-modulation instability (SMI). The ion motion also affects the generation of electron jets in astrophysical scenarios. In

the polar region of the pulsars, it is considered to be filled with electron-positron (equal mass species) plasma and energetic charged particles are being generated from the plasma waves. Therefore, including the effect of ion motion, the study of PWFA or the excitation of strong plasma waves is important. Including the effect of ion motion in PWFA concept, Rosenzweig et al. [80] reported a semi-analytical study in 1-D and provided the form of transformer ratio only for the beam density equal to half the plasma density and mass ratio (ratio of electron to ion mass) much less than unity. In this thesis, we have examined the effect of ion motion on the relativistic electron beam driven wakefield in a cold plasma, both theoretically and numerically in 1D, over a wide range of beam parameters and mass ratios. The study also includes the understanding and analyzing of the breaking of a relativistic electron-ion wake wave (i.e. Khachatryan mode [82]) in a cold plasma. A new limit of wave breaking for a relativistic Khachatryan mode [82] has been found, which lies much below the conventional theoretical limit given in the ref. [82]. This is due to the possibility of phase mixing process [85–88] which was ignored in ref. [82].

For practical reasons, in experiments for both PWFA and LWFA, the drivers are tightly focused to achieve a large enough intensity for exciting large plasma wake. The narrow spot sizes of the drivers induce forces in the transverse dimensions that are comparable to those in the longitudinal direction. This leads to significant multidimensional effects that are absent in one-dimensional theories. In such configurations, the beam expels all the plasma electrons nearby due to high space charge force and creates a pure ion channel just behind which propagates with a velocity equal to the velocity of the beam. When wakes are excited in this

manner it is called the blowout regime. For sufficiently intense beams, the structure of the blow-out can have a spherical in shape which is known as ‘bubble’ or ‘cavern’ [25, 49, 89, 90]. This regime was first identified by Sun et al. [91] in 1987 where they have derived the equilibrium profiles of both a laser and plasma density for a self-guided laser pulse sufficiently short that the ions do not move but sufficiently long that no wake is excited. As this analysis was for relatively long pulses where wakefields are not excited, its implication for plasma-based acceleration was not appreciated immediately. A few years later in 1991, Rosenzweig et al. [90] found an interesting regime for electron beam driven plasma wakefield through 2D fluid and PIC simulations. In this regime, a short (about plasma wavelength) and narrow (spot size smaller than plasma skin depth) electron bunch with sufficient charge can expel (blows out) the plasma electrons away from its path to form a pure ion region around and behind it. This phenomenon is very similar to what Sun et al. found for a laser. Most importantly, Rosenzweig et al. pointed out the major advantages for working in this regime. They are, i) the accelerating gradient is nearly constant throughout the structure which accelerates the witness bunch uniformly, ii) the focusing fields are linear inside the bubble which produces the energetic beam with low emittance, iii) the beam can propagate many betatron wavelengths without any significant diffraction as the energy loss is minimum for an electron beam propagating inside an ion channel. Thereafter, similar wakes have been excited using a short laser driver. It was shown that LWFA in this regime had the advantages of a uniform accelerating field and a linear focusing force [92]. Later on in 2002, with the help of three-dimensional (3D) particle-in-cell (PIC) simulations, Pukhov et al. [49] reported the excitation of ‘bubble’ like wake structure for ultrarelativistic, ultra-intense laser pulses having a length shorter than λ_p .

For such cases, the excited wake wave eventually breaks just after the formation of first buckets. Afterwards, due to the breaking of wake wave, the plasma electrons near the edge of the bubble get self-trapped and accelerated in the wake [93].

In 2-D, the analytical structures of the excitation of relativistic electron beam driven wakefield are mostly studied in the linear regime (beam having the density much less than the background plasma density) for special beam profiles [28,94,95]. In the non-linear regime, there is no exact analytical expression of 2-D wakefields. There exist an analytical model given by Lu et al [96] alone to predict the form of 2D wakefields for an arbitrarily shaped beam profile. They assumed that all electrons within a blowout radius are completely expelled. These radially expelled electrons form a narrow sheath just beyond the blowout radius which is surrounded by a region which response weakly. This assumption is reasonable when the spot size of the electron beam and laser are substantially less than the blowout radius. They modeled the profile of surrounding electron sheath by a step function (see Fig. (1) in ref. [96]). They also considered the thickness of the sheath is constant throughout the blowout. By using this theory one can predict the wakefield amplitudes and blowout radius in terms of the electron beam or laser beam parameters, as well as predict the nonlinear modifications to the wakes wavelength and waveform.

However, all these linear and non-linear analytical works have been derived from the quasi-static framework where the evolution of driver in a self-consistent manner has been ignored. Moreover, for sufficiently intense beams, the model of Lu et al. [96] also fails to predict the exact structure of blowout and the strength of the electric field near the edge of the blowout where the self-injection takes place.

Therefore, relaxing all these assumptions included in the theory, extensive numerical simulations have been performed to provide a reasonable empirical guidance in multi-dimensional, non-linear PWFA regime. However, most of these simulations have been carried out using particle-in-cell (PIC) simulation techniques (e.g. OSIRIS, QUICKPIC, EPOCH, XOOPIC and many more) [64, 72, 73, 84, 96–99]. These PIC simulations which compute the motion of billions of charge particles in the electromagnetic field for a long time at a microscopic level are computationally heavy and time-consuming. Therefore we require powerful computation facilities for the simulation purpose. Therefore we seek the possibility of fluid simulation (macroscopic) as a simplification to PIC simulation for analyzing and providing a reasonable empirical guidance in PWFA concept. We have developed and employed a fully explicit, relativistic, electromagnetic, 2-D fluid code to study the relativistic electron beam driven wakefield in cold plasma over a wide range of beam parameters for several beam configurations. We have studied the structure of wakefield ranging from linear to non-linear (blow-out) regime. A characteristic study of 2-D phase mixing of wake wave is also presented.

Plan of the Thesis

The present thesis is devoted to an extensive theoretical and numerical study of relativistic electron beam driven wakefield with the help of a fluid depiction. The beam and the background electron system are treated as two different fluid systems which are coupled through the Maxwell's equations. The numerical study has been carried for such a system using fluid simulation techniques (fluid code) both in 1-D and 2-D. Presently, the simulations in this area have been carried out using extensive particle-in-cell (PIC) simulations (e.g. OSIRIS, QUICKPIC, EPOCH,

XOOPIC and many more) [64, 72, 73, 84, 96–99]. These PIC simulations compute the trajectories of billions of particles at the most fundamental level (microscopic). The evolution of the position and momentum components of billions of particles in a self consistent electromagnetic field requires powerful computational facilities. On the other hand, the fluid approach is a macroscopic description where the individual particle is not evolved. It involves the average response of fluid elements which are essentially the moments of particle distribution functions. Ideally, fully kinetic descriptions are the more appropriate description for describing the physical phenomena in a system. But, due to their complexity, the use of such an approach is impractical. Furthermore, in comparison to kinetic simulations, the fluid approximation is much simpler to implement and solve. It can be used to describe complex phenomena in multi-dimensional geometry with realistic boundary conditions. The main drawback of fluid descriptions, as already stated, is their inability of describing the phenomena where information at particle level are desirable. Phenomena involving non-local transport or heating are some examples specially when the fluid depiction has been closed at the momentum transport level. In this thesis, we seek the possibility of fluid simulations as a simplified alternative for sophisticated PIC simulations. It is shown that many information with regards to the wakefield excitation can be recovered rather accurately from this simplified treatment. Furthermore, we have also shown by injecting test particles in the fluid simulations, the energy gained by them when they are placed at appropriate location of the wakefield structure, this being one of the prime objective of the particle acceleration process. We provide a brief summary of the salient observations carried out in each of the chapters.

In the second chapter (**chapter-2**), we have studied the excitation of relativistic electron beam driven wakefield using 1-D fluid simulation techniques for both rigid and non-rigid driver over a wide range of beam parameters (density, length, and velocity). Rigid beam defines such a bunch which can penetrate an infinite length in a plasma without any significant deformation, whereas a non-rigid beam loses its identity after propagating some distance. The criteria required for a beam to behave rigidly has also been identified and checked in this thesis. Further, an earlier 1-D nonlinear analytical work of Rosenzweig et al. [31] which was reported only for a rigid, homogeneous beam having density less than or equal to half of the plasma density, is extended for an arbitrary value of beam density. The numerical and analytical results have been compared for several plasma periods. Interesting features which arise when the self-consistent evolution of the beam is considered has also been reported. A summary of these results has been published in *Physics of Plasmas* 22, 073109 (2015), *Title: Fluid simulation of relativistic electron beam driven wakefield in a cold plasma*, *Authors: Ratan Kumar Bera, Sudip Sengupta and Amita Das*.

In the third chapter in the thesis (**chapter-3**), with the help of fluid simulation technique, we analyze the space-time evolution of relativistic electron beam driven wakefield in a cold plasma. We have found that the excited wakefield obtained from simulation deviates from the analytical structure after several plasma periods. The plasma density profile gradually modifies with time and exhibits sharp spikes after several plasma periods in the simulation. The corresponding electric field acquires sawtooth-like structure after several plasma periods. This is a clear signature of wake wave breaking [85–88,100]. Before wave breaking, it is observed that the wake

wave is identical to the corresponding Akhiezer-Polovin mode [81]. The breaking of the wake wave has been understood in terms of phase mixing of Akhiezer-Polovin mode [88]. A summary of these results has been published in *Physics of Plasmas* 23, 083113 (2016), Title: *Relativistic electron beam driven longitudinal wake-wave breaking in a cold plasma*, Authors: Ratan Kumar Bera, Arghya Mukherjee, Sudip Sengupta and Amita Das.

In the fourth chapter of this dissertation (**chapter-4**), the excitation of relativistic electron beam driven wakefield in a cold plasma has been investigated where the effect of ion motion is included. We have examined the structure of wakefields for different beam parameters and mass ratios (electron's to ion's mass) using 1-D fluid simulation techniques. It is observed that the transformer ratio that measures the efficiency of the acceleration saturates to unity for an over-dense beam in both the electron-positron and hydrogen plasmas. Therefore, there will be no gain for an over-dense beam in 1-D. It is also seen that the excited wake wave breaks exhibiting sharp density spikes in the simulation at later times. For the sake of understanding the wake wave breaking, it is also observed that the excited wake wave is equivalent to Khachatryan mode [82], before it breaks. We have, however, shown that the wave breaking limit lies much below the analytical limit derived by Khachatryan et al. The breaking of a wake wave or an equivalent Khachatryan mode has been understood in terms of phase mixing process [85–88]. A summary of these results are ready for submission Title: *Accessibility and stability of an electron-ion mode in plasma wakefield acceleration*, Authors: Ratan Kumar Bera, Sudip Sengupta and Amita Das.

In the fifth chapter (**chapter-5**), a two-dimensional fluid simulation has been employed to study the multidimensional behavior of the relativistic electron beam driven wakefield in a cold plasma. It is observed that for both under-dense as well as over-dense beams having large transverse extent compared to its longitudinal length, the axial profiles of the excited wakefield obtained from our simulation matches with the 1-D results of presented in Chapter 2 and reported in our publication Ratan et al. [101]. In the other limit i.e. when the transverse dimension of the beam is smaller or equal to its longitudinal extension, the simulation results deviate considerably from the 1-D results. A 2-D analytical study of the linear wake structure is also presented and compared with the simulations for the condition of small amplitude excitations. Our 2-D fluid simulation exhibits the blow-out structure for an intense beam that have been reported in PIC simulations and modelled by the prescription of Lu et al. [25,96], before phase mixing occurs. A method of estimating phase mixing time in the fluid simulations is also presented. Further, injecting the test particles in the simulation, we have studied the energy acquired by the test electrons. A maximum energy gain of $\sim 2.6\text{GeV}$ by the electrons from the back of the driver beam of energy $\sim 28.5\text{GeV}$ in a 10 cm long plasma is shown to be achieved. This is in conformity with the experimental results of ref. [69]. This shows that the fluid simulations which are much simpler and faster compared to Particle-in-Cell simulation techniques can in fact depict the wake structure reasonably well and also provide good estimate for particle acceleration. We have also experimented with the location of the injection of test particles and show that maximum energy gain can get doubled $\sim 5.2\text{GeV}$, when the bunch of test particles are placed near the axial edge of the first blowout structure. A summary of these results are available as a per-print *arXiv: 1803.00300, Title: 2-D fluid simulation*

*of a rigid relativistic electron beam driven wakefield in a cold plasma, Authors:
Ratan Kumar Bera, Amita Das, and Sudip Sengupta.*

Finally, in the last chapter (**chapter-6**), we present the conclusions of the work reported in the present thesis. We then provide a glimpse of the possible future research problems which can be carried out as direct extension of the results reported in this thesis.

2

Excitation of relativistic electron beam driven wakefield in a cold plasma in 1-D

The objective of this chapter ^{} is to investigate the structure of 1-D wakefields excited by injecting a relativistic electron beam in a cold plasma. By proposing a two-fluid description of plasma wave excitation, the structure of wakefield has been studied using fluid simulation techniques over a wide range of beam parameters. An analytical work in a quasi-static framework, for an arbitrary beam density, is also presented.*

Introduction

In plasma wakefield acceleration (PWFA), the wakefield is created using an ultra-relativistic electron beam propagating inside a plasma medium. The injected electron beam behaves like a trigger for the residual electron oscillation leading to a

^{*} Ratan Kumar Bera, Sudip Sengupta, and Amita Das, *Fluid simulation of relativistic electron beam driven wakefield in a cold plasma*, *Physics of Plasmas* 22, 073109 (2015).

plasma wave which has a phase velocity equal to the beam velocity. Similar to two-stream instability, here the driver beam loses its energy to the background plasma electrons to produce wake (behind the beam) wave. Hence if a late coming electron beam rides on this wake in a proper phase, it can be accelerated to higher energies. Therefore, for an efficient and useful acceleration process, a complete characterization of the excited wakefield over a wide range of beam parameters is required. A substantial amount of theoretical investigations in the linear regime of PWFA has been made by several authors. One-dimensional theory of PWFA in the non-linear regime has also been reported by several authors viz. Rosenzweig et al. [31], Ruth et al. [78] and Amatuni et al. [79] based on the Akhiezer-Polovin [81] treatment. Such theoretical treatments are limited by a number of approximations. A full nonlinear theory of PWFA taking account of the self-consistent evolution of the driver beam is still largely an unexplored area of research.

In this chapter, we present the excitation of wakefield driven by a relativistic electron beam in a cold plasma, proposing a two-fluid description of plasma wave excitation in 1-D. We have studied the excitation over a wide range of beam parameters, using fluid simulation techniques. In this study, the generation of wakefield has been investigated considering a homogeneous beam (rectangular profile). In the first set of simulations, we have examined the formation of wakefield considering a relativistic, pulsed electron beam where the self-consistent evolution of the beam is excluded. The simulation results have been compared with the analytical work of Rosenzweig et al. [31] and verified in the limit of beam density lower than or equal to half the plasma density. The analytical work given by Rosenzweig et al [31] has been extended to beam density larger than half of plasma density, and

the results have been compared with the simulation results. The efficiency of the excitation is measured by Transformer ratio (R), which is defined by the ratio of the maximum accelerating field (E_+) at the wake to the maximum decelerating field (E_-) inside the driver bunch. It is seen that transformer ratio varies with the beam pulse length (l_b) and density of beam (n_b) and becomes maximum when the beam density is exactly equal to half of the plasma density. Interestingly at late times of simulation, we have observed that the wake-field structure in all cases exhibits spiky features which cannot be described by Rosenzweig's theory. In the second set of simulations, we have included the beam evolution in the self-consistent electric field. In this particular case, we observe many interesting features. Depending on the beam pulse length compared to plasma wavelength, the electron beam may either split into many parts or may get compressed. Below we present the governing equations for the electron beam driven wakefield excitations in a cold plasma.

Governing Equations

The basic equations governing the space-time evolution of a relativistically intense wakefield excited by an ultra-relativistic electron beam propagating through a cold homogeneous demagnetized plasma, are the relativistic fluid-Maxwell equations. These are the continuity equations and the relativistic momentum equations for both plasma and beam electrons, and Poisson's equation for the wake electric field. Since ions do not respond in these time scales, equations describing ion dynamics are hence neglected. Ions are assumed to provide a stationary positively charged neutralizing background. Assuming the plasma parameters do not vary in the transverse direction (transverse to the beam propagation direction), the

governing equations in 1-D, are

$$\frac{\partial n}{\partial t} + \frac{\partial(nv)}{\partial z} = 0 \quad (2.1)$$

$$\frac{\partial p}{\partial t} + v \frac{\partial p}{\partial z} = -eE \quad (2.2)$$

$$\frac{\partial n_b}{\partial t} + \frac{\partial(n_b v_b)}{\partial z} = 0 \quad (2.3)$$

$$\frac{\partial p_b}{\partial t} + v_b \frac{\partial p_b}{\partial z} = -eE \quad (2.4)$$

$$\frac{\partial E}{\partial z} = 4\pi e(n_0 - n - n_b) \quad (2.5)$$

where $p = m_e \gamma v$ and $p_b = m_e \gamma_b v_b$ are the z -component of momentum of plasma electrons and beam electrons of mass m_e having z -component of velocity v and v_b respectively. $\gamma = \left(1 - \frac{v^2}{c^2}\right)^{-1/2}$ and $\gamma_b = \left(1 - \frac{v_b^2}{c^2}\right)^{-1/2}$ are the relativistic factors for plasma electrons and beam electrons having density n and n_b respectively. E and n_0 represents self-consistent electric field and equilibrium plasma density respectively. Equations (2.1) - (2.5) are the key equations required to investigate relativistic electron beam driven wakefield excitation in a cold unmagnetized plasma. Although the equations look simple, it is difficult to obtain exact analytical expression of the excited wakefield by directly solving them. In the rigid beam limit (*i.e.* in the limit $v_b \rightarrow 1$, equations (2.3) and (2.4) are neglected), the stationary wave frame solution of equations (2.1), (2.2) & (2.5) has been given by Rosenzweig et al. [?]. Their solution is valid in the limit of beam density smaller

than or equal to half the plasma density ($\alpha = n_b/n_0 \leq 1/2$). In his paper, we have extended the Rosenzweig solution to arbitrary ratios of beam to plasma density (*i.e.* arbitrary values of α). We have further simulated equations (1)-(5) (*i.e.* including beam evolution) using a 1-D fluid simulation techniques (discussed later in detail).

1-D Fluid Simulation of electron beam driven wake-field excitation

In this section we present the methodology of fluid simulation techniques for the excitation of wakefield. Physical quantities can be expressed in dimensionless units by making the following replacements for the density, velocity and electric field:

$$t \rightarrow \omega_{pe} t, z \rightarrow \frac{\omega_{pe} z}{c}, E \rightarrow \frac{eE}{m_e c \omega_{pe}}, v \rightarrow \frac{v}{c}, p \rightarrow \frac{p}{m_e c}, n \rightarrow \frac{n}{n_0}, n_b \rightarrow \frac{n_b}{n_0}.$$

Thus the above equations (2.1) - (2.5) can be written in the normalized units as,

$$\frac{\partial n}{\partial t} + \frac{\partial(nv)}{\partial z} = 0 \quad (2.6)$$

$$\frac{\partial p}{\partial t} + v \frac{\partial p}{\partial z} = -E \quad (2.7)$$

$$\frac{\partial n_b}{\partial t} + \frac{\partial(n_b v_b)}{\partial z} = 0 \quad (2.8)$$

$$\frac{\partial p_b}{\partial t} + v_b \frac{\partial p_b}{\partial z} = -E \quad (2.9)$$

$$\frac{\partial E}{\partial z} = (1 - n - n_b) \quad (2.10)$$

The general solution of the above equations (2.6-2.10), which represents the form of wake in terms of density, velocity, and the electric field has been obtained numerically in this chapter. A one-dimensional fluid code based on flux-corrected transport scheme given by Boris et al. [102] has been developed for solving these equations. Flux-Corrected Transport scheme which is based on Lax Wendroff method [103] is an accurate and easy to use algorithm for solving a nonlinear, time-dependent generalized continuity equations which occur in fluid dynamics, reactive, multiphase, elastic plastic flows, plasma dynamics, and magneto-hydrodynamics. Using this scheme, Boris et al. [102] developed a suite of subroutines known as LCPFCT (Laboratory of Computational Physics, Flux-Corrected Transport) which is a freely available code (<https://www.nrl.navy.mil/lcp/LCPFCT>) written in Fortran language. This is a standard package whose stability properties has already been established in a variety of contexts by many users [41,104]. LCPFCT solves the conservative form of equations or the generalized continuity equations of type $\frac{\partial \rho}{\partial t} + \vec{\nabla} \cdot \vec{\Gamma} = S$; where ρ and $\vec{\Gamma}$ represents the physical quantities and their flux respectively. S refers to the source or sink in the equation. Therefore the continuity or advection type of equations can be solved using this suite of subroutine. For solving the momentum equations, we have used CNVFCT suite of subroutine which solves the convective form of equations of type $\frac{\partial \rho}{\partial t} + (\vec{v} \cdot \vec{\nabla}) \cdot \rho = S$; where \vec{v} is the instantaneous flow velocity associated with the physical quantities ρ . The stability properties of this subroutine have also been checked reproducing several well-known results e.g. plasma oscillations, acoustic modes etc. Poisson equation

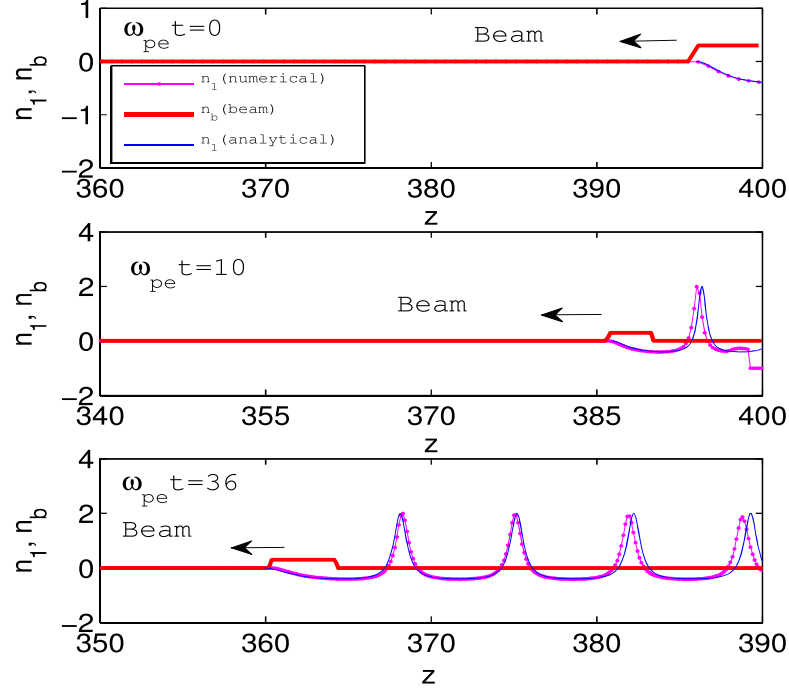


Figure 2.1: Plot of numerical and analytical normalized perturbed plasma density (n_1) profiles for $n_b = 0.3$, $v_b = 0.99$, $l_b = 4/2\pi$ at different times.

has been solved using tridiagonal matrix method. This is a simplified form of Gaussian elimination that can be used to solve tridiagonal systems of equations. Using these set of subroutines, we have developed our electrostatic fluid code for the excitation of wakefield in a cold plasma.

In our simulation, the beam is allowed to propagate inside the plasma starting from one end of the simulation window to the other end and the whole beam-plasma system is evolved according to equations (2.1-2.5) with non-periodic (open) boundary conditions. In open boundary conditions, the wave propagates to the boundary and passes through without being reflected or absorbed at the boundary. The excited wave retains its shape accordingly with time. For the initialization of the

simulation, the self-consistent profiles for density, electric field, and fluid velocity have been taken from the analytical work of Rosenzweig et al. [31]. We have also simulated cases where the Rosenzweig's solution is not initialized (discussed later). It is to be noted here, that the structure of the excited wakefield is independent of the initial profiles and always converges to the Rosenzweig's solution. In the simulations, the spatial resolution Δz has been chosen in such a way that

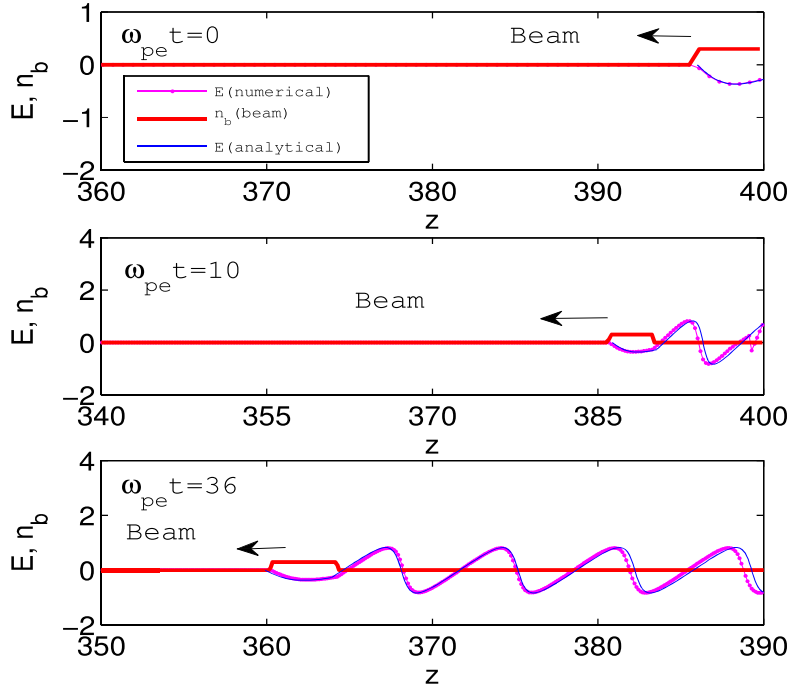


Figure 2.2: Plot of numerical and analytical normalized electric field (E) profile for $n_b = 0.3$, $v_b = 0.99$, $l_b = 4/2\pi$ at different times.

the plasma wave-length ($\frac{2\pi c}{\omega_{pe}}$) is adequately resolved. The temporal resolution i.e. time step (Δt) is then calculated from Courant-Friedrichs-Lewy (CFL) condition $\Delta t = C_n \Delta z / u_{max}$, where u_{max} and C_n , are the maximum fluid velocity and CFL number [102]. In our simulations, the maximum fluid velocity $u_{max} = 1$ as the maximum velocity of any fluid element can reach up to is the speed of light and

$C_n = 0.2$ for a good temporal resolution and stability. The numerical observations illustrating new physical effects have been also confirmed by changing the grid size (Δz), C_n and Δt to many orders. In time, we have followed the profiles of electric field, velocity, plasma electron density and beam electron density at the wake region as well as inside the beam. In the first set of the simulation, we have excluded the beam evolution (rigid beam case) whereas in the second set we have taken account of beam evolution. Both these cases are presented in the following sections.

Numerical Observations

In this section, we present our simulation results obtained for different driver parameters. The simulations which have been performed here illuminates many physical aspects of relativistic electron beam driven wakefield in a cold plasma. Below we have presented and discussed these results in detail.

Wake field excited by a rigid beam driver

In this set of simulations, the excitation of wakefield has been studied without considering the beam evolution in the self-consistent electrostatic field. We have ignored the equation (2.9) in the simulation. Therefore, the beam can propagate with a constant velocity v_b . This approximation is valid for a sufficiently energetic beam ($\gamma_b \gg 1$) which moves as a rigid piston without losing any significant amount of energy. In a realistic situation, this is not a typical case. The beam loses significant amount of energy to create the wakefield. Figures (2.3, 2.4) and figures (2.5, 2.6) present simulation (and analytical) results for $\alpha = 0.5$ and $\alpha = 0.7$

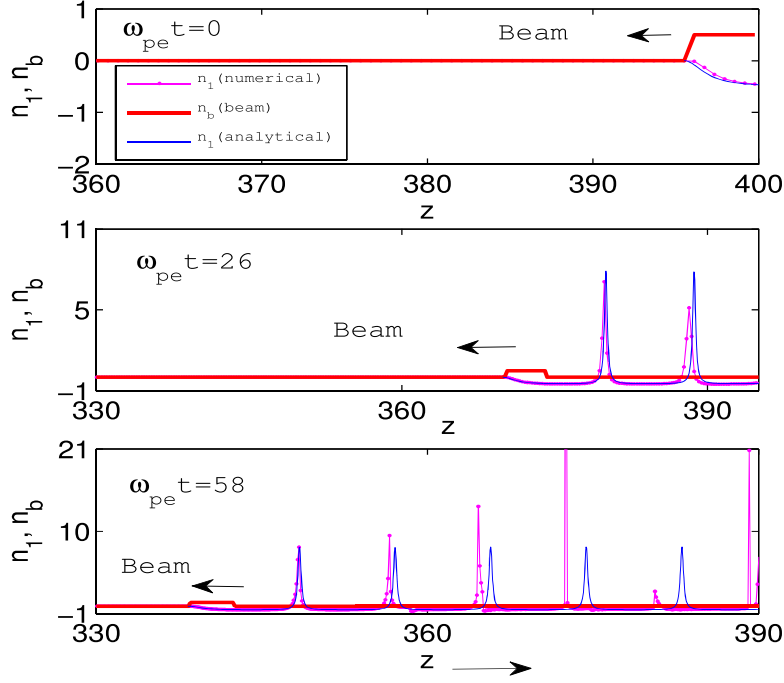


Figure 2.3: Plot of numerical and analytical normalized perturbed plasma density (n_1) profiles for $n_b = 0.5$, $v_b = 0.99$, $l_b = 4/2\pi$ at different times.

respectively for $l_b < \lambda_p$. Simulation runs are repeated for $l_b > \lambda_p$ (beam length greater than plasma wavelength) for same values of α and similar results are observed. In such cases, we have evolved equations (2.6,2.7, 2.8 and 2.10) for different values of n_b and v_b , and followed the electric field, velocity and electron density in time. Figures (2.1) and (2.2) respectively show the perturbed electron density and the electric field at different times for $n_b = 0.3$ and for $l_b < \lambda_p$ (beam length smaller than plasma wavelength). Numerical results are shown in magenta and the analytical results (derived later in this paper) are shown in blue. One of the interesting feature observed in all these simulations is that at late times the perturbed electron density show spiky features which are not discussed in analytical work of Rosenzweig et al. [?]. We comment on this in a later section. Figure (2.7)

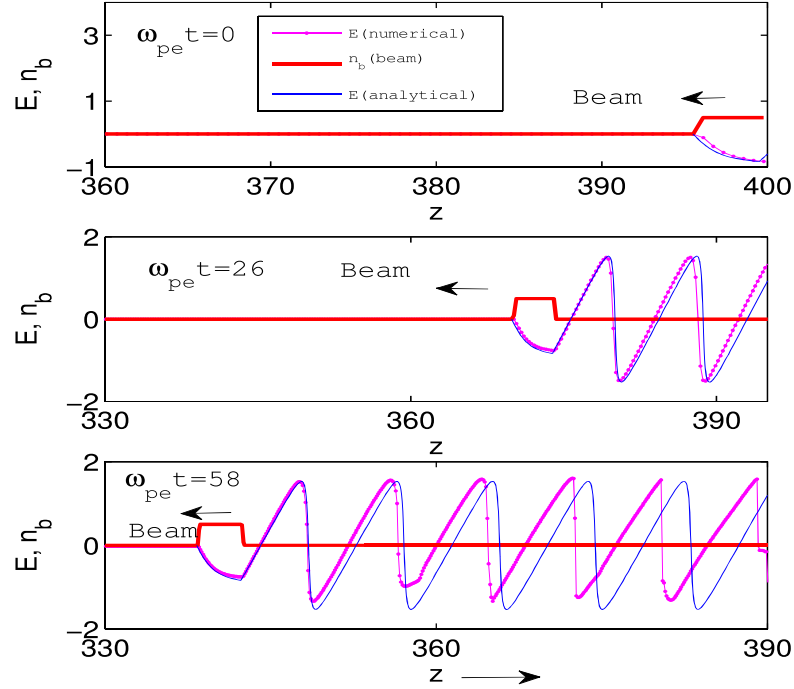


Figure 2.4: Plot of numerical and analytical normalized electric field (E) profiles for $n_b = 0.5$, $v_b = 0.99$, $l_b = 4/2\pi$ at different times.

shows the variation of transformer ratio R (ratio of peak accelerating field behind the beam to the peak decelerating field inside the beam) as a function of α for both $l_b > \lambda_p$ and $l_b < \lambda_p$. The points are obtained from simulation whereas the continuous line has been obtained analytically (as derived later).

Excitation of wake field including beam evolution

In this section, we present more generalized numerical observations where the self-consistent evolution of the beam is included. We have included full set of beam evolution equations (2.3, 2.4) in the simulation. These equations (2.1-2.5) are solved using 1D fluid simulation code with non-periodic boundary conditions. For different values of α , the evolution of wake field and beam profile is recorded in

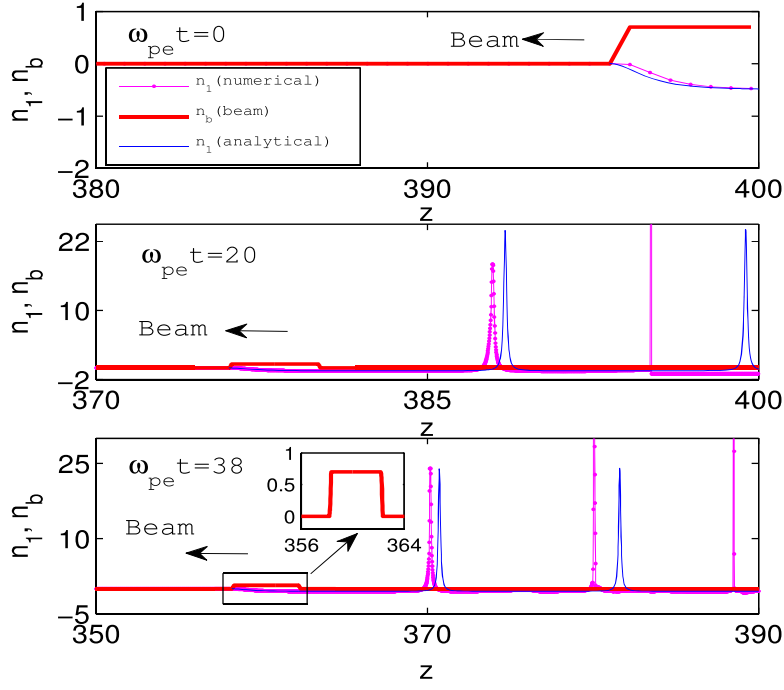


Figure 2.5: Plot of numerical and analytical normalized perturbed plasma density (n_1) profiles for $n_b = 0.7$, $v_b = 0.99$, $l_b = 4/2\pi$ at different times.

simulation. Figures (2.8) and (2.9) show the perturbed electron density and electric field profile respectively for $l_b < \lambda_p$ and $\alpha = 0.3$ with $\beta_b \rightarrow 1$. Except for a phase difference, the results are similar to what is observed in figures (2.1) and (2.2). For $\beta_b \rightarrow 1$, the beam evolution is negligible within the simulation time. For $\beta_b \leq 0.99$ significant modification of beam density profile is observed with time which in turn modifies the wake field structure. Modification of beam density profile not only depends on α (ratio of beam to plasma density) but also on the ratio of beam length (l_b) to plasma wave length (λ_p). Higher the beam density faster is the rate of modification of the beam density profile. Figures (2.10) and (2.11) show the perturbed electron density for $l_b < \lambda_p$ and $l_b > \lambda_p$ respectively for $\alpha = 0.3$.

We make here the following observations. For $l_b < \lambda_p$, the beam get compressed

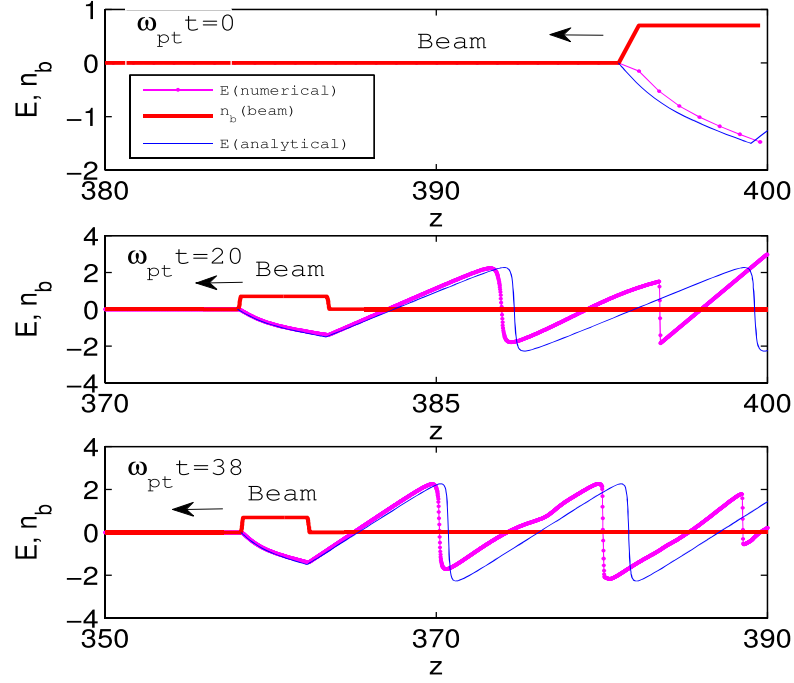


Figure 2.6: Plot of numerical and analytical normalized electric field (E) profiles for $n_b = 0.7$, $v_b = 0.99$, $l_b = 4/2\pi$ at different times.

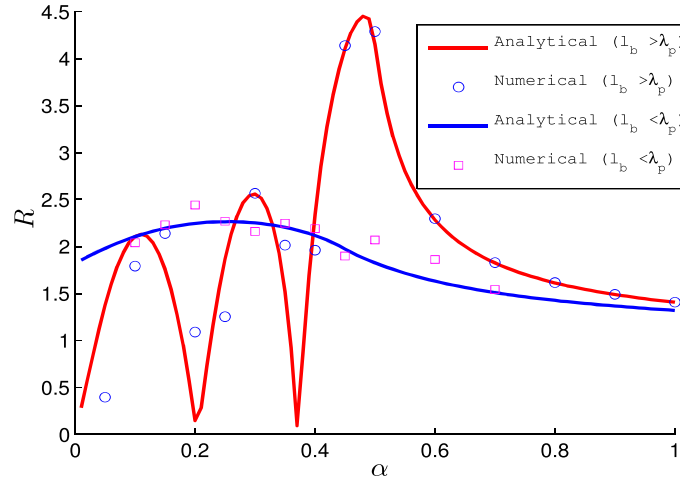


Figure 2.7: Plot of transformer ratio (R) as a function of beam density (α) for $l_b/\lambda_p = 4/2\pi$ and $l_b/\lambda_p = 3$.

and its velocity gradually decreases. For $l_b > \lambda_p$, the beam splits into different beam-lets with different amplitude, each moving with different speed $||$. In the next section, we give analytical description of the problem in the limit $\beta_b \rightarrow 1$.

Analytical Description of Beam driven wakefield

In this section, we present the analytical solution of beam driven wake wave in a cold plasma. The solution has been obtained in a stationary wave frame of the wakefield equations in the rigid beam limit (i.e. neglecting beam evolution equations) for arbitrary values of normalized beam density α . For the sake of completeness the solution in the regime $\alpha \leq \frac{1}{2}$, which had been obtained earlier by Rosenzweig et al. [31] is also presented here. All the fluid variables (n , p and E) are assumed to be functions of wave frame variable τ , which is defined as $\tau = (t - \frac{z}{\beta_{ph}})$, where z is the direction of propagation of the beam (and wake) and β_{ph} is the normalized phase velocity of the wake, which is equal to the normalized beam velocity β_b . The beam density ($=\alpha$) is assumed to be constant in the region $0 \leq \tau \leq \tau_f$, where $\tau_f = \frac{l_b}{\beta_{ph}}$; here l_b is the normalized length of the beam. As the beam moves into the region $\tau < 0$, it creates a wake in the region $\tau \geq 0$. The schematic diagram of the beam propagation in the quasistatic frame τ is shown in figure (2.12).

In this frame, the space and time derivatives of physical quantities can be replaced by,

$$\begin{aligned}\frac{\partial}{\partial z} &= -\beta_{ph}^{-1} \frac{d}{d\tau} \\ \frac{\partial}{\partial t} &= \frac{d}{d\tau}\end{aligned}$$

Using these above transformations, equation (2.1) can be written as,

$$\frac{d}{d\tau} \left(n \left(1 - \frac{\beta}{\beta_{ph}} \right) \right) = 0 \quad (2.11)$$

In terms of the variable τ , the above equation can be integrated to give,

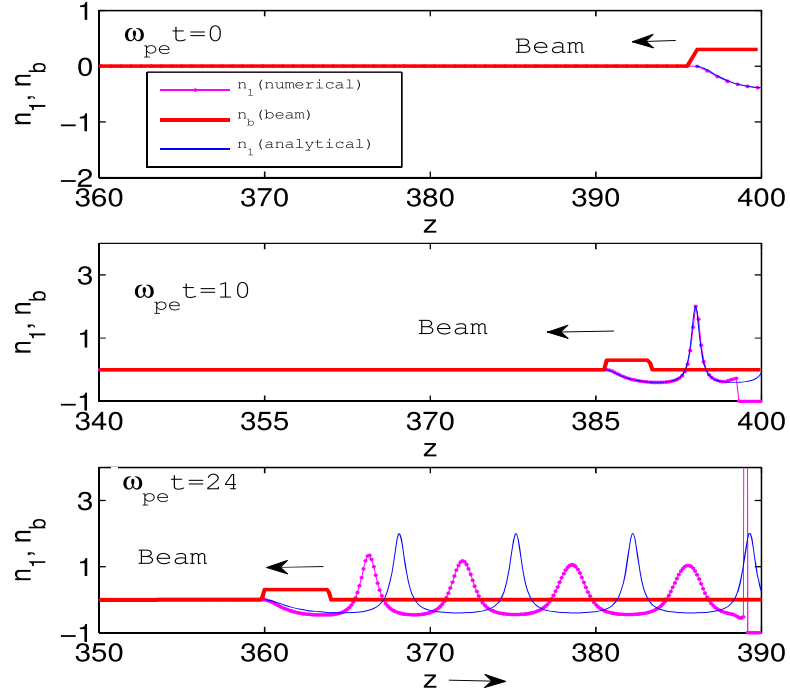


Figure 2.8: Numerical and analytical normalized perturbed density (n_1) profiles for the normalized beam density (n_b) = 0.3 at different times, including beam evolution for $l_b/\lambda_p = 4/2\pi$ with $v_b \rightarrow 1$.

$$n = \frac{\beta_{ph}}{\beta_{ph} - \beta} \quad (2.12)$$

In τ - frame, the momentum equation (2.2) and poisson equation (2.5) can be written as,

$$(\beta_{ph} - \beta) \frac{d(\gamma\beta)}{d\tau} = -E \quad (2.13)$$

$$\frac{dE}{d\tau} = -\beta_{ph}(1 - n - n_b) = \beta_{ph} \left(\frac{\beta}{\beta_{ph} - \beta} + n_b \right) \quad (2.14)$$

Differentiating both the side of the equation (2.13) w.r. t. τ , we have,

$$\frac{d}{d\tau}(\beta_{ph} - \beta) \frac{d(\gamma\beta)}{d\tau} = -\frac{dE}{d\tau} \quad (2.15)$$

Therefore, the above equation can be written as,

$$\beta_{ph} \frac{d^2(\gamma\beta)}{d\tau^2} - \frac{d}{d\tau}(\beta \frac{d(\gamma\beta)}{d\tau}) = -\frac{dE}{d\tau} \quad (2.16)$$

Now, we have the following expressions,

$$\frac{d\gamma}{d\tau} = \gamma^3 \beta \frac{d\beta}{d\tau}$$

$$\frac{d(\gamma\beta)}{d\tau} = \gamma^3 \frac{d\beta}{d\tau}$$

Using the above relations in equation (2.16), we have,

$$\beta_{ph} \frac{d^2(\gamma\beta)}{d\tau^2} - \frac{d^2\gamma}{d\tau^2} = -\frac{dE}{d\tau} \quad (2.17)$$

Substituting the form of $\frac{dE}{d\tau}$ in the above equation from equation (2.14), we have,

$$\frac{d^2}{d\tau^2} \left(\frac{1 - \beta\beta_{ph}}{\sqrt{1 - \beta^2}} \right) = \beta_{ph}^2 \left(\frac{\beta}{\beta_{ph} - \beta} + \alpha \right) \quad (2.18)$$

where $\beta = v$ and $\beta_{ph} = v_{ph}$. In the rigid beam limit, $\beta_{ph} = \beta_b \rightarrow 1$, where

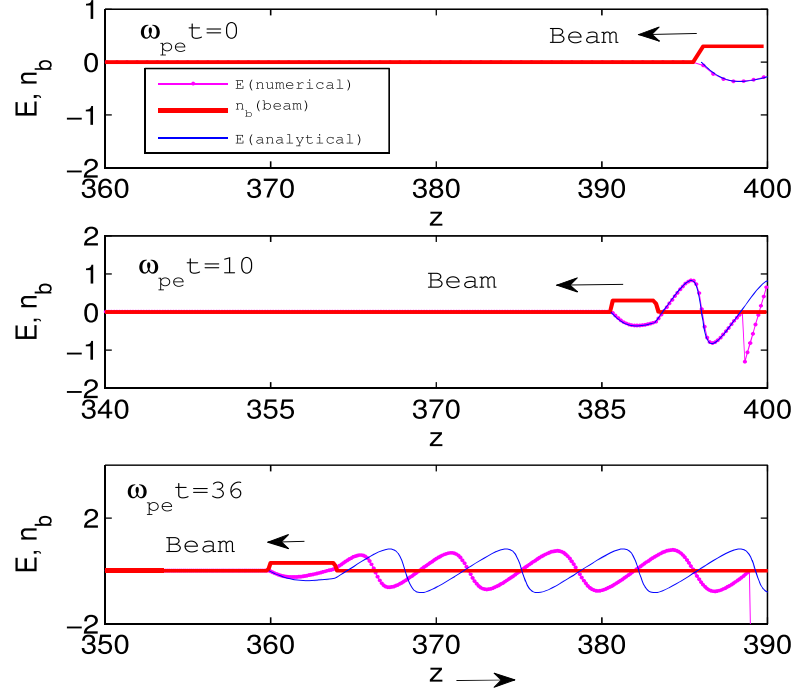


Figure 2.9: Numerical and analytical normalized electric field (E) profiles for the normalized beam density (n_b) = 0.3 at different times, including beam evolution for $l_b/\lambda_p = 4/2\pi$ with $v_b \rightarrow 1$.

$\beta_b = v_b$, v_b being the velocity of the beam. In this limit, defining a new variable $x(\tau) = \sqrt{\frac{1-\beta}{1+\beta}}$, equation (2.18) reduces to the following form

$$x'' = \frac{1}{2} \left(\frac{1}{x^2} - 1 + 2\alpha \right) \quad (2.19)$$

where ‘prime’ represents differentiation w.r.t variable τ . In terms of variable x , plasma electron density n and wake electric field E are respectively given by,

$$n = \frac{1}{2} \frac{1+x^2}{x^2} \quad (2.20)$$

$$\beta = \frac{1 - x^2}{1 + x^2} \quad (2.21)$$

$$E(x) = x'(\tau) \quad (2.22)$$

The electric field (equation (2.22)) is obtained by integrating the Poisson's equation and using the condition $x' = 0$ at $\tau = 0$. It is clear from above that the equation (2.19) has a finite discontinuity at the tail of the beam ($\tau = \tau_f$) and therefore has to be solved separately in two different regimes : inside ($\alpha \neq 0$) the beam and behind ($\alpha = 0$) the beam. In the following subsections (2.5.1 and 2.5.2), we respectively present the solution of equation (2.19) in these two separate regimes.

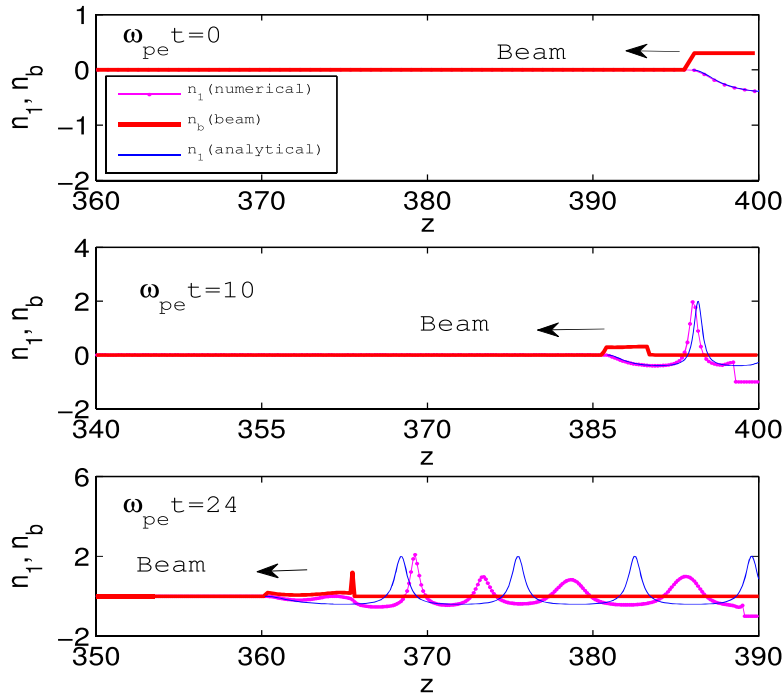


Figure 2.10: Numerical and analytical normalized perturbed density (n_1) profiles for the normalized beam density (n_b) = 0.3 at different times, including beam evolution for $l_b/\lambda_p = 4/2\pi$ with $v_b = 0.99$.

Values at the turning points		
x	1	$1/(1 - 2\alpha)$
β	0	$\frac{4\alpha(\alpha-1)}{(1+2\alpha)^2+1}$
n	1	$2\alpha(\alpha - 1) + 1$
E	0	0

Table 2.1: Value of plasma parameters at the turning points inside the beam.

Solution inside the beam

In this section, we present the analytical form of plasma parameters as a function of τ inside the beam ($\tau = 0$ to $\tau = \tau_f$). Multiplying equation (2.19) by x' and using the condition $x' = 0$ at $x = 1$ (i.e. $\beta = 0$), yields

$$[x'(\tau)]^2 = 2(1 - \alpha) - \frac{1}{x} - (1 - 2\alpha)x \quad (2.23)$$

which (using equation (2.22)) immediately gives the electric field inside the beam as

$$E(x) = x' = - \left(2(1 - \alpha) - \frac{1}{x} - (1 - 2\alpha)x \right)^{1/2} \quad (2.24)$$

(The -ve sign is chosen as there are excess electrons in the region of the beam). The turning points in the solutions inside the beam can be find out using $x' = 0$, where the amplitude of the electric field vanishes. Form equation (2.23), we have obtained two turning points, $x_- = 1$ and $x_+ = 1/(1 - 2\alpha)$, which shows that inside the beam oscillatory solution exists only for $\alpha < 1/2$. The values of the plasma parameters at the turning points are shown in the following table (2.1) At the turning points perturbed densities are respectively given by $n_1 = n - 1 = 0$ and $\delta n = -2\alpha(1 - \alpha)$. Therefore, for $\alpha = 1/2$, at the second turning point beam density is exactly neutralized by the perturbed plasma electron density; another

indication that oscillatory solution exists only for $\alpha < 1/2$. To obtain the electric field and density profile inside the beam, equation (2.23) needs to be integrated, which for $\alpha < \frac{1}{2}$ gives,

$$\tau = (1 - 2\alpha)^{-1/2} \int_1^x \sqrt{\frac{x}{(x-1)(\frac{1}{1-2\alpha} - x)}} dx$$

Integrating the above equation, the final expression of τ can be written as,

$$\tau = 2(1 - 2\alpha)^{-1} [E(m) - E(\psi, m)] \quad (2.25)$$

where $\psi = \cos^{-1}[\sqrt{(x-1)\frac{1-2\alpha}{2\alpha}}]$ and $m = 2\alpha$. Here $E(m)$ and $E(\psi, m)$ are respectively the complete and incomplete elliptical integrals of second kind. Equation (2.24) and (2.25) along with the expression for ψ gives the electric field inside the beam as a function of wave frame variable τ . The half-time periods of the oscillations in the plasma parameters inside the beam is obtained by integrating equation (2.23) between the two turning points $x_- = 1$ ($\psi = \pi/2$) and $x_+ = 1/(1 - 2\alpha)$ ($\psi = 0$) and is given by

$$(T/2) = 2(1 - 2\alpha)^{-1} [E(m) - E(0, m)]$$

where T is the time period of the oscillation with an angular frequency given by,

$$\omega = \frac{\pi(1 - 2\alpha)}{2E(m)} \quad (2.26)$$

This clearly indicates that as α increases, the oscillation frequency decreases monotonically and approaches zero for $\alpha = \frac{1}{2}$. Substituting $\alpha = \frac{1}{2}$ in equation

(2.23), the functional dependence of τ on x inside the beam is given by

$$\tau = [\sqrt{x(x-1)} + \ln(\sqrt{x} + \sqrt{x-1})] \quad (2.27)$$

which shows that for large x , $\tau \sim x$. Thus for $\alpha = 1/2$, x' and hence electric field inside the beam is nearly a constant.

For $\alpha > 1/2$, the expression for perturbed density at the second turning point shows that the beam is not completely neutralized by the plasma density. Therefore the electric field continuously grows without oscillating. For $\alpha > 1/2$, the solution of equation (2.23) can be expressed as,

$$\tau = (2\alpha - 1)^{-1/2} \int_1^x \sqrt{\frac{x}{(x-1)(x + \frac{1}{2\alpha-1})}} dx$$

Therefore, integrating the above equation, the final solution can be written as,

$$\tau = \frac{-2i}{\sqrt{2\alpha-1}} [\sqrt{m}E(i\sqrt{m}\xi, m^{-1}) - i(m-1)\xi] \quad (2.28)$$

where $\xi = \sinh^{-1}[\sqrt{(x-1)\frac{2\alpha-1}{2\alpha}}]$, $i = \sqrt{-1}$, $m = \frac{2\alpha}{2\alpha-1}$ and $E(i\xi, m)$ is the incomplete elliptic integral of second kind. Thus equation (2.24) and (2.28) along with the expression for ξ gives the electric field profile for $\alpha > 1/2$.

Solution behind the beam

To evaluate the wake electric field behind the beam, we begin from equation (2.19) with $\alpha = 0$. The first integral yields

$$\frac{(x')^2}{2} + \gamma = \gamma_m \quad (2.29)$$

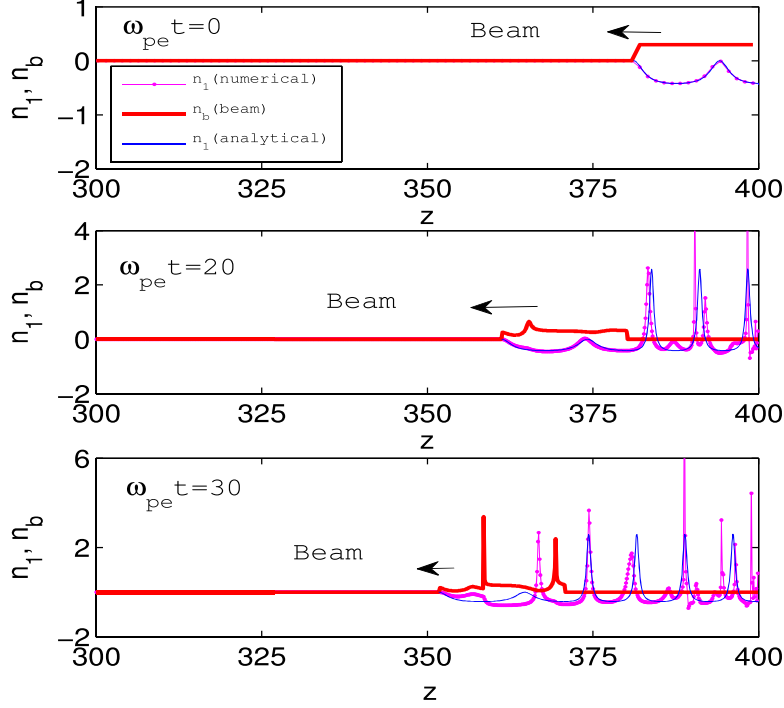


Figure 2.11: Numerical and analytical normalized perturbed plasma density (n_1) profiles for the normalized beam density (n_b) = 0.3 at different times, including beam evolution for $l_b/\lambda_p = 3$ with $v_b = 0.99$.

where $\gamma = \frac{1}{2}(x + \frac{1}{x})$ and γ_m is the maximum value of γ .

Since x'' has a finite discontinuity at $\tau = \tau_f$, x' and x are continuous function of τ . The electric field i.e. x' must be continuous at the end of the beam. Using the continuity in x' at $\tau = \tau_f$ and equations (2.24) and (2.29), we can write,

$$2\gamma_m - x_f - \frac{1}{x_f} = 2(1 - \alpha) - \frac{1}{x_f} - (1 - 2\alpha)x_f$$

Therefore the value of γ_m is given by

$$\gamma_m = (1 - \alpha) + \alpha x_f \quad (2.30)$$

where x_f is the value of x at $\tau = \tau_f$. Using this expression for γ_m , the electric field behind the beam is given by

$$E(x) = \pm \sqrt{2(1 - \alpha) + 2\alpha x_f - (x + 1/x)} \quad (2.31)$$

To obtain the electric field and density profile behind the beam, the equation (2.29) is integrated to give τ as a function of x . The equation (2.29) can be rearranged in the following fashion,

$$\frac{dx}{d\tau} = \frac{1}{\sqrt{x}} \sqrt{(x - a)(b - x)} \quad (2.32)$$

where $b = \gamma_m + \sqrt{\gamma_m^2 - 1}$ and $a = \gamma_m - \sqrt{\gamma_m^2 - 1}$. Integrating the equation 2.32, we get,

$$\int_{\tau_f}^{\tau} = \int_{x_f}^x \frac{\sqrt{x}}{\sqrt{(x - a)(b - x)}} \quad (2.33)$$

The solution of the above equation can be written as,

$$\tau = \tau_f + 2\sqrt{b}[E(\phi_f, m) - E(\phi, m)] \quad (2.34)$$

where $m = 2\sqrt{\gamma_m^2 - 1}/b$ and $x(x_f)$ is related to $\phi(\phi_f)$ as $x = \gamma_m + (\sqrt{\gamma_m^2 - 1})\cos(2\phi)$. Thus equation (2.31) and (2.34) along with the relation between x and ϕ gives the wake electric field profile behind the beam. In the following table (2.2), we present the values of plasma parameters at the turning points where $x' = 0$.

The oscillation frequency of the wake electric field is obtained by integrating equation (2.29) between the two turning points $x_{\pm} = \gamma_m \pm \sqrt{\gamma_m^2 - 1}$ (i.e $\phi = 0, \pi/2$) and is given by $\omega = \pi \left(2\sqrt{(\gamma_m + \sqrt{\gamma_m^2 - 1})E(m)} \right)^{-1}$. Analytically obtained profiles of perturbed density and wake electric field is plotted in all the figures in blue,

Values at the turning points		
x	$a = \gamma_m - \sqrt{\gamma_m^2 - 1}$	$b = \gamma_m - \sqrt{\gamma_m^2 - 1}$
β	$\frac{1-a^2}{1+a^2}$	$\frac{1-b^2}{1+b^2}$
n	$\frac{1+a^2}{2a^2}$	$\frac{1+b^2}{2b^2}$
E	0	0

Table 2.2: Value of plasma parameters at the turning points outside the beam.

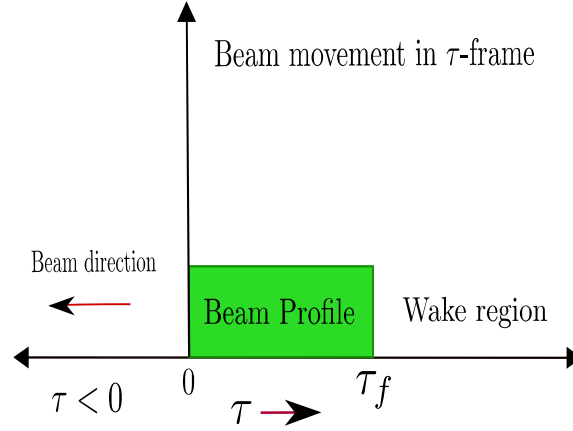


Figure 2.12: Schematic diagram of the beam-plasma interaction in τ - frame.

showing a reasonably good fit with numerical results. The deviations observed at late times in the simulation is due to a phase mixing effect which is discussed in the summary section. Using the expressions for wake electric fields inside (equation (2.24)) and outside (equation (2.31)) the beam, the Transformer ratio (R), which is defined as the ratio of maximum accelerating field (E_+) at the wake to the maximum decelerating field (E_-) inside the beam can be evaluated. The expression of

R in different regime of α are respectively given by

$$\begin{aligned} R(\alpha < \frac{1}{2}) &= \sqrt{2\alpha(x_f - 1)} / \sqrt{2(1 - \alpha) - 2\sqrt{1 - 2\alpha}} \\ R(\alpha = \frac{1}{2}) &= \sqrt{x_f} \\ R(\alpha > \frac{1}{2}) &= \sqrt{\frac{2\alpha(x_f - 1)}{2(1 - \alpha) - \frac{1}{x_f} + (2\alpha - 1)x_f}} \end{aligned}$$

The variation of transformer ratio (R) with respect to beam density (α) for different beam pulse length (τ_f) is shown by a continuous line in figure (2.7). Here again the analytical results show a good fit with numerical work. It is clear from the figure that the transformer ratio R is maximum when the beam density is exactly equal to the half of the plasma density.

Summary

We have studied the space-time evolution of wakefield excited by an ultra-relativistic electron beam ($\beta_b \rightarrow 1$) numerically using fluid simulation as well as analytically using stationary wave ansatz. Our simulation results show a reasonably good match with the analytical work, for several plasma periods. It is observed that at late times in the simulation, the perturbed density in all cases show spiky features, which is accompanied by sawtooth-like structures in the electric field profile. These features are well-known signatures of wave breaking [85–87,100,105]. In next chapter, a detail study on the modification of wake wave resulting in the breaking of wake wave has been discussed in detail. One of the most exciting features observed in the simulation that the beam gets modified in the self-consistent electric field during the propagation inside the plasma. Our simulation results with the

normalized beam velocities $\beta_b \leq 0.99$ show that the modification of beam density depends on the ratio of beam length to plasma wavelength. For $l_b < \lambda_p$, the beam gets compressed and its velocity gradually decreases. For $l_b > \lambda_p$, the beam splits into different beam-lets with different amplitude, each moving with different speed. The splitting and bunching effect of a beam in the self-consistent electromagnetic field is a well known effect as given in references [27, 106].

3

Breaking of relativistic electron beam driven longitudinal wake wave in a cold plasma

*The objective of this chapter * is to investigate the space-time evolution of longitudinal wakefield excited by a relativistic electron beam in a cold plasma. The space-time evolution exhibits a gradual modification in the wakefield profile which breaks due to phase mixing process after several plasma periods. The breaking of wake wave has been understood in terms of phase mixing of Akhiezer-Polovin [81] mode.*

* Ratan Kumar Bera, Arghya Mukherjee, Sudip Sengupta and Amita Das, *Relativistic electron beam driven longitudinal wake-wave breaking in a cold plasma*, *Physics of Plasmas* 23, 083113 (2016)

Introduction

In the previous chapter, one-dimensional fluid simulations have been performed to study the longitudinal structure of the electron beam driven wakefield in a cold plasma, over a wide range of beam parameters. In addition, an analytical work was also presented in the quasistatic framework. It was shown that the simulation results match with the analytical results over a wide range of beam parameters, for several plasma periods. At late times, the simulation results deviate from the analytical results. It is observed that, the plasma density and electric field profiles gradually evolve with time and the density profile forms sharp structures which is accompanied by the sawtooth like structures in the electric field profile.

In this chapter, we present a detailed study on the modification of the excited wakefield and a plausible physical reason behind the formation of sharp structures in the simulation. Therefore, we have carried out fluid simulation for different beam parameters and follow the space and time evolution of the excitation for a long time. In all cases, we have considered the excitation for a rigid beam ($\gamma_b \gg 1$) to avoid the changes in the wake profile due to self-consistent beam evolution; where $\gamma_b = 1/\sqrt{1 - v_b^2}$ is the Lorentz factor associated with the beam velocity (v_b). In the rigid beam limit, the evolution of the driver beam has been ignored in the self-consistent electric field. Therefore the electron beam propagates with a constant velocity for a long time without any significant deformation. In the previous chapter, we have shown that the rigidity of the beam is valid for hundreds of plasma periods if the velocity of the beam is higher than 0.99. Therefore we have used $v_b = 0.99$ in all the simulations presented here. It is observed that the density profile

gradually modifies with time and form sharp spike structure which are accompanied by sawtooth-like structures in the electric field profile after several plasma periods. This is a clear signature of wave breaking [85–87,100,105]. For every beam density (n_b) and beam velocity (v_b), the wake wave finally shows wave breaking, after several plasma periods. An analytical calculation of wake wave breaking in terms of input parameters (beam density, beam velocity, and beam length) is shown here. The analytical dependence of wake wave breaking time on the beam parameters verifies the wake wave breaking time obtained from simulation. Interestingly, the wake wave structure matches with longitudinal Akhiezer-Polovin mode [81] before it breaks (shown later). The analytical form of wake wave breaking time also matches the existing Akhiezer-Polovin wave breaking time formula given by Arghya et al. [88].

Governing Equations and Fluid simulation techniques

This section presents the basic equations governing the space and time evolution of ultra-relativistic electron beam driven wakefield in a cold plasma. These equations are the relativistic fluid-Maxwell equations presented in the previous chapter. These equations contain the continuity equations and the equation of motion for both plasma electron and beam electron. These equations are also connected with Poisson's equation. We have used the same set of normalized form of equations in this chapter to study the space-time evolution of the excitation (see chapter 2). In all the cases, we have performed simulations ignoring the beam evolution (2.1-2.5) in this study. This is true for a sufficiently energetic beam (rigid beam). We have solved these equations for different beam parameters using 1-D fluid sim-

ulation techniques (discussed in chapter 2). In the simulation, we have followed the excited wakefield profile for longer periods of time. The observations made in this study is presented below.

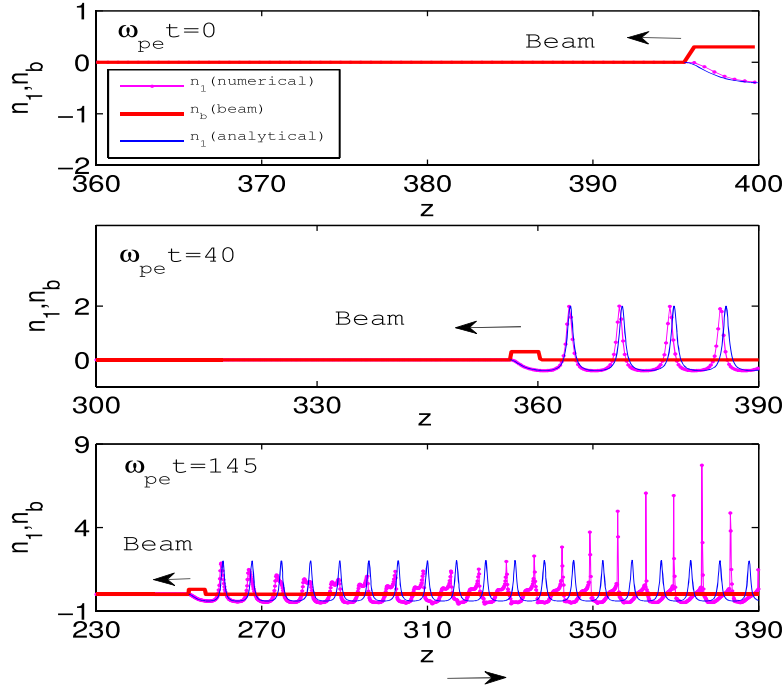


Figure 3.1: Numerical and analytical normalized perturbed electron density (n_1) profile at different times for the normalized beam density (n_b) = 0.3, the beam velocity ($v = b$) = 0.99, and the beam length (l_b) = 4

Numerical Observations and Discussions

In this section, we present the numerical observations made in the study of relativistic electron beam driven wakefield excitation in a cold plasma. The simulation results are shown in figures (3.1-3.4)) for different values of beam density (n_b) and beam velocity (v_b). In all cases, the simulation is carried out for a fixed normalized beam length (l_b) = 4. Figs. (3.1) and (3.2), respectively, show the perturbed elec-

tron density and the wake electric field for $n_b = 0.3$ and $v_b = 0.99$. Same quantities

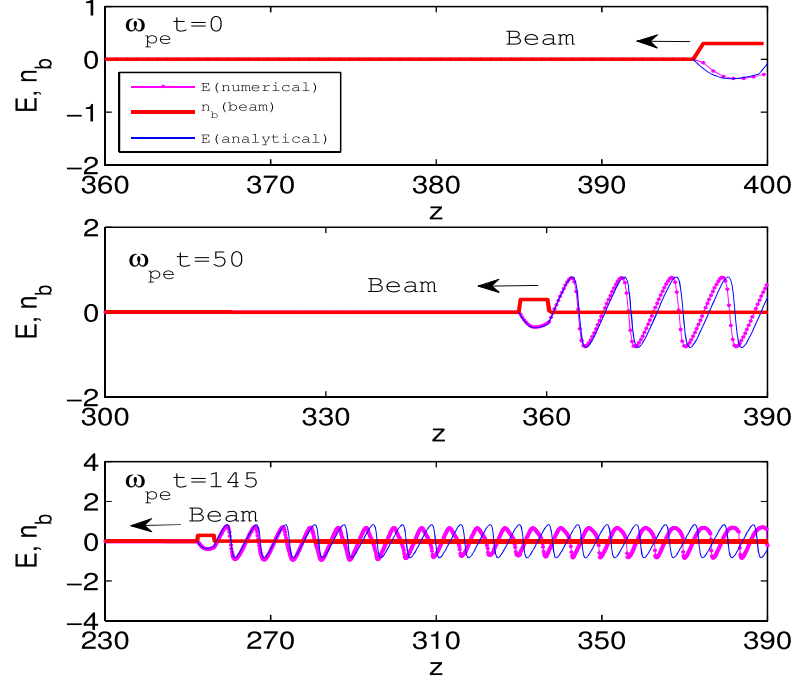


Figure 3.2: Numerical and analytical normalized electric field (E) profile at different times for the normalized beam density (n_b) = 0.3, the beam velocity ($v = b$) = 0.99, and the beam length (l_b) = 4

are shown in figures (3.3)) and (3.4)) for a different beam density $n_b = 0.4$, keeping the beam velocity fixed (at $v_b = 0.99$). Finally, Figures (3.5)) and (3.6)) , respectively, show the perturbed electron density and wake electric field for $n_b = 0.4$ and a different beam velocity $v_b = 0.8$. In all the figures, the numerical results are shown in magenta and the analytical results (derived in the previous chapter for completeness) are shown in blue.

In every case, the excited wakefield profile matches quite well with the analytical work by Rosenzweig et al. [80] and with numerical work by Ratan et al. [101], for

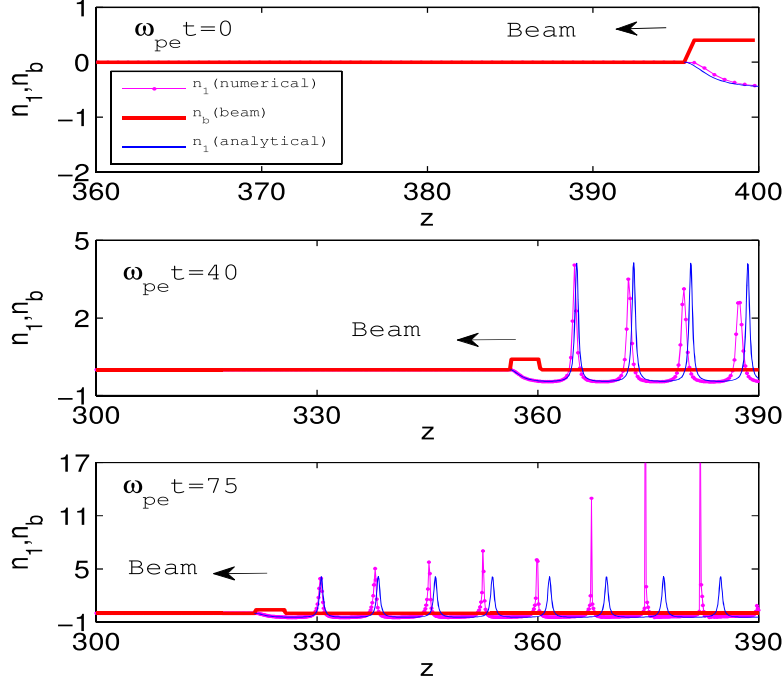


Figure 3.3: Numerical and analytical normalized perturbed electron density (n_1) profile at different times for the normalized beam density (n_b) = 0.4, the beam velocity ($v = b$) = 0.99, and the beam length (l_b) = 4

several plasma periods. As mentioned in the previous chapter, the wake wave profile gradually modifies with space and time and finally breaks. Here we have also observed the same response of the wakefield which finally breaks after several plasma periods. (see figures (3.1)-(3.6)). The breaking of the wake wave is observed when the density profile of the wake wave gets spiked. For different values of beam density (n_b) and beam velocity (v_b) with a constant beam length (l_b), we have performed simulations and scaled the wave breaking time (τ_{mix}) of wake wave with these parameters in figures ((3.7)- (3.9)).

We have identified that the breaking time of the wakefield is different for dif-

ferent beam density (n_b) and beam velocity (v_b). The wake wave breaks earlier for higher beam density (n_b) than the lower beam density for constant v_b and l_b and breaks later for higher beam velocity (v_b) than the lower velocity for constant n_b and l_b . It is observed that the amplitude of the density, electric field and velocity profile of wakefield depends with the beam density (n_b), beam length (l_b) and its velocity (v_b). Here we have carried out the simulation for beam density smaller than half of the background plasma density. For the beam density equal

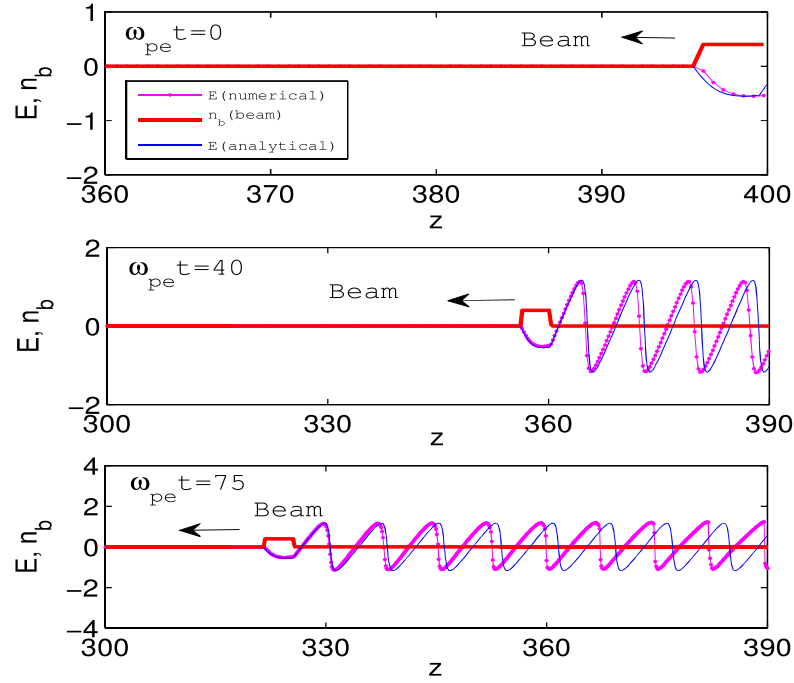


Figure 3.4: Numerical and analytical normalized electric field (E) profile at different times for the normalized beam density (n_b) =0.4, the beam velocity ($v = b$) =0.99, and the beam length (l_b)= 4

or even higher than half of the plasma density, the wake wave breaks immediately in simulation, before two or three plasma periods (see in ref. [101]). It is clearly shown that the excited wakefield profile is also indistinguishable from the longi-

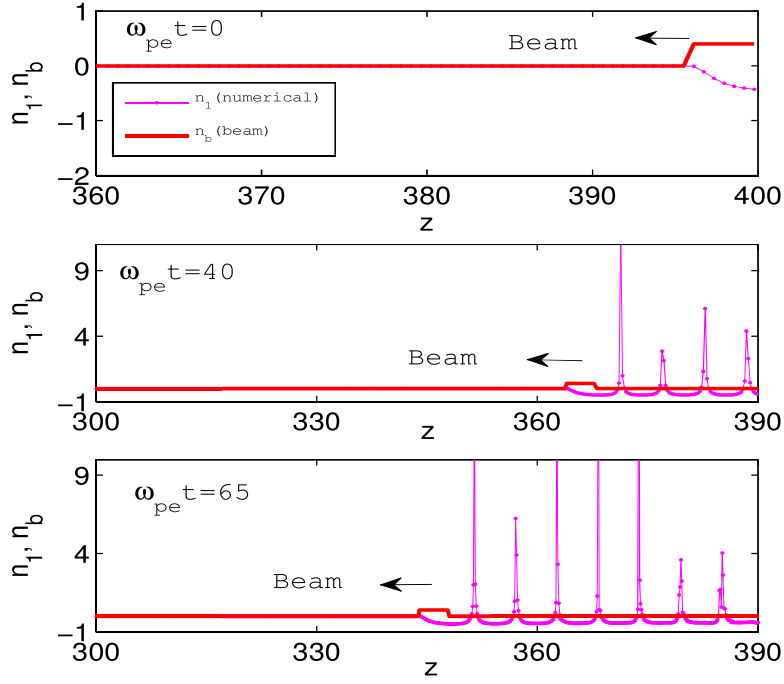


Figure 3.5: Numerical and analytical normalized perturbed electron density (n_1) profile at different times for the normalized beam density (n_b) = 0.4, the beam velocity ($v = b$) = 0.8, and the beam length (l_b) = 4

tudinal Akhiezer-Polovin (AP) mode (see figure (3.10)). Analytically we can show that the expression of frequency of wake wave and AP wave is exactly same. In order to describe the physics behind the beam driven wake wave breaking, we have adopted the well existing theory of phase mixing of longitudinal Akhiezer-Polovin (AP) mode which is discussed in the following section. An analytical expression of breaking time is also calculated in terms of these parameters. The simulation results fit the analytical formula perfectly.

Analysis of wake wave breaking

In this section, we have presented the physical mechanism behind breaking of the wake waves in detail. It is to be noted that the equations (2.1-2.5) outside the beam (i.e. $n_b = 0$) are the same set of equations needed for examining the structure and characteristics of an Akhiezer-Polovin (AP) mode (see equations (1-3) in ref. [87]). It is well known that Akhiezer-Polovin (AP) mode is only relativistically intense fundamental propagating mode that exists in a cold plasma. The excitation and characteristics of Akhiezer-Polovin mode has been investigated extensively by several authors [87, 88, 107]. AP mode can be parametrized by two parameters, u_m^{AP} and β_{ph} , where u_m^{AP} and β_{ph} represents maximum fluid velocity and phase velocity of AP wave respectively. In ref. [107], the solution of an AP mode for a given value of u_m^{AP} and β_{ph} was given in terms of plasma density (n_{AP}) in a normalized form as,

$$n_{AP} = \frac{\beta_{ph}}{\beta_{ph} - u_{AP}} \quad (3.1)$$

where $u_{AP} = \frac{p}{\sqrt{1+p^2}}$ is the velocity of the electrons having momentum p . The expression of u_{AP} can be obtained as a function of $\tau = (t - z/\beta_{ph})$ from the following equation,

$$\frac{d^2 p}{d\phi^2} + \frac{p}{\sqrt{1+p^2}} = 0 \quad (3.2)$$

Here the following transformation is used,

$$\left(1 - \frac{u}{\beta}\right) \frac{d}{d\tau} = \frac{d}{d\phi}$$

The solution of equation 3.2 can be written as (see equations (18-27) in ref. [107]),

$$\tau = \left(2 \frac{E(\theta, R)}{R'} - R' K(\theta, R) \right) - \frac{2R}{\beta R'} \sin \theta \quad (3.3)$$

where $(A - 1) \sin^2 \theta = A - \sqrt{1 + p^2}$, $R = \sqrt{\frac{A-1}{A+1}}$, $R' = \sqrt{1 - R^2}$ and $A = 1/\sqrt{1 - (u_m^{AP})^2}$. Here u_m^{AP} is the maximum value of u_{AP} which determines the amplitude of the AP mode. The frequency of the AP mode is given by,

$$\omega_{AP} = \frac{\pi R'}{(2E(R) - R'^2 K(R))} \quad (3.4)$$

Therefore, for a given value of u_m and β_{ph} , the structure of AP mode and its frequency can be obtained using equations (3.1-3.4). As stated above, the equations outside the beam are exactly similar to the equations required for exciting an AP mode. Therefore there must exist an identical Akhiezer-Polovin mode corresponding to the wake wave, which can be excited using the same value of u_m and β_{ph} as that of the wake wave. In the previous chapter (section 2.5), we presented the analytical expressions of plasma electron density (n), velocity (u) and electric field (E) of the wake wave for different beam density (n_b), beam length (l_b) and beam velocity (v_b). The amplitude and phase velocity of the wake can be determined from the beam parameters (n_b , v_b and l_b). Following our earlier analytical work presented in chapter (2), we can write the analytical solutions of the relativistic electron beam driven wakefield in $\tau = (t - \frac{z}{\beta_{ph}})$ frame as,

$$n = \frac{1}{2} \frac{1 + x^2}{x^2} \quad (3.5)$$

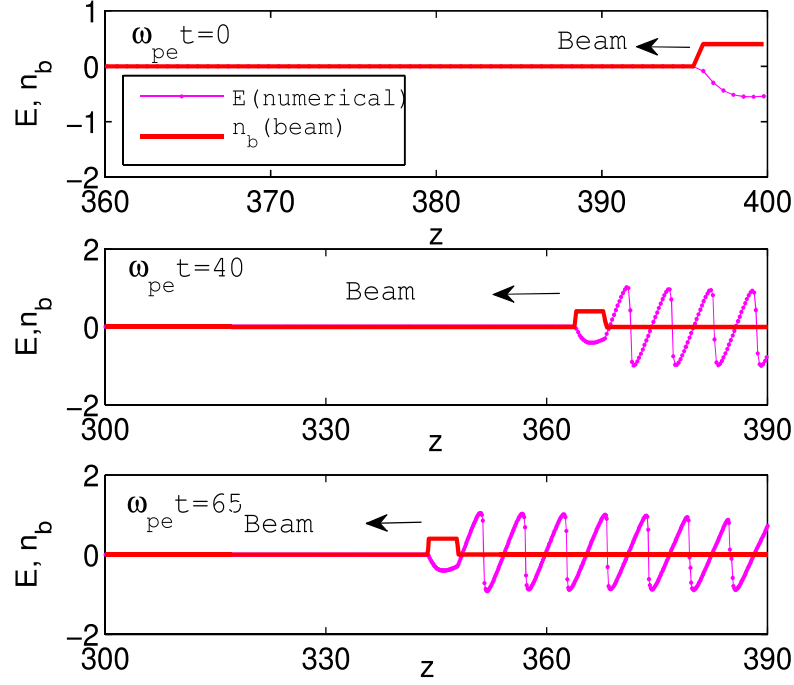


Figure 3.6: Numerical and analytical normalized electric field (E) profile at different times for the normalized beam density (n_b) = 0.4, the beam velocity ($v = b$) = 0.8, and the beam length (l_b) = 4

$$\beta = u = \frac{1 - x^2}{1 + x^2} \quad (3.6)$$

$$E = -x'(\tau) \quad (3.7)$$

where 'prime' represents differentiation with respect to variable τ . n , u and E represents the electron density, velocity and electric field respectively. The form of " x " is obtained inside the bunch for $\beta_{ph} = 1$ as a function of τ from,

$$(x')^2 = \left(2(1 - \alpha) - \frac{1}{x} - (1 - 2\alpha)x \right) \quad (3.8)$$

where α is beam density (n_b) and the form of x as a function of τ outside the bunch (wake region) is evaluated from,

$$(x')^2 = \left(2\gamma_m - x - \frac{1}{x}\right) \quad (3.9)$$

where $\gamma_m = \frac{x'^2}{2} + \gamma = (\sqrt{1 - u_m^2})^{-1}$, maximum value of Lorentz factor (γ) associated with plasma electron velocity (u) and u_m represents the maximum value of u . Using the continuity condition of x' at $\tau = \tau_f$ (end of beam), we obtained the value of γ_m as,

$$\gamma_m = (\sqrt{1 - u_m^2})^{-1} = (1 - \alpha) + \alpha x_f \quad (3.10)$$

where $x_f = x(\tau_f)$, $\tau_f = 2\pi l_b / \lambda_p$ and $\lambda_p = \frac{2\pi c}{\omega_{pe}}$, plasma wavelength. Substituting the value of γ_m in the expression of u_m , we have the following expression for u_m .

$$u_m = \sqrt{1 - \frac{1}{((1 - \alpha) + \alpha x_f)^2}} \quad (3.11)$$

where x_f is obtained either from the solution of equation (3.8) at $\tau = \tau_f$ or the solution of equation (3.9) at τ_f . In the previous chapter, equation (3.8) was solved in three different regimes of beam density ($\alpha < 1/2$, $\alpha = 1/2$ and $\alpha > 1/2$). In this chapter, the simulations illustrating the breaking of wake wave have been carried out for the beam density $\alpha < 1/2$. Therefore, we only present the solution of the equation (3.8) for $\alpha < 1/2$. The solution of equation (3.8) for $\alpha < 1/2$ was given as,

$$\tau = 2(1 - 2\alpha)^{-1}[E(m) - E(\psi, m)] \quad (3.12)$$

where $\psi = \cos^{-1}[\sqrt{(x - 1)\frac{1 - 2\alpha}{2\alpha}}]$ and $m^2 = 2\alpha$. Here $E(m)$ and $E(\psi, m)$ are respectively the complete and incomplete elliptical integrals of second kind. We

have obtained value of x_f using equation (3.12) for a given value of α and l_b . Finally, we have calculated u_m by substituting x_f in equation (3.11). Substituting the value of u_m in the equation (3.10), we have obtained the value of γ_m which decides the structure of the wake wave (see equation (3.9)). The structure of wake wave was found from the solution of equation(3.9) as,

$$\tau = \tau_f + 2\sqrt{b}[E(\phi_f, m) - E(\phi, m)] \quad (3.13)$$

where $b = \gamma_m + \sqrt{\gamma_m^2 - 1}$, $m^2 = 2\sqrt{\gamma_m^2 - 1}/b$ and $x(x_f)$ is related to $\phi(\phi_f)$ as $x = \gamma_m + (\sqrt{\gamma_m^2 - 1})\cos(2\phi)$. The normalized frequency of the wake wave may be written as,

$$\omega_{wake} = \frac{\pi}{\left(2\sqrt{(\gamma_m + \sqrt{\gamma_m^2 - 1})E(m)}\right)} \quad (3.14)$$

Note that using the identity of elliptical integral $E(2\sqrt{m'}/(1+m')) = (2E(m') - \sqrt{1-m'^2}K(m'))$ [108], it can be easily shown that the expression of frequency of the wake wave is exactly similar to the form of frequency of an AP mode (see equation 3.4). We have estimated the value of u_m and $\beta_{ph} = \beta_b$ of wake wave in terms of beam density (n_b), beam length (l_b) and beam velocity (v_b), where β_{ph} is taken to be equal to beam velocity (β_b). It is found that the analytically calculated value of u_m matches the numerically obtained value for different beam parameters. Furthermore, for a given beam parameters, we have used the value of u_m and β_{ph} of the wake wave as u_m^{AP} and β_{ph} in equations (3.1-3.3) and obtained the structure of corresponding AP mode. Here we have shown the plot of perturbed density ($n_1 = n - 1$) profile of a corresponding AP mode for an wake wave excited for $n_b = 0.3$, $l_b = 4$ and $\beta_{ph} = 0.99$ in Fig. (3.7). As expected, Fig.(3.7) shows that the excited wake wave is exactly identical to the corresponding AP mode. In other

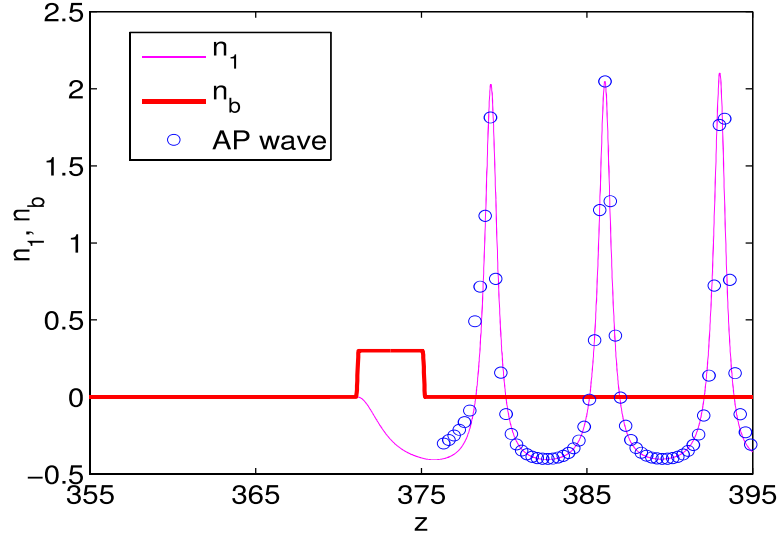


Figure 3.7: Plot of perturbed density profile (n_1) of wake wave (magenta) and Akhiezer-Polovin mode (blue circles) for normalized beam density (n_b) = 0.3, beam velocity (v_b) = 0.99, and beam length (l_b) = 4 at $\omega_{pe}t$ 25

words, we can state that wake wave is nothing, but a longitudinal AP mode in a cold plasma. Therefore, the characteristics of the wake wave can be studied by analyzing the properties of an AP mode.

In simulation, we have observed that this wake wave (or AP wave) breaks via phase mixing mechanism after several plasma periods. Hence a plausible explanation for the appearance of density spikes in the wakefield structure lie in the basics of phase mixing of longitudinal Akhiezer-Polovin (AP) wave. It is known that the amplitude of any relativistically intense wave is limited by its wave breaking limit. Extensive study on wave breaking phenomena has been addressed by several authors [85–87, 100, 105]. The wave breaking mechanism is explained by the process when frequency of the oscillation depends on space which results in the crossing of fluid elements. The crossing of the fluid elements make the wave incoherent

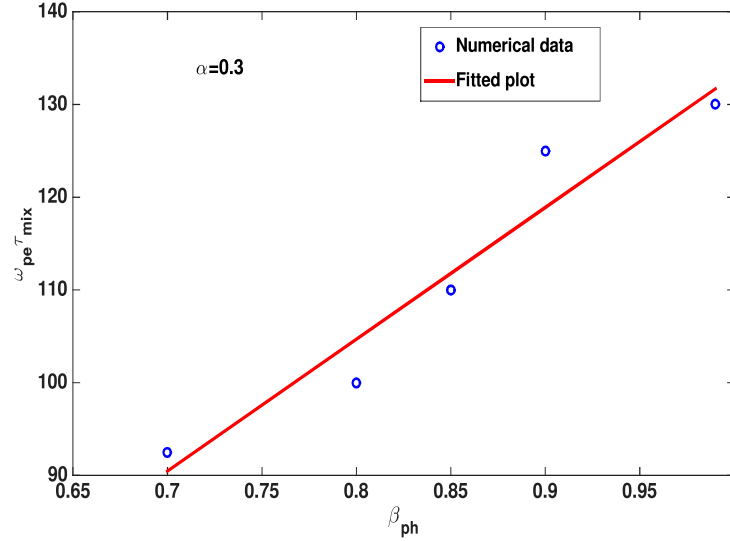


Figure 3.8: Plot for numerically obtained (circles) and fitted (solid) scaling of phase mixing time (τ_{mix}) with the phase velocity (β_{ph}) for the normalized beam density (n_b)=0.3 and the beam length (l_b)= 4

and the energy contained in a coherent wave structure is transferred into random particle motion [85–87, 100, 105].

It is well known that a pure longitudinal AP mode does not break if its amplitude is restricted by the wave breaking limit ($E_{WB} = \sqrt{2(\gamma_{ph} - 1)}$), where $\gamma_{ph} = \left(\sqrt{1 - \beta_{ph}^2}\right)^{-1}$, is the relativistic factor associated with the phase velocity (v_{ph}) of the AP wave with electric field of amplitude E_{WB} . For a relativistically intense wave ($\beta_{ph} \rightarrow 1$), the amplitude for wave breaking is extremely large ($E_{WB} \rightarrow \infty$). Hence, we expect that AP mode or wake wave of arbitrary amplitude should sustain for long time which is not observed in this context. In 2012, Prabal et al. [87] shown that AP wave can break below its wave breaking limit via the process of phase mixing if it is subjected to a small arbitrary longitudinal perturbation. Recently Arghya et al. [88] presented an analytical formula for this

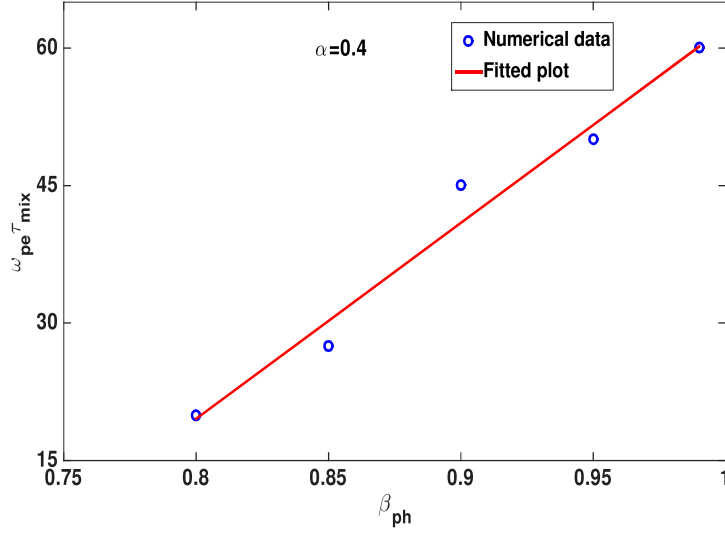


Figure 3.9: Plot for numerically obtained (circles) and fitted (solid) scaling of phase mixing time (τ_{mix}) with the phase velocity (β_{ph}) for the normalized beam density (n_b) = 0.4 and the beam length (l_b) = 4

phase mixing time or wave breaking time of longitudinal AP wave, which depends on the input parameters of the AP wave. The estimated phase mixing time (τ_{mix}) depends on phase velocity of the wave (β_{ph}) and peak value of fluid velocity u_m for a sinusoidal longitudinal perturbation of velocity amplitude δ as following,

$$\tau_{mix} \approx \frac{2\pi\beta_{ph}}{3\delta} \left[\frac{1}{u_m^2} - \frac{1}{4} \right] \quad (3.15)$$

We have also identified the breaking of the wake waves for different beam density (n_b) and beam velocity (β_{ph}). For different beam parameters, we have shown that the excited wake wave profile is identical with the corresponding AP mode before it breaks. After several plasma periods, the perturbed plasma electron

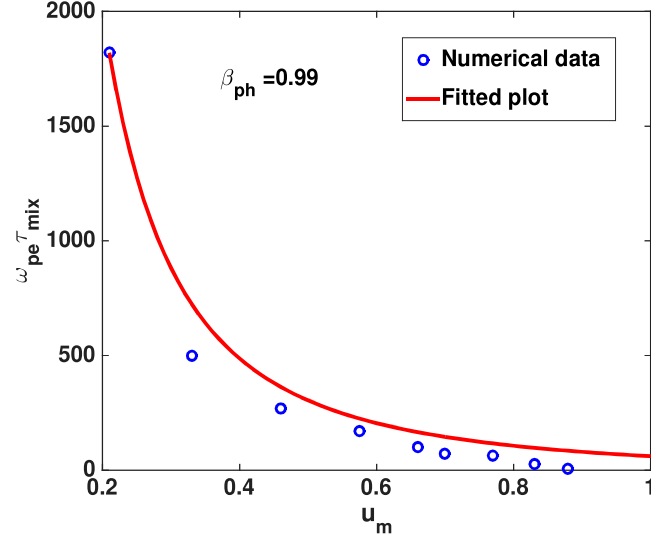


Figure 3.10: Plot for analytical (solid) and numerical (circles) scaling of phase mixing time (τ_{mix}) as a function of maximum fluid velocity (u_m) for normalized beam velocity (v_b) = 0.99 and beam length (l_b) = 4.

density shows an irregular and spiky behavior and finally breaks (see figures (3.1)-(3.6)). In simulations, we have measured the wake wave breaking time (minimum time required to break) for different beam density (n_b) and beam velocity (v_b). The breaking time in simulation refers such a time when the first density spike occurs. Analytically, we have also determined the breaking time (τ_{mix}) using equation (3.15) for different values of u_m and beam velocity(v_b) where u_m is obtained from equation (3.11). These results are plotted in figures (3.8) (3.9), and (3.10). Here we see that the analytically obtained values show a good comparison to the numerical values.

Summary

Study of space-time evolution of relativistic electron beam driven wake wave shows to the breaking of wake wave at late times. After several plasma periods, we have observed that the numerical perturbed density profile of wake wave steepens which is accompanied by the sawtooth structure in electric field profile. This is a well-known effect called wave-breaking (or wake wave breaking) [85–87,100,105], which arises due to the relativistic mass variation of electrons. It is shown that the wake wave modifies gradually and breaks after a certain time (wave -breaking time) via phase mixing mechanism. We have presented that the excited wake wave is identical with the corresponding longitudinal Akhiezer-Polovin mode [81] (obtained using same parameters value) in a cold plasma before it breaks. Therefore this breaking of wake wave is well understood in terms of longitudinal AP wave breaking phenomena. Analytically, we have scaled the wake wave breaking time (τ_{mix}) in terms of beam parameters (beam density, beam length and beam velocity), which was estimated earlier by Arghya et al. [88] in terms of AP wave parameter (maximum fluid velocity and phase velocity of the wave). It is shown that the numerically obtained breaking time matches with analytical predicted value.

4

Accessibility and stability of an electron-ion mode in plasma wakefield acceleration

The objective in this chapter ^{} is to investigate the excitation of wakefield driven by a relativistic electron beam in a cold plasma, where the effect of ion motion is included. Proposing three fluid description of the plasma, an 1-D fluid simulations have been employed in this chapter. The simulation results have been also compared with analytical results. The wave breaking limit for a longitudinal relativistic electron-ion mode is also presented.*

^{*} Ratan Kumar Bera, Sudip Sengupta, and Amita Das, *Accessibility and stability of an electron-ion mode in plasma wakefield acceleration*, Ready for Submission

Introduction

In chapters (2 and 3), the excitation of relativistic electron beam driven wakefield has been studied for a wide range of beam parameters, where the effect of ion motion was completely neglected. This is because of their heavy mass. Being a heavy species, ions do not respond much in the electron time scale. They only provide a neutralizing background in the studies. Therefore, the equations responsible for the dynamics of ions motion have been neglected in the previous chapters and also in the several earlier works [31, 78, 79]. In 1998, Khachatryan et al. [82] reported in the study of strong plasma waves ($\gamma \gg 1$) that plasma ions (even heavy ions) make an essential contribution to the process of charge separation under the influence of such a strong field; where $\gamma = (1 - v^2/c^2)^{-1/2}$ is the Lorentz factor associated with the velocity (v) of the electrons. Later in 2005, Rosenzweig et. al. [83] reported that the motion of ions plays an important role in PWFA which produces large perturbations in ion density, giving rise to transverse fields that in turn disrupt the motion of the beam. Recently, in the study by Vieira et al. [84], it was shown that ions can essentially affect the future proton driven plasma wakefield acceleration. Their motion can limit the energy transfer from the driver to the accelerated particles by reducing the accelerating gradient which is a result of early saturation in the self-modulation instability (SMI). Therefore, including the effect of ion motion, the study of PWFA or the excitation of strong plasma waves requires a special attention. In terms of theoretical work, including the effect of ions motion, a semi-analytical form (no exact solution) of the electron beam driven wakefield in 1-D is presented using multiple fluid models in ref. [80]. They calculated an approximate value of the transformer ratio (ratio of maximum

accelerating gradient behind the beam to the maximum decelerating gradient inside the beam) which determines the efficiency of the excitation, only for beam density equal to the half the plasma density and in the limit $\mu \ll 1$; where μ represents the ratio of electron to ion's mass. For arbitrary beam parameters including the effect of ion motion, a complete characterization of PWFA mechanism is still a largely unexplored area of research.

In this chapter, we have employed one-dimensional fluid simulation to study the electron beam driven wakefield (or strong plasma waves excite by relativistic electron beam) over a wide range of beam parameters and mass ratios by proposing three-fluid (plasma electron, plasma ion, and beam electrons) description of the plasma wave excitation. It is observed that our simulation results show a good agreement with the semi-analytical results given by Rosenzweig et al. [1] for different beam densities and mass ratios. We have also found that the excitation is independent of the initialization of plasma parameters. The numerically excited profile ultimately converts to Rosenzweig's solution. Clearly, this again confirms that Rosenzweig's solution is the only solution (mode) available in the cold, homogeneous plasma when an electron beam passes through it. We have studied the transformer ratio (R) which determines the efficiency of the acceleration process as a function of mass ratio and beam density. In the simulation, it is observed that the density profile of the excited wake deviates from the analytical solution after several plasma periods. The excited wake gradually modifies with time and becomes spiky after several plasma periods. The corresponding electric field profile turns into a saw-tooth form which is a clear signature of wave breaking [85–87, 105]. This particular feature observed in the present simulation has been found to be absent

in the analytical calculations given in ref. [80]. It is also seen that the Rosenzweig's solution outside the beam (or numerically excited wake before breaking) is identical to corresponding Khachtryan's mode [82], excited using the same parameter values of the wakefield. The wave breaking limit obtained from our simulation lies much below the analytically estimated value given by [82] (see appendix A.2 for detail derivation). These observed differences between our simulation results and analytically predicted results have been understood in terms of phase mixing process [87,88]. In the analytical calculation given by Khachatryan, the possibility of phase mixing was ignored.

Governing Equations

The basic equations governing the excitation of 1-D relativistic electron beam driven wakefield in a cold plasma are the relativistic fluid-Maxwell equations. These equations contain the continuity and momentum equations for electron beam, plasma electrons and plasma ions. Poisson's equation is used to calculate the electric field. We have considered the the electron beam is moving along z -direction in an infinite, homogeneous plasma channel. Here we focus on exciting a relativistic electron beam driven wakefield only in the longitudinal direction (along the beam propagation). Therefore, neglecting the variation of plasma parameters (density, velocity and electric field for both the electrons and ions) in transverse directions (transverse to the beam propagation), the basic normalized governing equations in 1-D can be written as,

$$\frac{\partial n}{\partial t} + \frac{\partial(nv)}{\partial z} = 0 \quad (4.1)$$

$$\frac{\partial p}{\partial t} + v \frac{\partial p}{\partial z} = -E \quad (4.2)$$

$$\frac{\partial n_i}{\partial t} + \frac{\partial(n_i v_i)}{\partial z} = 0 \quad (4.3)$$

$$\frac{\partial p_i}{\partial t} + v_i \frac{\partial p_i}{\partial z} = \mu E \quad (4.4)$$

$$\frac{\partial n_b}{\partial t} + \frac{\partial(n_b v_b)}{\partial z} = 0 \quad (4.5)$$

$$\frac{\partial p_b}{\partial t} + v_b \frac{\partial p_b}{\partial z} = -E \quad (4.6)$$

$$\frac{\partial E}{\partial z} = (n_i - n - n_b) \quad (4.7)$$

where $p = \gamma v$, $p_i = \gamma_i v_i$ and $p_b = \gamma_b v_b$ are the z -components of momentum of plasma electron, plasma ion and beam electron having z -component of velocity v , v_i and v_b respectively. Here, $\gamma = (1 - v^2)^{-1/2}$, $\gamma_i = (1 - v_i^2)^{-1/2}$ and $\gamma_b = (1 - v_b^2)^{-1/2}$ are the relativistic factors associated with plasma electron, plasma ion and beam electron respectively. In the above equations, n , n_i and n_b represents the density of plasma electron, plasma ion and electron beam respectively. E and μ represents the z -component of the electric field and mass ratio (ratio of electron to ion mass) respectively. We have used the normalization factors as, $t \rightarrow \omega_{pe} t$, $z \rightarrow \frac{\omega_{pe} z}{c}$, $E \rightarrow \frac{eE}{m_e c \omega_{pe}}$, $v \rightarrow \frac{v}{c}$, $v_i \rightarrow \frac{v_i}{c}$, $v_b \rightarrow \frac{v_b}{c}$, $p \rightarrow \frac{p}{m_e c}$, $p_i \rightarrow \frac{p_i}{m_e c}$, $p_b \rightarrow \frac{p_b}{m_e c}$, $n \rightarrow \frac{n}{n_0}$, $n_i \rightarrow \frac{n_i}{n_0}$ and $n_b \rightarrow \frac{n_b}{n_0}$. The normalization method was discussed in chapter (2) in detail. Equations (4.1-4.7) are the key equations needed to examine the excitation of 1-D relativistic electron beam driven wakefield in a cold plasma.

Fluid simulation of the relativistic electron beam driven wakefield

In this section, we present numerical techniques used to study the relativistic electron beam driven wakefield excitation in a cold plasma. We have developed a fluid code using LCPFCT subroutines, which is based on flux-corrected transport scheme [102]. The basic principle of this scheme is based on the generalization of two-step Lax-Wendroff method [103]. The detail simulation techniques have been discussed in chapter 3.

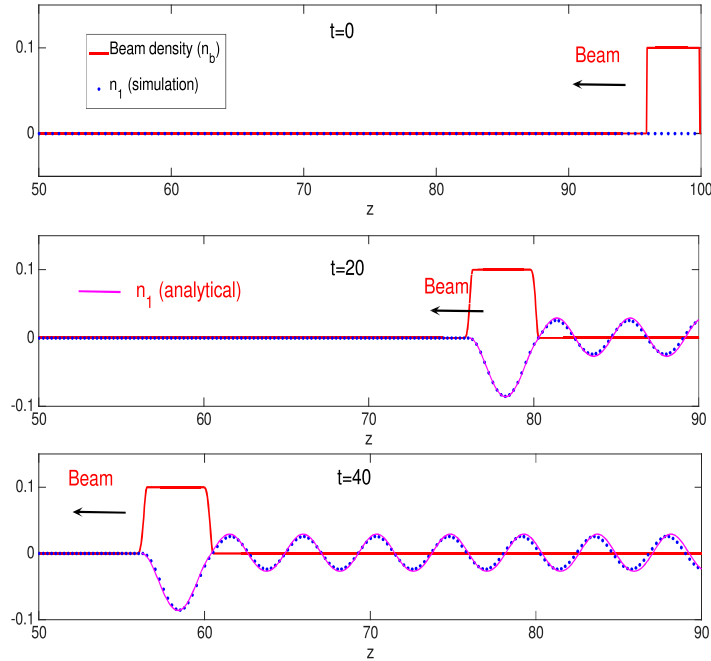


Figure 4.1: Plot of normalized perturbed electron density (n_1) profile at different times for the normalized beam density (n_b)=0.1, $l_b = 4$ beam velocity (v_b) =0.99 and $\mu = 1$.

In this case, we have performed our simulation for a rigid beam. Rigid beam

defines such a beam which can penetrate infinite length in plasma without any significant deformation. This is true only for a sufficiently energetic beam. In chapter (2), we showed that beam can be considered to be rigid only if the velocity of the beam $v_b \geq 0.99$. In this limit, beam evolution equations (4.5) and (4.6) can be neglected. Therefore, in all the simulations, the beam propagates along z - direction with a speed $v_b = 0.99$ to avoid the self-consistent effect of the beam. We have solved the equations ((4.1),(4.2), (4.3),(4.4) and (4.7)) with non-periodic boundary conditions along z - direction. Here the driver beam is allowed to propagate from one end of the simulation window to its other end. The effect of beam has been included in equation (4.7). We have initialized our system in two different ways, self-consistent way and also when the beam is “simply put” inside the plasma. We find that our simulation results are independent of the initialization method; the solution always converges to the same wake field profile in both the cases. This fact, *i.e.* independence of wakefield profile to initialization method, is also discussed in the chapter (2). In this chapter, we present the simulation results when the beam is simply put in the plasma.

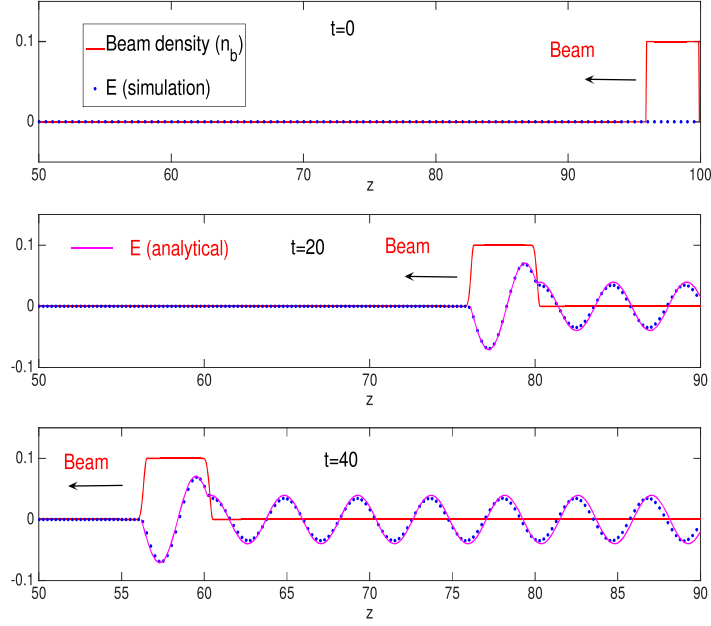


Figure 4.2: Plot of normalized electric field (E) profile at different times for the normalized beam density (n_b)=0.1, beam velocity (v_b)=0.99, $l_b = 4$ and $\mu = 1$.

Numerical observations and discussion

In this section, we present the numerically obtained profiles of perturbed electron density (n_1) and electric field (E) profile with time for different beam density and mass ratio. In all our simulations, we have used beam velocity $v_b = 0.99$ and beam length $l_b = 4$. The numerical perturbed density (n_1) and electric field (E) profiles of the excited wake wave are shown in figures (4.1) and (4.2) respectively at different times for $n_b = 0.1$ and $\mu = 1$.

The numerical perturbed density (n_1) and electric field (E) profiles are plotted in figures (4.3) and (4.4) respectively at different times for $n_b = 0.2$ and $\mu = 1$. We have obtained the corresponding analytical profiles of wakefield excited for

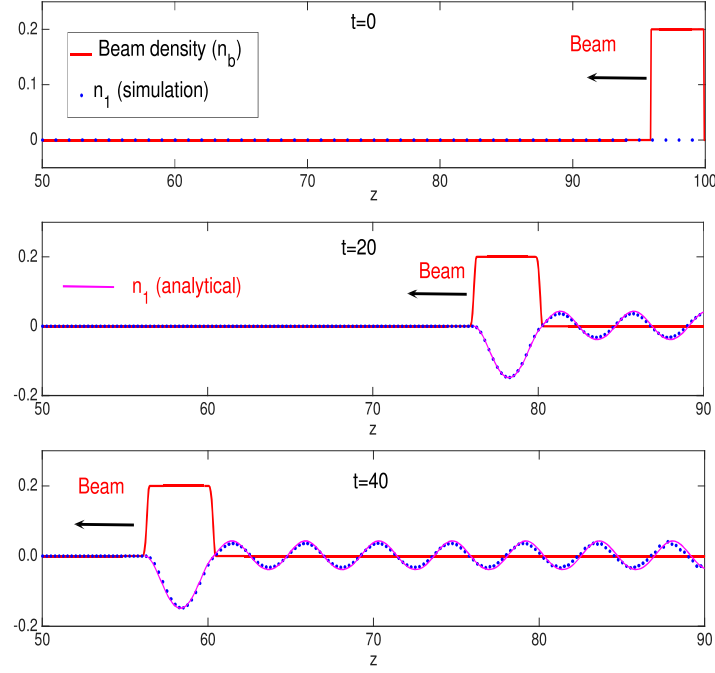


Figure 4.3: Plot of normalized perturbed electron density (n_1) profile at different times for the normalized beam density (n_b)=0.2, beam velocity $v_b = 0.99$, $l_b = 4$ and $\mu = 1$.

the same parameters used in our simulation from the semi-analytical calculation given in ref. [80]. These analytical profiles (in magenta lines) are shown in figures (4.1-4.4). It is clear from figures (4.1-4.4) that the numerical profiles match well with the analytical profiles for different beam densities and mass-ratios. In figure (4.5), we have shown the plot of perturbed electron density profile (n_1) obtained for $\mu = 1/1836$, $n_b = 0.2$ at $\omega_{pe}t = 50$ along with the profile, where the effect of ion motion is completely neglected [31, 101, 109]. It is clear from the figure (4.5) that ion motion may be neglected for small values of μ . In figure (4.6), we have plotted analytical values of transformer ratio $R = \frac{E_+}{E_-}$ obtained from [80] along with numerical values as a function of μ for two different values of $n_b = 0.1$ and

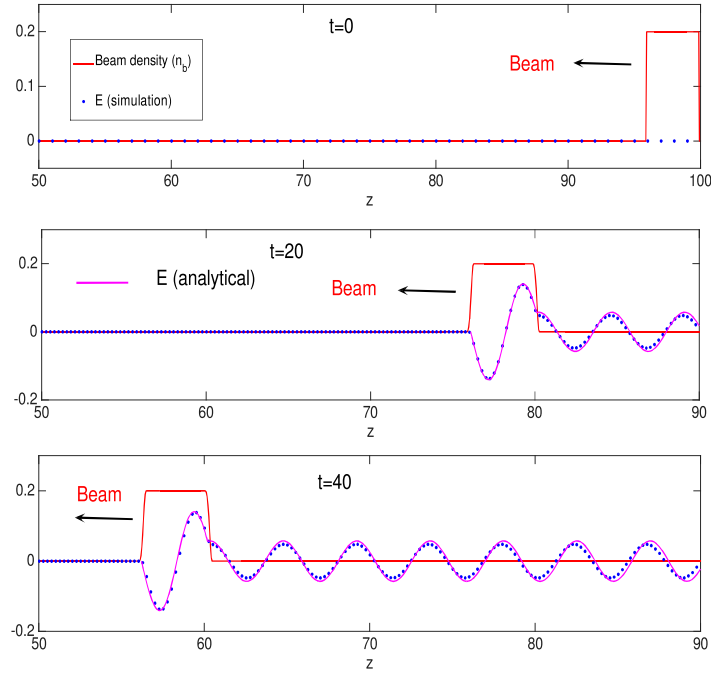


Figure 4.4: Plot of normalized electric field (E) profile at different time for the normalized beam density (n_b)=0.2, beam velocity $v_b = 0.99$, $l_b = 4$ and $\mu = 1$.

0.5; where E_+ and E_- are the maximum value of accelerating electric field behind the beam and maximum decelerating electric field inside the beam respectively. We have found that numerically obtained transformer ratio matches well with the analytical values.

In figure (4.7), we have plotted the transformer ratio (shown in squares) obtained from fluid simulation on the top of its analytical values (solid red line) obtained from semi-analytical theory [80] for $\mu = 1/1836$ as a function of beam density (n_b). In addition, we have also plotted the analytical result for the transformer ratio R vs. beam density n_b , given in ref. [101] for $\mu = 0$ on top of the $\mu = 1/1836$ curve. As expected the curve for $\mu = 0$ closely matches the curve for $\mu = 1/1836$. Further, we have also plotted the semi-analytical values (shown in

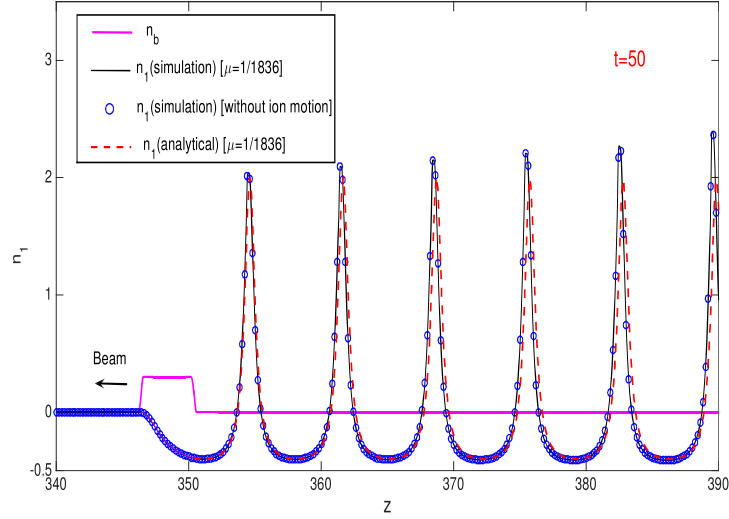


Figure 4.5: Plot of normalized perturbed electron density (n_1) profile at different times for the normalized beam density (n_b)=0.3, beam velocity $v_b = 0.99$ and $l_b = 4$ and $\mu = 1/1836$.

dotted line) obtained for $\mu = 1$ from ref. [80] along with some values obtained from simulation. We find a good match between theory and simulation. It is observed that in both cases transformer ratio R settles down to unity for large values of n_b . This implies that there is no gain in 1-D for an over-dense beam. The transformer ratio determines the energy gain of the acceleration along the dephasing length, which is the maximum length over which electrons are accelerated. Typically, higher the value of transformer ratio (R) larger the energy gain in the process of acceleration.

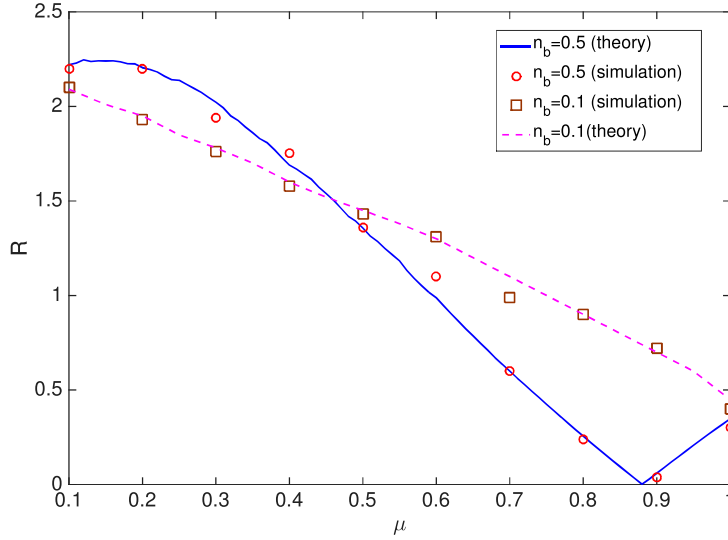


Figure 4.6: Plot of transformer ratio (R) vs. mass ratio (μ) for $n_b = 0.5$ and $n_b = 0.1$

Breaking of electron-ion wake waves in a cold plasma

We have observed in our simulation that the numerical profiles of perturbed electron density (n_1) and electric field (E) match with the analytical results, for several plasma periods (see figures (4.1-4.5)). After several plasma periods, subsequently, they start to deviate. The amplitude of the electron density gradually increases and shows spiky behavior at later times ($\omega_{pe}t = 123$) shown in figure (4.8). This feature, indicating the density bursts, is known as wave breaking [85–87, 105].

It is well known that, including the ion dynamics, the solution of 1-D relativistic fluid-Maxwell equations (equations (1), (2), (3), (4) and without the beam term in Poisson equation (7)) in a cold plasma is a “Khachatryan mode” [82] which is parametrized in terms of μ , β_{ph} and E_{max} ; where β_{ph} and E_{max} are respectively

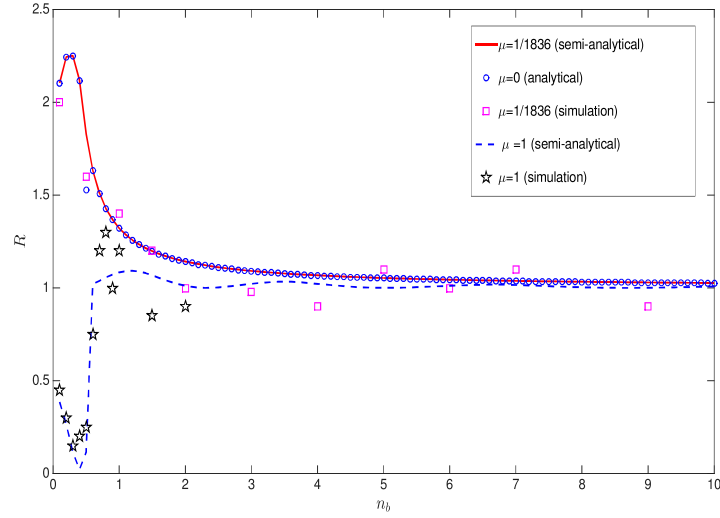


Figure 4.7: Plot of semi-analytical and numerical values of transformer ratio (R) as a function of beam density (n_b) for $\mu = 1$ and $\mu = 1/1836$. The blue circles indicate the values of transformer ratio obtained from the analytical expression given by Ratan et. al. [*Physics of Plasmas*, 22, 073109 (2015)] for $\mu = 0$.

the phase velocity and the maximum amplitude of the electric field associated with the wave. Therefore the electron beam driven wakefield (structure behind the beam) which is a solution of (equations (1-4, 7)) with $n_b = 0$, should be a corresponding Khachatryan mode excited using the same values of μ , $\beta_{ph} = v_b$ and E_{max} of the wake wave. Using the value of μ , β_{ph} and E_{max} from the simulation, we have plotted the corresponding Khachatryan's mode on top of the wake wave excited for $n_b = 0.1$, $v_b = 0.99$, $l_b = 4$ and $\mu = 1$ in figure (4.9). It is seen that the structure of the wake wave shows a good match with the corresponding Khachatryan mode. Therefore the wake wave breaking can be understood in terms of breaking of Khachatryan's mode.

In 1998, Khachatryan et al. [82] analytically calculated the wave breaking limit

for a relativistically intense plasma wave (including ion motion) in terms of the maximum amplitude of electric field as, $E_{WB} = \sqrt{2}\gamma_{ph}[1 + (1 - \nu_1^{\frac{1}{2}}\nu_2^{\frac{1}{2}})/\mu]$; where $\nu_1 = 1 + \mu$, $\nu_2 = 1 + [\mu(\gamma_{ph} - 1)/(\gamma_{ph} + 1)]$ and $\gamma_{ph} = (1 - \beta_{ph}^2)^{-\frac{1}{2}}$ (see appendix A.2 for detail calculation). For a wave in a medium, wave breaking limit decides the maximum sustainable amplitude of the wave. If the amplitude exceeds that limit, the wave breaks resulting in the destruction of coherent motion [85, 86, 105]. In simulation, at the point of wave breaking, we note the corresponding maximum

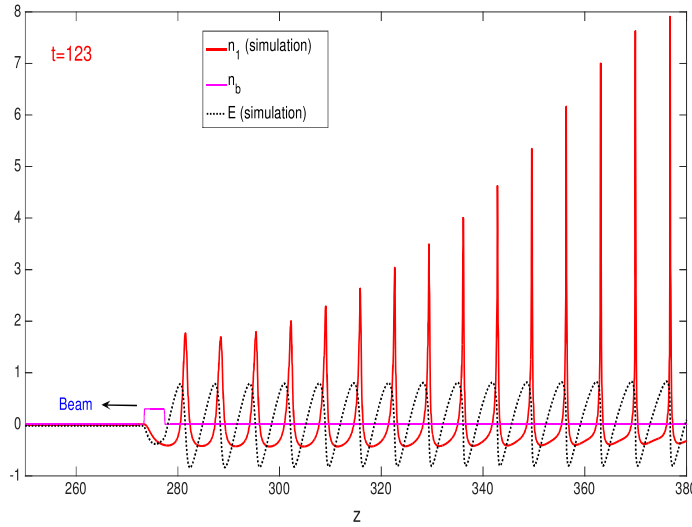


Figure 4.8: Plot of plasma electron density (n_1) at different times $t = 123$ for $\mu = 1/1836$, $n_b = 0.3$, $v_b = 0.99$ and $l_b = 4$.

amplitude of electric field (E_{WB}) for different values of μ , where $n_b = 0.2$, $l_b = 4$ and $v_b = 0.99$. In figure (4.10), we have plotted both numerical and theoretical values of E_{WB} as a function of the mass ratio (μ). It is seen that the wave-breaking limit of numerically excited wake-wave lies much below the analytically estimated limit. Here the wake wave breaks much below the analytical wave breaking limit. In other words, the wake wave breaks before it reaches to its wave breaking amplitude. It is

because of phase mixing process, which arises because of relativistic mass variation effects [85–87]. Physically, the propagation of the non-evolving driver beam inside the cold plasma, excites a wake wave along with small numerical perturbations which are inevitably present in the simulations (and also in a realistic situation). These perturbations result in a slow variation of physical quantities associated with the wake wave and produce a real physical effect which is described by the phase mixing process. Inside the beam, such a phenomenon does not occur as the wake is forced to oscillate at a frequency which is decided by the beam density. These

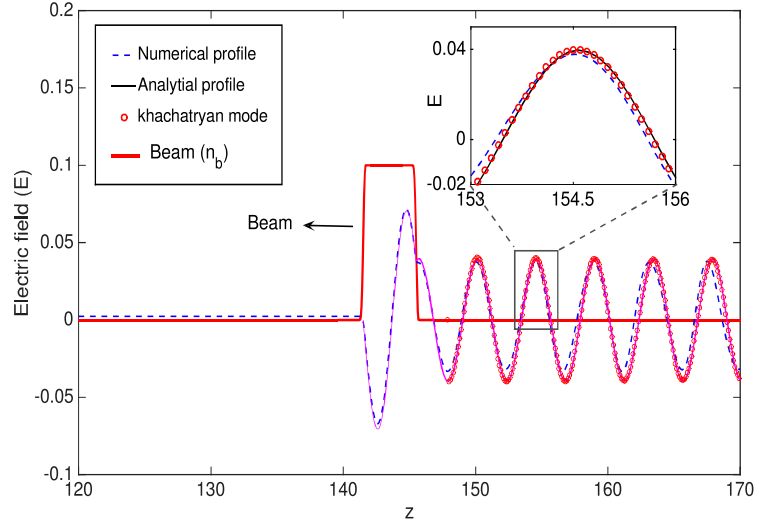


Figure 4.9: Comparison of numerical electric field profile (E) with the analytical and Khachatryan mode for $n_b = 0.1$, $l_b = 4$, $v_b = 0.99$ and $\mu = 1$.

perturbations to the Khachatryan mode, causes the frequency of the wake wave to become a function of position. This is because the frequency of an oscillating electron fluid element depends on relativistic mass (energy) which in turn becomes a function of position because of the perturbations. The spatial dependence of frequency eventually results in the crossing of electron fluid elements resulting in

breaking of the wake wave even in a cold plasma [85–87, 105]. In an earlier work by Ratan et al. [101], for immobile ions, it was shown that the excited wake wave is a corresponding Akhiezer -Polovin (AP) mode [81], before it breaks. In their simulation, the wake breaks in the same way due to numerical fluctuations which perturbs the AP mode and helps to break. For a perturbed Akhiezer-Polovin mode (*i.e.* with immobile ions), the spatial dependence of frequency has been explicitly shown numerically in refs. [87] and analytically in ref. [88]. Therefore, in our simulation for mobile ions, it is clear that the wake wave breaks due to phase mixing process before it reaches its wave breaking limit (E_{WB}). Khachatryan et al. [82] calculated the wave breaking limit without considering the contribution of phase mixing process in their theory.

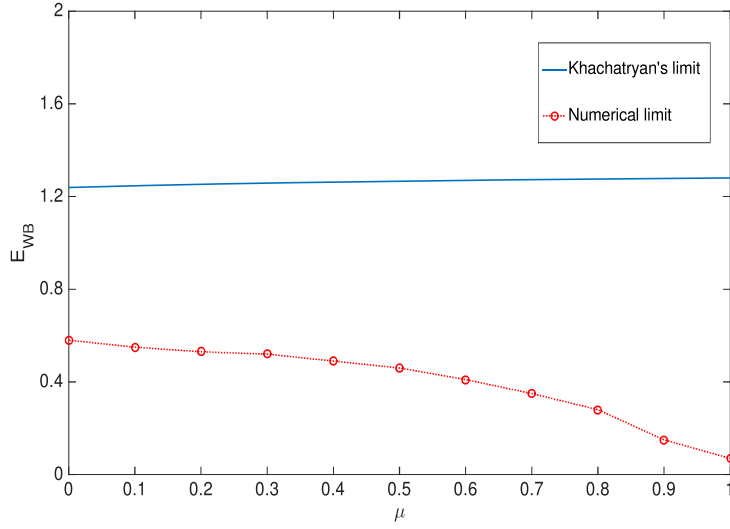


Figure 4.10: Plot of maximum amplitude of wave breaking electric field (E_{WB}) as a function of mass ratio (μ) for $n_b = 0.2$, $l_b = 4$ and $v_b = 0.99$ or $\gamma_{ph} = 7.08$.

Summary

We have studied the excitation relativistic electron beam driven wakefield in a cold plasma using fluid simulation techniques where the effect of ion motion is included. We have shown that simulation results match with the analytical results given by Rosenzweig et al. [80] for different beam density and mass ratio. It is found that the excited wakefield in our simulation is independent of the initial choice of plasma parameters. The excited wakefield ultimately converts to the Rosenzweig's solution, which is unique in nature. We have seen that, for an over-dense beam, the transformer ratio saturates to unity for both the electron-positron and hydrogen plasmas in 1-D. There will be no gain for the over-dense beam. At later times, we have observed that the numerically excited wakefield profile gradually deviates from the analytical result and finally breaks via phase mixing process. We have shown that the excited wake wave is alike to the corresponding Khachatryan's wave [82]. We have numerically obtained the wave breaking limit which is found to be much below the analytically estimated values by Khachatryan et al. [82]. This is so as Khachatryan et al. [82] were ignored the possibility of phase mixing in the analytical work.

5

2-D fluid simulation of relativistic electron beam driven wakefield in a cold plasma

The objective of this chapter ^{} is to investigate 2-D wakefields driven by a relativistic electron beam in cold plasma. A 2-D fully relativistic electromagnetic fluid code has been developed and employed for the excitation of wakefield for several beam configurations over a wide range of beam parameters. The effect of finite transverse beam size on the excitation of 2-D wakefields is investigated. The excitation of blow-out structure which has a key role for generating good quality energetic beam is also presented in this chapter. Further, injecting test electrons in the fluid simulations, the energy gain in the process of acceleration is studied which show a good agreement with the experimental observations.*

^{*} Ratan Kumar Bera, Amita Das, and Sudip Sengupta, *2-D fluid simulation of a rigid relativistic electron beam driven wakefield in a cold plasma*, [arXiv: 1803.00300](#)

Introduction

In plasma wakefield acceleration (PWFA), the charge particles get accelerated by the electric field associated with the plasma wave excited by injecting an ultra-relativistic electron beam in a plasma medium. This scheme offers a most suitable way to boost the energy of the existing linacs. The success of PWFA scheme has been demonstrated in a number of experiments by accelerating charged particles to GeV energies [66,69,72,73]. In terms of theoretical work, till date, both linear and nonlinear theory in 1-D has been well established to examine PWFA scheme for several driver configurations [31,78–80,101,109] (presented in the earlier chapters). The excitation of two-dimensional beam driven wakefield has been studied by several authors only in the linear regime [28,94,95,110]. In the nonlinear regime, the two-dimensional modeling of PWFA has been provided by the work of Lu et al. [96] alone. Their theoretical work was modeled in a quasi-static frame with several approximations which fails to predict the correct form of wakefield near the edge of the blow-out structure after wave breaking. Therefore, in higher dimensions, most of the experimental PWFA results have been guided by the extensive numerical simulations. Till date, most of the simulations have been performed using particle-in-Cell (PIC) techniques e.g. OSIRIS, EPOCH, QUICKPIC etc [64,72,73,84,96–99]. These PIC codes which model plasmas by calculating the trajectories of billions of particles as they respond to external forces and to the forces particles exert on each other work at the most fundamental and microscopic level. These codes are fully explicit, multi-dimensional, fully parallelized, fully relativistic, PIC codes. The simulation using these codes in an ordinary computers are computationally heavy and time-consuming. Therefore powerful computational fa-

cilities are required for an efficient performance working with these sophisticated PIC codes. In this chapter, we therefore seek the possibility of fluid simulations which are much simpler and faster than any sophisticated PIC simulations, to provide a reasonable empirical guidance in PWFA context.

In this chapter, a two-dimensional fluid simulations have been employed to study the excitation of relativistic electron beam driven wakefield in a cold plasma by proposing a two-fluid description of plasma wave excitation. We have performed our simulations for several beam configurations. It is observed that for both under-dense and an over-dense beam having a large transverse extension than the longitudinal extension, the axial profiles of the excited wakefield obtained from our simulation show a good agreement with the 1-D results of Ratan et al. [101]. In the other limit i.e. when the transverse dimensions of the beam are smaller or close to its longitudinal extension, the simulation results deviate considerably from the 1-D results. This study clearly shows that the transverse size of the beam plays an important role in the transformation of electro-static to an electromagnetic nature of the excitation. A 2-D analytical study of the wakefield structure in the linear regime is also presented and compared well with the fluid simulation result for small amplitude excitations. Further, we have performed our simulations for a short, over-dense beam where linear approximations are no longer valid. In this regime, the excitations exhibit a “blowout” structure which is an ion cavity free from cold plasma electron. This arises due to high space-charge force for a short and over-dense beam which evacuates all the plasma electrons from its vicinity and thereby creates a pure ion channel behind. The key features of this ion channel propagating near the speed of light and surrounded by a thin electron sheath

are, i) the mono-energetic electron beam can self-generated, ii) the accelerating gradients are nearly constant and the focusing fields are linear iii) driver beam can propagate many betatron wavelengths without any significant spreading as most of the electrons of the driver propagate in the ion channel. Therefore most of the PWFA experiments are designed in this regime for producing high-quality beams [69,72,73,90,96]. The analytical modeling of the blow-out in a quasi-static frame has already been given by Lu et al. [96] where the surrounding electron sheath has been modeled as a step profiles. In our simulation, we have observed that the excited blowout structure in terms of electric field and density matches with the analytically modeled results of Lu et al. [25,96]. These comparisons are made before the wake wave breaks and fluid simulations subsequent to breaking become irrelevant. The breaking of wake wave has been confirmed with several observations. It is well known that the wake wave breaks when the excursion length of an electron in the wake exceeds the radius of curvature of the blowout [111]. It is indeed seen in the fluid simulations that, after breaking, the excursion length becomes higher than the radius of curvature of the blowout. Another strong observation is that we have observed the simultaneous spiky feature in the density profile which is a clear signature of wave breaking in the fluid simulation. In addition, the wave breaking time has been identified in fluid simulations by tracking the total energy of the system which does not remain conserved after breaking. When the wave breaks, the blowout structure gets destroyed in our fluid simulations as the crossing of the particles/ fluid elements can not be described in fluid theory. However, it is seen that the excitation can survive hundred of plasma periods without any significant deformation for $\frac{n_b}{n_0} \leq 5$. For $n_b > 5$, the blowout breaks and destroys after few plasma periods. In all simulations, we have considered the beam

density in the range, $0 \leq n_b \leq 5$.

Next, we have injected test particles (electrons) in the fluid simulation to estimate the energy gain in the process of acceleration. The fluid simulations are good enough for providing the potential structure in the wake for different beam configurations. Due to the absence of particle characteristics in the fluid model, fluid simulations are irrelevant to predict about energy gain in the process of acceleration. Therefore, we have used test electrons in the fluid simulation for such studies. It is observed that the test electrons from the back of the driver beam of energy 28.5GeV can gain up to a maximum energy of 2.6 GeV in a 10 cm long plasma channel. These results show a good conformity with the experimental results given in ref. [69], where an energy gain of 2.6 GeV in a 10 cm long plasma is shown. This shows the fluid simulations which are much simpler and faster than any sophisticated PIC simulations are pretty adequate representing the wakefield structure and also prove a good estimation of the energy gain in the process of acceleration. Furthermore, we have experimented with the location of injection of the test electrons and observe that the energy gain can be doubled to $\sim 5.2\text{GeV}$ when they were placed near the axial edge of the first blowout potential structure.

Governing Equations

The basic equations governing the excitation of 2-D relativistic electron beam driven wakefield in a cold plasma are the relativistic fluid-Maxwell equations. The equations contain the equation of continuity and the equation of momentum for both plasma electrons and beam electrons. We have used Maxwell's equations

for the evolution of electromagnetic fields. The dynamics of ion have been ignored because of their heavy mass. They only provide a neutralizing background. Therefore, the basic governing equations for the excitation of two-dimensional relativistic electron beam driven wakefield in a cold plasma are,

$$\frac{\partial n}{\partial t} + \vec{\nabla} \cdot (n\vec{v}) = 0 \quad (5.1)$$

$$\frac{\partial \vec{p}}{\partial t} + (\vec{v} \cdot \vec{\nabla})\vec{p} = -e\vec{E} - \frac{e}{c}(\vec{v} \times \vec{B}) \quad (5.2)$$

$$\frac{\partial n_b}{\partial t} + \vec{\nabla} \cdot (n_b\vec{v}_b) = 0 \quad (5.3)$$

$$\frac{\partial \vec{p}_b}{\partial t} + (\vec{v}_b \cdot \vec{\nabla})\vec{p}_b = -e\vec{E} - \frac{e}{c}(\vec{v}_b \times \vec{B}) \quad (5.4)$$

$$(\vec{\nabla} \times \vec{B}) = -\frac{4\pi e}{c}(n\vec{v} + n_b\vec{v}_b) + \frac{1}{c}\frac{\partial \vec{E}}{\partial t} \quad (5.5)$$

$$(\vec{\nabla} \times \vec{E}) = -\frac{1}{c}\frac{\partial \vec{B}}{\partial t} \quad (5.6)$$

$$\vec{\nabla} \cdot \vec{E} = 4\pi e(n_0 - n - n_b) \quad (5.7)$$

$$\vec{\nabla} \cdot \vec{B} = 0 \quad (5.8)$$

where $\vec{p} = m_e\gamma\vec{v}$ and $\vec{p}_b = m_e\gamma_b\vec{v}_b$ is the momentum of plasma electron and beam electron having density n and n_b respectively. Here $\gamma = \left(1 - \frac{v^2}{c^2}\right)^{-1/2}$ and $\gamma_b = \left(1 - \frac{v_b^2}{c^2}\right)^{-1/2}$ is the relativistic factor associated with the plasma electron and beam electron having velocity \vec{v} and \vec{v}_b respectively. In the above equations, \vec{E} and \vec{B} represents the electric and magnetic field respectively. Now, we have made the following replacements in the physical quantities, $t \rightarrow \omega_{pe}t$, $(x, y) \rightarrow \frac{\omega_{pe}(x, y)}{c}$, $\vec{E} \rightarrow \frac{e\vec{E}}{m_e c \omega_{pe}}$, $\vec{B} \rightarrow \frac{e\vec{B}}{m_e c \omega_{pe}}$, $\vec{v} \rightarrow \frac{v}{c}$, $\vec{v}_b \rightarrow \frac{v_b}{c}$, $\vec{p} \rightarrow \frac{\vec{p}}{m_e c}$, $\vec{p}_b \rightarrow \frac{\vec{p}_b}{m_e c}$, $n \rightarrow \frac{n}{n_0}$, and

$n_b \rightarrow \frac{n_b}{n_0}$. Using these normalizations in the above equations (5.1-5.8), we have,

$$\frac{\partial n}{\partial t} + \vec{\nabla} \cdot (n\vec{v}) = 0 \quad (5.9)$$

$$\frac{\partial \vec{p}}{\partial t} + (\vec{v} \cdot \vec{\nabla})\vec{p} = -\vec{E} - (\vec{v} \times \vec{B}) \quad (5.10)$$

$$\frac{\partial n_b}{\partial t} + \vec{\nabla} \cdot (n_b \vec{v}_b) = 0 \quad (5.11)$$

$$\frac{\partial \vec{p}_b}{\partial t} + (\vec{v}_b \cdot \vec{\nabla})\vec{p}_b = \vec{E} - (\vec{v}_b \times \vec{B}) \quad (5.12)$$

$$\frac{\partial \vec{E}}{\partial t} = (n\vec{v} + n_b \vec{v}_b) + (\vec{\nabla} \times \vec{B}) \quad (5.13)$$

$$\frac{\partial \vec{B}}{\partial t} = -(\vec{\nabla} \times \vec{E}) \quad (5.14)$$

$$\vec{\nabla} \cdot \vec{E} = (1 - n - n_b) \quad (5.15)$$

$$\vec{\nabla} \cdot \vec{B} = 0 \quad (5.16)$$

Equations (5.9-5.16) are the key equations to study the 2-D excitation of relativistic electron beam driven wakefield in a cold plasma. We have numerically and analytically (in linear regime) solved the above equations to study the structure of 2-D wakefields.

2-D fluid simulation techniques

In this section, we present the 2-D fluid simulation techniques used for the excitation of relativistic electron beam driven wakefield in a cold plasma. We have solved

the equations (5.9-5.16) using two-dimensional fluid simulation techniques. The equations are solved in 2-D geometry (“x-y” plane) and the electron beam is propagating along x -direction. This means that the excitations are observed at $z = 0$ plane in a cylindrical geometry ($r = \sqrt{y^2 + z^2}$, ϕ , x) having azimuthal symmetry (see figure 5.3). We have developed a fully-explicit, relativistic, electromagnetic fluid code using LCPFCT suite of subroutines based on flux-corrected transport scheme [102]. The one-dimensional LCPFCT subroutines have been used repetitively to construct the 2-D fluid code by splitting the time steps in the different directions (x and y). The detail of the simulation techniques is discussed in the appendix (A.1). In our simulation, we have used non-periodic boundary conditions (open) to retain the form of wake wave at the boundary. Initially, we have introduced the beam at one end of the simulation window which propagates with a velocity along x -direction towards another end. The results have been recorded in terms of the spatial profiles of n , n_b , \vec{v} , \vec{v}_b , \vec{E} , and \vec{B} at each time step. At each time step, it is checked that the results must satisfy the equations (5.15) and (5.16). We have also checked the conservation of energy in the simulation using equation (A.35) (see appendix A.1). We have used this code for several studies e.g. electromagnetic soliton propagation in plasmas, non-linear plasma oscillations, and finite beam-plasma systems. The results have been bench-marked for some standard known results against the widely used Particle-In-Cell code OSIRIS [104, 112].

Simulation results

In this section, we present our numerical observations and a detail discussion based on these observations. The excitation of wakefield is carried out for a bi-Gaussian beam having density profile $n_b = n_{b0} \exp(-\frac{x^2}{2\sigma_x^2}) \exp(-\frac{y^2}{2\sigma_y^2})$; where σ_x and σ_y repre-

sents the length of beam along longitudinal and transverse directions respectively. In all the simulations, the evolution of the beam has been excluded. Therefore, the beam is moving with a constant velocity inside the plasma. In this limit, the equation (5.12) for the evolution of the beam in a self-consistent manner has been ignored. The propagation of the beam having a constant velocity has been taken into account by solving the continuity equation (5.11). Therefore the beam propagates inside the plasma as a rigid piston. For an electron beam case, the driver evolves on a length scale roughly given by the Betatron wavelength, which is $2\pi\sqrt{2\gamma_b}$ for a beam particle in an ion channel. Therefore the rigid beam approximation is valid for a sufficiently energetic beam i.e. $\gamma_b \gg 1$. In our simulations, the relativistic factor of the beam γ_b is indeed much larger as the velocity of the beam $v_b \geq 0.9999$, very close to the speed of light. This fact has been discussed in several earlier works [25, 101, 109]. Thus we have ignored the self-consistent evolution of the driver in the time scale of wakefield generation. Below we present our simulation results studying different aspects of relativistic electron beam driven wakefield excitation.

Effect of finite transverse beam size

In this section, we have performed our simulations for different beam length ratios which are defined as $l_s = \sigma_x/\sigma_y$, the ratio of longitudinal beam length to transverse beam length. Fig. (5.1) and (5.2) shows the excited wakefield profiles in terms of electron density (n), longitudinal electric field (E_x), and z -component of magnetic field (B_z) for $l_s = 0.5/\sqrt{15} = 0.129 < 1$ and $l_s = \sqrt{15}/0.5 = 4.4 > 1$ respectively; where the peak density of the beam $n_{b0} = 0.1$ and velocity $v_b = 0.9999$ in both the cases.

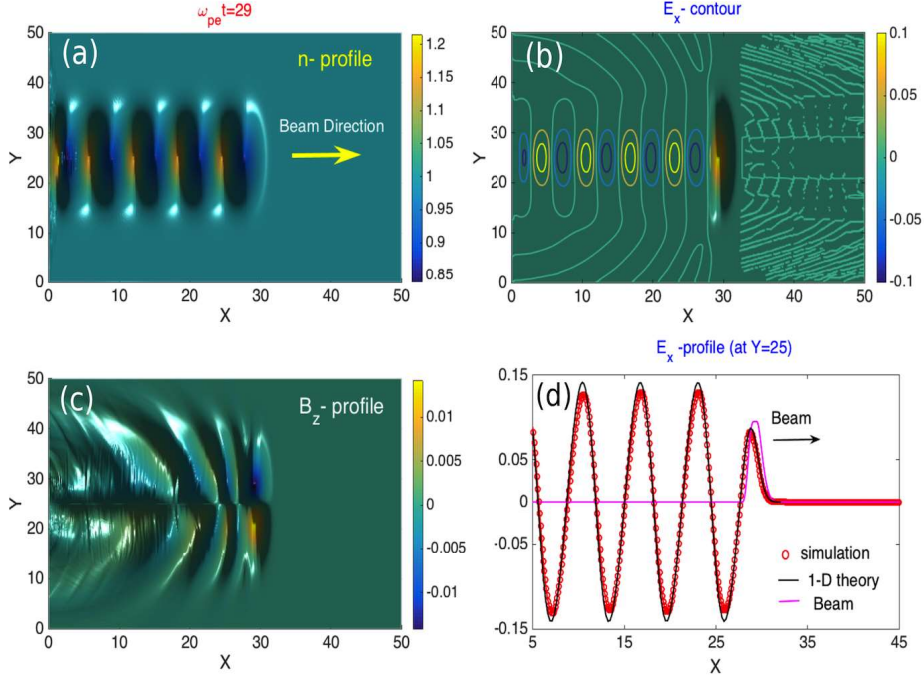


Figure 5.1: Plot of (a) normalized electron density (n), (b) contour of longitudinal electric field (E_x), (c) z - component of magnetic field (B_z) profile, (d) axial profile of analytical (solid black) and numerical (circle) longitudinal electric field at $\omega_{pe} t = 29$ for a bi-Gaussian beam of normalized peak density (n_{b0})=0.1, beam velocity (v_b)=0.9999, $\sigma_x = 0.5$ and $\sigma_y = \sqrt{15}$.

The last sub-plots (d) of these figures (5.1-5.2) show the axial profile of longitudinal electric field (E_x) obtained from our 2-D simulation by integrating along the transverse directions and the 1-D profile given in ref. [101] for the same values of the beam parameters. It is seen that the simulation results match with the 1-D results for $l_s < 1$ and deviate for $l_s > 1$. It indicates that, for a beam having a small transverse extension compared to its longitudinal length, the effect of transverse magnetic field plays an important role. The transverse magnetic field bends the motion of the electrons. Hence the charge separation decreases in the longitudinal direction and we observe a significant suppression in the amplitude

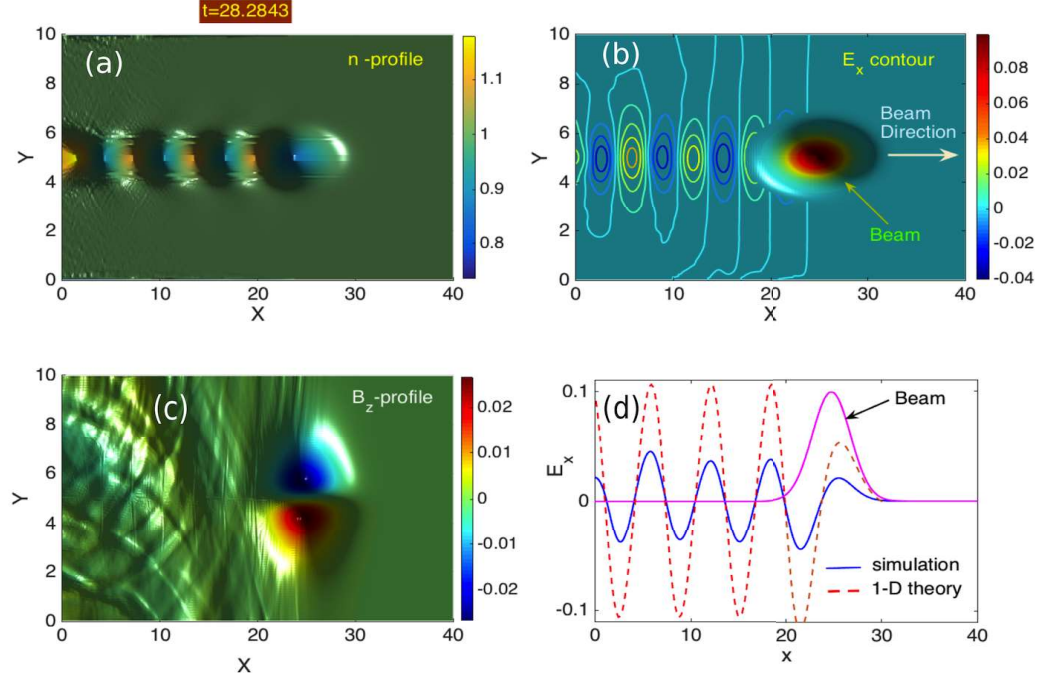


Figure 5.2: Plot of (a) normalized electron density (n), (b) contour of longitudinal electric field (E_x), (c) z - component of magnetic field (B_z) profile, (d) axial profile of analytical (solid black) and numerical (circle) longitudinal electric field at $\omega_{pe}t = 28.28$ for a bi-Gaussian beam of normalized peak density (n_{b0})=0.1, beam velocity (v_b)=0.9999, $\sigma_x = \sqrt{5}$ and $\sigma_y = 0.5$.

of the longitudinal electric field in 2-D than that obtained from 1-D theory. To examine the numerical structure of the 2-D wakefields, we present an analytical solution of wakefields in the next section.

2-D linear theory of electron beam driven wakefields

An analytical solution of relativistic electron beam driven wakefields in the linear regime (i.e. $n_b \ll 1$) is presented in this section. The analytical solutions are obtained in cylindrical co-ordinate (r, θ, x) system, where $r = \sqrt{y^2 + z^2}$ and $\theta = \tan^{-1}(\frac{z}{y})$ represents the radial and azimuthal coordinates corresponding to

cartesian co-ordinates (x, y, z) (see figure 5.3).

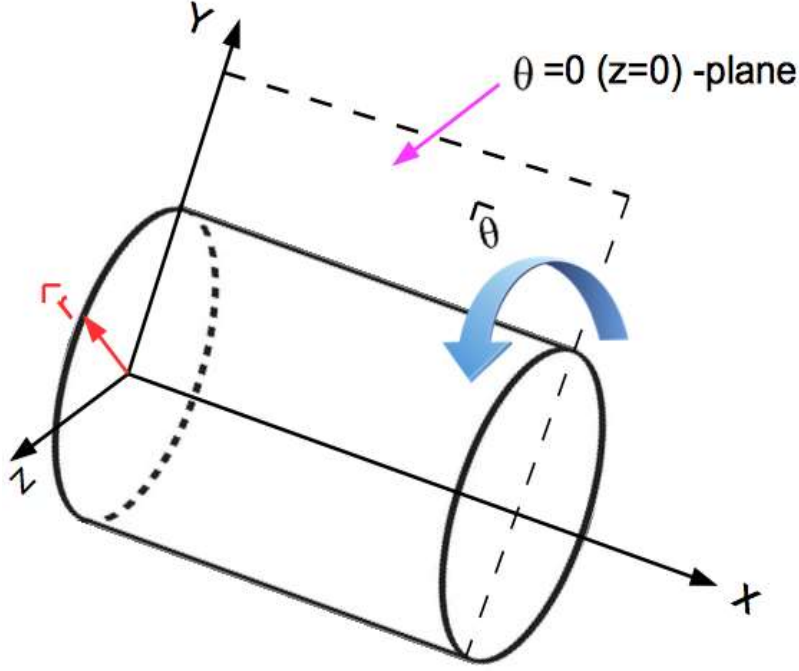


Figure 5.3: A schematic diagram of slab representation for cylindrical geometries.

We have also considered the azimuthal (θ) symmetry in the derivation i.e. $\partial/\partial\theta \equiv 0$. In the frame, $(\xi = x - v_b t, r)$ and $v_b = 1$, the beam exists in the region $-\xi_f \leq \xi \leq 0$ (see figure (5.4)); where $\xi_f = 2\pi l_b/\lambda_p$ defines the value of ξ at the tail of the beam and $\lambda_p = \frac{c}{\omega_{pe}}$ is the skin depth of the plasma. In this frame (ξ, r) , the fluid-Maxwell equations (5.9-5.16) inside the beam can be reduced to the following set of equations (see appendix (A.3) for detail derivation).

$$\partial_\xi^2 n_1^{in}(\xi, r) + n_1^{in}(\xi, r) = -n_b(\xi, r) \quad -\xi_f \leq \xi \leq 0 \quad (5.17)$$

$$(\nabla_r^2 - 1)(A_{1x}^{in} - \phi_1^{in}) = -n_1^{in} \quad -\xi_f \leq \xi \leq 0 \quad (5.18)$$

where $n^{in} = n^{in} - 1$, ϕ_1^{in} and A_{1x}^{in} represents the normalized perturbed values of plasma density (n) scalar potential (ϕ^{in}) and x -component of vector potential (A^{in}) inside the beam respectively. Clearly, the profile of $n_1(\xi, r) = 0$, $\vec{v}(\xi, r) = 0$, $\vec{E}(\xi, r) = 0$ and $B(\xi, r) = 0$, at the front of the beam ($\xi > 0$), as the beam propagates equal to the speed of light. The solution of the above equation (5.17)

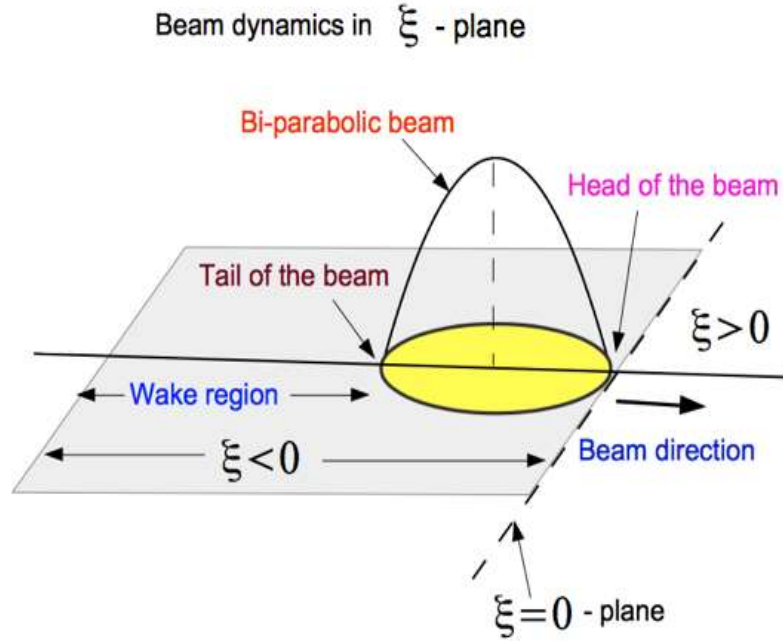


Figure 5.4: A schematic diagram of beam dynamics in (ξ, r) -plane.

for a given n_b provides the form of perturbed plasma density $n_1^{in}(\xi, r)$ inside the beam $-\xi_f \leq \xi \leq 0$. Substituting the form of n_1^{in} in the R.H.S of the equation (5.18) and then integrating, the solution of $(A_{1x}^{in} - \phi_1^{in})$ can be obtained inside the beam. Using the expression of $(A_{1x}^{in} - \phi_1^{in})$, the longitudinal electric field (E_{1x}^{in}) inside the beam is then calculated from the following equation.

$$E_{1x}^{in} = \frac{\partial}{\partial \xi}(A_{1x}^{in} - \phi_1^{in}) \quad (5.19)$$

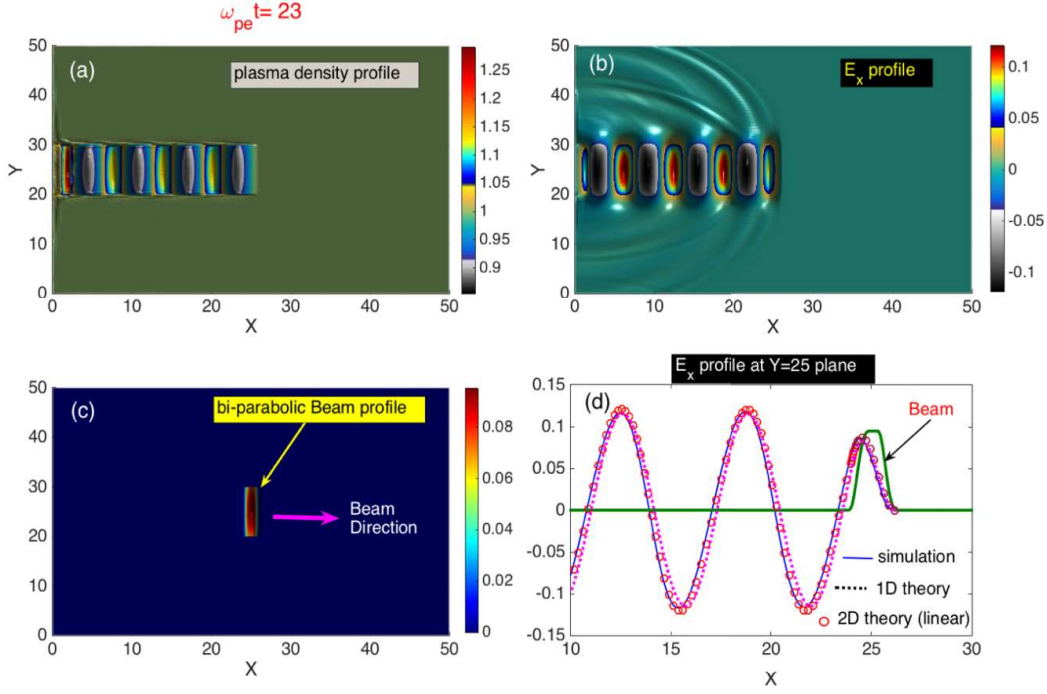


Figure 5.5: Plot of (a) normalized electron density (n), (b) longitudinal electric field (E_x), (c) beam profile, (d) profile of analytical (solid black) and numerical (circle) Axial profile of longitudinal electric field at $\omega_{pe} t = 23$ for a bi-parabolic beam of normalized peak density (n_{b0})=0.1, beam velocity (v_b) =0.9999, $b = 0.5$ and $a = \sqrt{15}$.

At the wake of the beam ($-\infty \leq \xi \leq -\xi_f$), the equations (5.17) and (5.18) can be re-written as,

$$\partial_{\xi}^2 n_1^{wake}(\xi, r) + n_1^{wake}(\xi, r) = 0; \quad -\infty \leq \xi \leq -\xi_f \quad (5.20)$$

$$(\nabla_r^2 - 1)(A_{1x}^{wake} - \phi_1^{wake}) = -n_1^{wake}; \quad -\infty \leq \xi \leq -\xi_f \quad (5.21)$$

It is to be noted that the solution of the equation (5.21) depends on the the form of n_1^{wake} outside the beam which is obtained from equation (5.20) with a proper boundary conditions. The longitudinal field (E_{1x}^{wake}) is then obtained from,

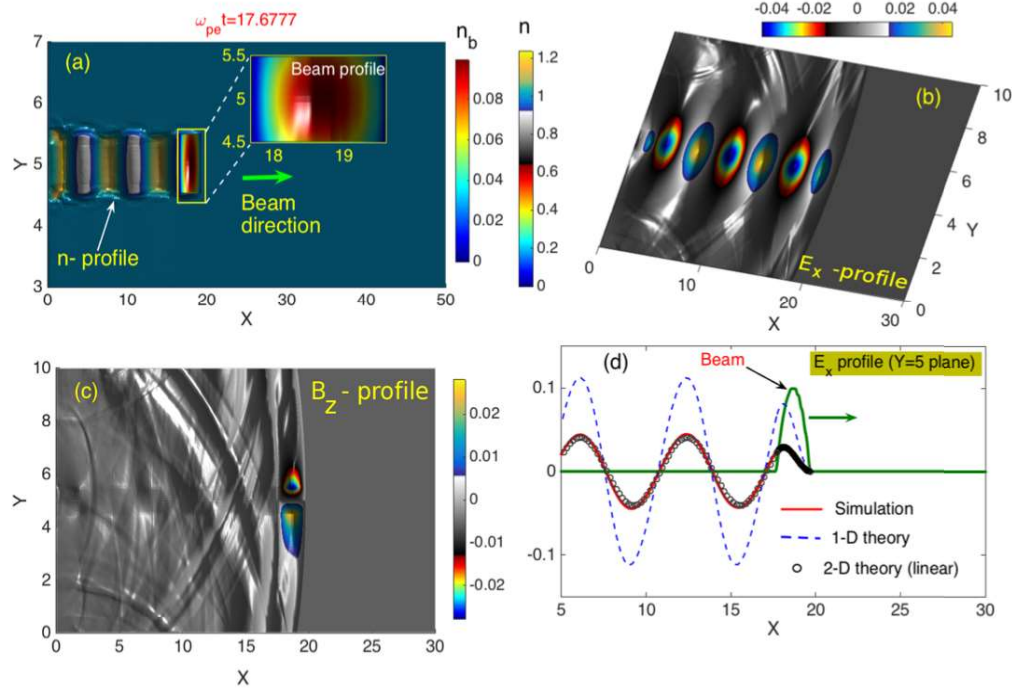


Figure 5.6: Plot of (a) normalized electron density (n), (b) longitudinal electric field (E_x), (c) z - component of magnetic field (B_z) profile, (d) Axial profile of analytical (solid black) and numerical (circle) longitudinal electric field at $\omega_{pe}t = 17$ for a bi-parabolic beam of normalized peak density (n_{b0})=0.1, beam velocity (v_b) =0.9999, $b = \sqrt{5}$ and $a = 0.5$.

$$E_{1x}^{wake} = \frac{\partial}{\partial \xi} (A_{1x}^{wake} - \phi_1^{wake}) \quad (5.22)$$

The solutions of equations (5.17)-5.22) represent the analytical form of perturbed plasma density and longitudinal electric field both inside and outside the beam. Now we assume the separation of variables in n_b as following,

$$n_b(\xi, r) = n_{b0}g(\xi)f(r); \quad -\xi_f \leq \xi \leq 0 \quad (5.23)$$

Substituting the form of n_b in equation (5.17), we get,

$$\partial_\xi^2 n_1^{in}(\xi, r) + n_1^{in}(\xi, r) = -n_{b0}g(\xi)f(r) \quad -\xi_f \leq \xi \leq 0 \quad (5.24)$$

The solution of the above equation can be written as (see appendix A.4.1),

$$n_1^{in} = -n_{b0}f(r) \int_\infty^\xi d\xi' g(\xi') \sin(\xi - \xi'); \quad -\xi_f \leq \xi \leq 0 \quad (5.25)$$

Here $\sin(\xi - \xi')$ is the Green's function corresponding to equation (5.24). As $\xi = x - v_b t$, therefore ξ' has to be started from ∞ to ξ . The Green's function goes to zero for $\xi' > \xi$. Therefore, the solution of the equation (5.25) takes the following form,

$$n_1^{in} = -n_{b0}f(r) \int_\xi^\infty g(\xi') \sin(\xi' - \xi) d\xi' = -n_{b0}f(r)G(\xi); \quad -\xi_f \leq \xi \leq 0 \quad (5.26)$$

It is to be noted that the change in the lower limit in the integral implies the causality in the system; forces applied in the future can not affect the solution at any moment. However, at the front of the beam ($\xi > 0$), the perturbed plasma density $n_1(\xi, r) = 0$, as the perturbation can not travel more than speed of light. Therefore, the solution of $G(\xi)$ can be written as,

$$G(\xi) = \int_\xi^0 g(\xi') \sin(\xi' - \xi) d\xi'$$

Therefore, the form of the perturbed plasma density inside the beam is,

$$n_1^{in} = -n_{b0}f(r) \int_\xi^0 g(\xi') \sin(\xi' - \xi); \quad -\xi_f \leq \xi \leq 0 \quad (5.27)$$

Substituting the form of n_1^{in} in the equation (5.18), we get,

$$(\nabla_r^2 - 1)(A_{1x}^{in} - \phi_1^{in}) = -n_{b0}f(r)G(\xi); \quad -\xi_f \leq \xi \leq 0 \quad (5.28)$$

The solution of the above equation (5.28) can be written as,

$$(A_{1x}^{in} - \phi_1^{in}) = -n_{b0}G(\xi)F(r); \quad -\xi_f \leq \xi \leq 0 \quad (5.29)$$

Where $F(r) = \int_0^r r' f(r') I_0(r') K_0(r) dr' + \int_r^\infty r' f(r') I_0(r) K_0(r') dr'$. Here I_0 and K_0 represents modified Bessel function of first and second kind respectively (see appendix A.4.2 for detail derivation). Therefore, the longitudinal field inside the beam is,

$$E_{1x}^{in} = -n_{b0} \frac{\partial G(\xi)}{\partial \xi} F(r) \quad (5.30)$$

At the wake of the beam, the solution of the equation (5.20) can be written as,

$$n_1 = A(r) \sin(\xi) + B(r) \cos(\xi) \quad -\infty \leq \xi \leq -\xi_f \quad (5.31)$$

where $A(r)$ and $B(r)$ are the integration constants. It is to be noted that the plasma density (n_1) and the derivative of the plasma density w.r.t. ξ , $\frac{dn_1}{d\xi}$ has to be continuous at the end of the beam $\xi = -\xi_f$. Therefore, we have the following boundary conditions.

$$n_1^{wake}(-\xi_f, r) = n_1^{in}(-\xi_f, r)$$

$$\partial_\xi n_1^{wake}(-\xi_f, r) = \partial_\xi n_1^{in}(-\xi_f, r)$$

Using these two conditions, we get,

$$A(r)\sin(-\xi_f) + B(r)\cos(-\xi_f) = -n_{b0}f(r)G(-\xi_f)$$

$$A(r)\cos(-\xi_f) - B(r)\sin(-\xi_f) = -n_{b0}f(r)G'(-\xi_f)$$

Solving the above equations of $A(r)$ and $B(r)$, we get,

$$A(r) = -n_{b0}f(r)(G(-2b)\sin(-2b) + G'(\xi_f)\cos(-2b)) \quad (5.32)$$

$$B(r) = -n_{b0}f(r)(G(-\xi_f)\cos(-\xi_f) - G'(-\xi_f)\sin(-\xi_f)) \quad (5.33)$$

Substituting the form of n_1^{wake} in equation (5.21), we have,

$$(\nabla_r^2 - 1)(A_{1x}^{wake} - \phi_1^{wake}) = -n_{b0}f(r); \quad -\infty \leq \xi \leq -\xi_f \quad (5.34)$$

The solution of the above equation is therefore,

$$(A_{1x}^{wake} - \phi_1^{wake}) = M(r)\sin(\xi) + N(r)\cos(\xi); \quad -\infty \leq \xi \leq -\xi_f \quad (5.35)$$

where $M(r)$ and $N(r)$ can be obtained from,

$$M(r) = -n_{b0}F(r)(G(-2b)\sin(-2b) + G'(\xi_f)\cos(-2b)) \quad (5.36)$$

$$N(r) = -n_{b0}F(r)(G(-\xi_f)\cos(-\xi_f) - G'(-\xi_f)\sin(-\xi_f)) \quad (5.37)$$

The exact analytical solution is obtained here for a bi-parabolic beam having density $n_b = n_{b0}(1 - \frac{(\xi+b)^2}{b^2})(1 - \frac{r^2}{a^2}) = n_{b0}g(\xi)f(r)$; where a and b defines the extension of the beam along ξ and r respectively. In (ξ, r) frame, the beam thus exists in

the region $-2b \leq \xi \leq 0$, where the peak of the beam density is located at $\xi = -b$. Therefore, the form of $G(\xi)$ can be written as,

$$G(\xi) = \int_{\xi}^0 \left(1 - \frac{(\xi + b)^2}{b^2}\right) \sin(\xi' - \xi) d\xi'$$

Integrating the above equation of $G(\xi)$, we have,

$$G(\xi) = \left(1 - \frac{(\xi + b)^2}{b^2}\right) + \frac{2}{b} \sin(\xi) + \frac{2}{b^2} (1 - \cos(\xi)) \quad (5.38)$$

Finally, the form of n_1^{in} for the bi-parabolic beam inside the beam ($-2b \leq \xi \leq 0$) can be written as,

$$n_1^{in} = -n_{b0} \left(1 - \frac{r^2}{a^2}\right) \times \left[\left(1 - \frac{(\xi + b)^2}{b^2}\right) + \frac{2}{b} \sin(\xi) + \frac{2}{b^2} (1 - \cos(\xi)) \right] \quad -2b \leq \xi \leq 0 \quad (5.39)$$

The form of $F(r)$ can be obtained by integrating the following equation,

$$F(r) = \int_0^r r' \left(1 - \frac{r'^2}{a^2}\right) I_0(r') K_0(r) dr' + \int_r^a r' \left(1 - \frac{r'^2}{a^2}\right) I_0(r) K_0(r') dr'$$

The solution of the above equation is,

$$F(r) = 2 \left[I_0(r) K_0(a) + \frac{1}{2} \left(1 - \frac{r^2}{a^2}\right) - \frac{2}{a^2} \right]$$

Substituting the form of $F(r)$ in equation (5.29), we have,

$$\begin{aligned} (A_{1x}^{in} - \phi_1^{in}) = & -2n_{b0} \left(\left(1 - \frac{(\xi+b)^2}{b^2}\right) + \frac{2}{b} \sin(\xi) + \frac{2}{b^2} (1 - \cos(\xi)) \right) \\ & \times \left[I_0(r) K_0(a) + \frac{1}{2} \left(1 - \frac{r^2}{a^2}\right) - \frac{2}{a^2} \right] \quad -2b \leq \xi \leq 0 \end{aligned} \quad (5.40)$$

The longitudinal electric field inside the beam is,

$$E_{1x}^{in} = \frac{\partial}{\partial \xi}(A_{1x}^{in} - \phi_1^{in}) = 2n_{b0} \left[I_0(y)K_0(a) + \frac{1}{2}(1 - \frac{y^2}{a^2}) - \frac{2}{a^2} \right] \times \left[(-\frac{2(\xi+b)}{b^2}) + \frac{2}{b}\cos(\xi) + \frac{2}{b^2}\sin(\xi) \right] \quad -2b \leq \xi \leq 0 \quad (5.41)$$

Using the form of $G(\xi)$ and $F(r)$, one can easily derive the exact form of $A(r)$, $B(r)$, $M(r)$ and $N(r)$ from equations (5.32, 5.33, 5.36, and 5.37). The perturbed plasma density and the longitudinal electric field at wake can be written as,

$$n_1^{wake} = A(r)\sin(\xi) + B(r)\cos(\xi) \quad -\infty \leq \xi \leq -2b \quad (5.42)$$

$$E_{1x}^{wake}(\xi, r) = \frac{\partial}{\partial \xi}(A_{1x} - \phi_1) = M(r)\cos(\xi) - N(r)\sin(\xi) \quad -\infty \leq \xi \leq -2b \quad (5.43)$$

We have also performed fluid simulations using a bi-parabolic beam for different beam length ratios. The simulation results are shown in (5.5) and (5.6) for $l_s = \frac{b}{a} = 0.129 < 1$ and $l_s = \frac{b}{a} = 4.4 > 1$ respectively; where $n_{b0} = 0.1$ and $v_b = 0.9999$ in both the cases. In the last subplots of figs.(5.5 (d)) and (5.6 (d)), we have plotted the axial profile ($y = 0$ plane) of longitudinal electric field obtained from our simulation along with the 2-D linear analytical profile obtained from equations (5.41) and (5.43) at $r = 0$ and 1-D theoretical profiles given in ref. [101]. For the 1-D results, the equation (8) and equation (8) for $\alpha = 0$ given in ref. [101], are solved numerically for a bi-parabolic beam profile; where α is the beam density. We have observed that the 2-D results obtained from our simulation match with the 2-D theoretical results for any arbitrary values of b/a . This validates our simulation result for the excitation of relativistic electron beam driven wakefield in a cold plasma. An interesting observation has been made for a beam having

$\frac{b}{a} \geq 1$ (see figure 5.6). In this particular case, the longitudinal electric field profile obtained from 2-D theory which also matches with the simulation results deviates from 1-D result. This certainly concludes that the finite transverse size of the beam plays an important role in the excitation. For a beam having transverse size larger than the longitudinal extension, the excitation acquires electrostatic characteristics. Whereas, excitations exhibit electromagnetic characteristics for a beam having transverse size smaller or equal to the longitudinal extension. Due to finite transverse size, the electric fields acquires curvature leading to the appearance of the transverse magnetic fields. These transverse magnetic fields restrict the movement electrons longitudinally and hence the longitudinal charge separation decreases. Therefore, the amplitude of the longitudinal electric field decreases.

Fluid simulation in the blowout regime

Here we present the excitation of wakefield for a beam density larger than the background plasma density. In figure (5.7), we plot the excitation of wakefield in terms of longitudinal electric field and perturbed plasma density for $n_{b0} = 1$, $v_b = 0.9999$, $\sigma_x = \sqrt{2}$ and $\sigma_y = 0.4$. It is observed that the excitation exhibits blowout structure in the simulation.

Fig (5.8) shows the excitation for $n_{b0} = 1$, $v_b = 0.9999$, $\sigma_x = \sqrt{2}$ and $\sigma_y = 1$ where we have also plotted the analytical profile of longitudinal electric field and corresponding curve of blowout radius obtained from the analytical modeled results presented in ref. [96]. In Fig (5.9), we have plotted the excitation for $n_{b0} = 7$, $v_b = 0.9999$, $\sigma_x = \sqrt{2}$ and $\sigma_y = 1$ and the corresponding analytical curve of blowout radius obtained from [96]. The analytical blowout curve and longitudinal electric field profile are obtained by solving the equations (46) and (47) given in

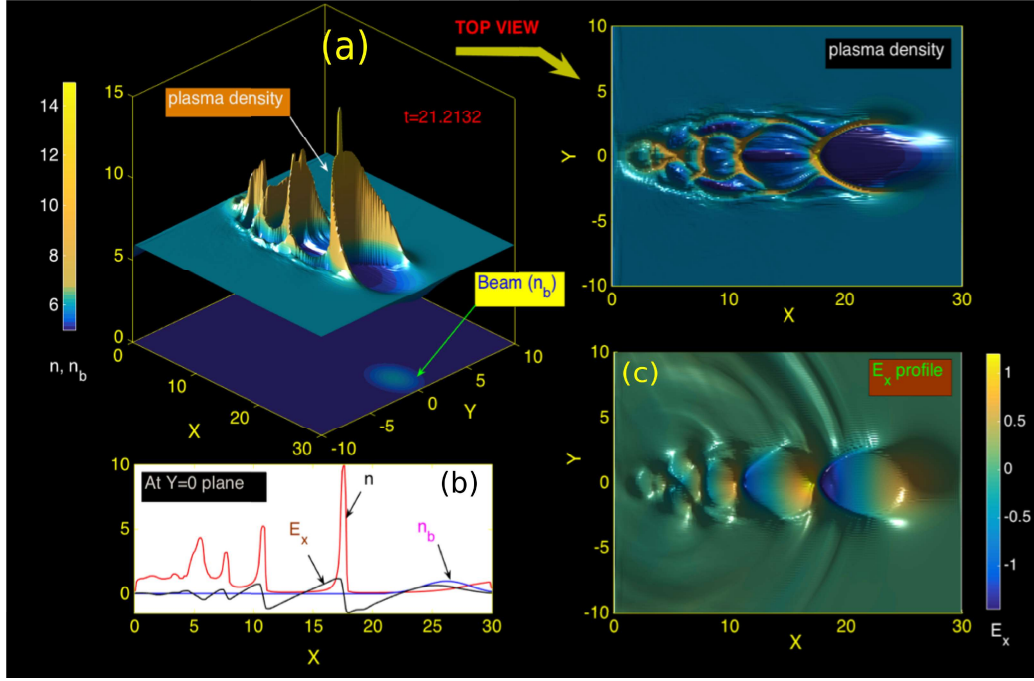


Figure 5.7: Plot of (a) normalized plasma electron density (n) profile, (b) axial profile of density, electric longitudinal electric field (E_x) profile for a bi-Gaussian beam of normalized peak density (n_{b0})=1, beam velocity (v_b)=0.9999, $\sigma_x = \sqrt{1}$ and $\sigma_y = 0.4$ at $t = 21.21$.

ref. [96], using the same parameter values. It is seen that our simulation results show a good agreement with the analytical results. However, for a beam density $n_{b0} = 7$, $v_b = 0.9999$, $\sigma_x = \sqrt{2}$ and $\sigma_y = 0.4$, the numerical results deviate from analytical theory after several plasma periods (see fig.(5.10)). This size of the excited blowout structure gradually increases and eventually destroys exhibiting sharp spikes in the density profile and sawtooth-like structures in the electric field profile, after several plasma periods ($\sim t = 8$). This is a clear signature of wave breaking [85–88]. It is well known that the wake wave breaks when the excursion length exceeds the value of the radius of curvature [111]. In fig. (5.10), it is clear that the wave first breaks at the axial edge of the blowout. We have calculated

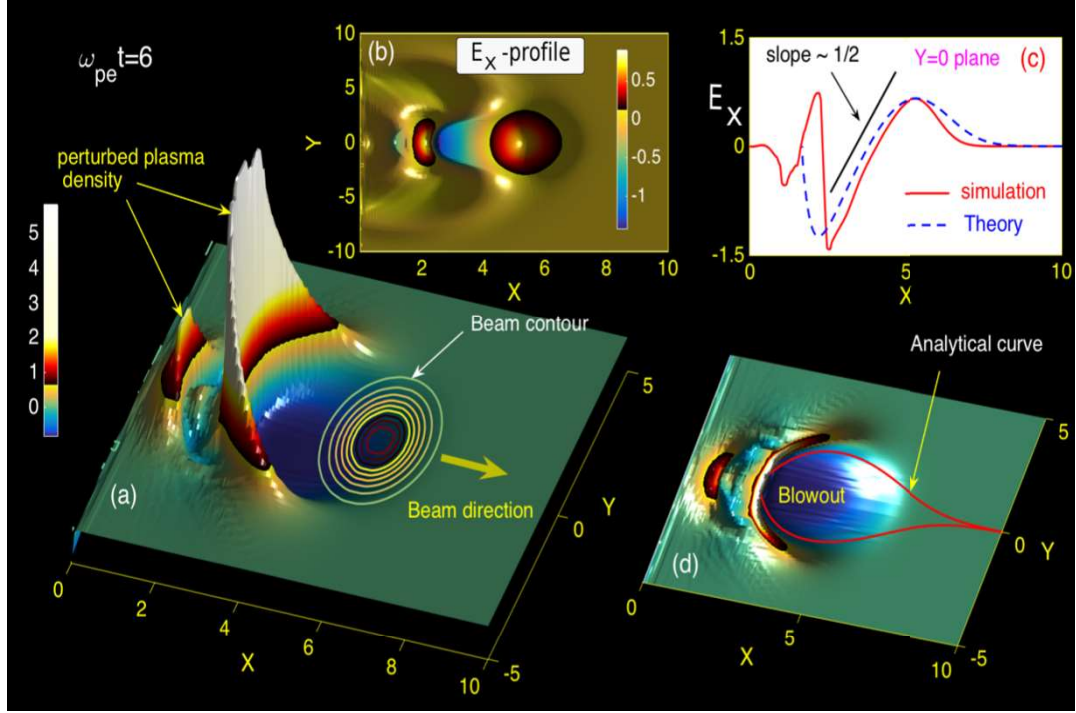


Figure 5.8: Plot of (a) normalized perturbed electron density (n_1) profile, (b) longitudinal electric field (c) axial profile of analytical and numerical longitudinal electric field profile (d) analytical obtained blowout curve (red line) for a bi-Gaussian beam of peak density (n_{b0})=1, beam velocity (v_b) =0.9999, $\sigma_x = \sqrt{2}$ and $\sigma_y = 1$ at $\omega_{pe}t = 6$.

the value of the radius of curvature $R = 3.5$ at the axial edge of the blowout by fitting a circle. The excursion length is defined as $l_e = \frac{E_{max}}{\omega^2}$; where E_{max} and ω is the maximum electric field at the blowout and the characteristic frequency of the wake [113]. Before the wave breaking time i.e. at $t = 2.8$, the values of maximum electric field $E_{max} = 2.9$ and $\omega \sim \omega_{pe}$. This implies that the excursion length $l_e = \frac{E_{max}}{\omega^2} = 2.9$ is less than the radius of the curvature R . After the wake breaks at $t = 8$, the maximum amplitude of the electric field increases to $E_{max} = 4.2$. Therefore the excursion length $l_e = \frac{E_{max}}{\omega^2} = 4.2$ becomes higher than the radius of the curvature R . We have also found that, in fluid simulation, the total energy

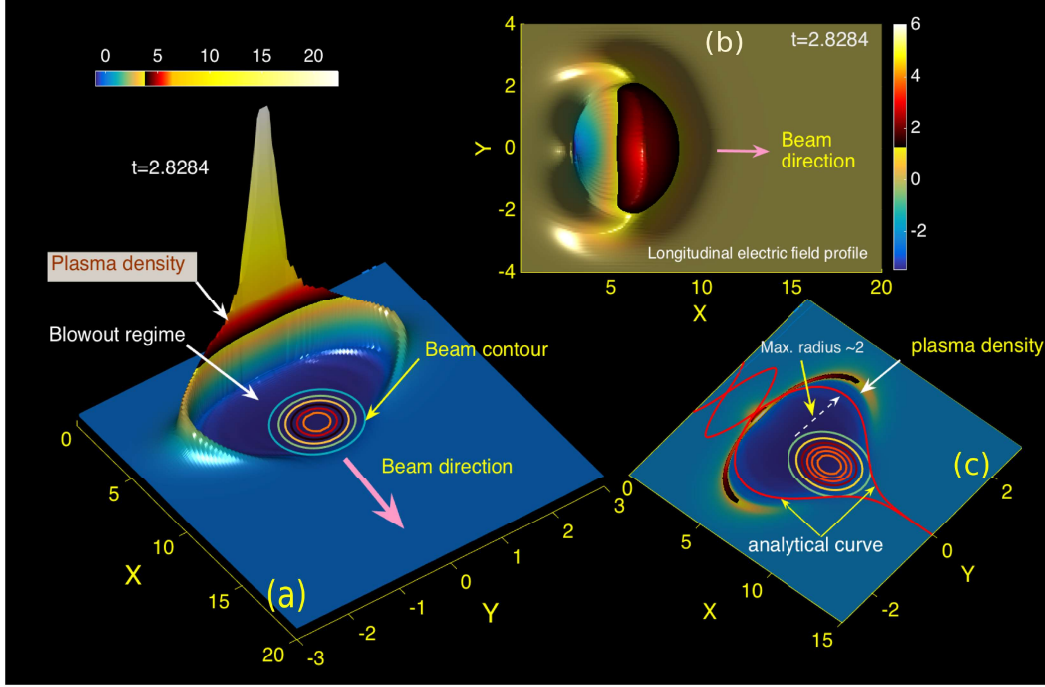


Figure 5.9: Plot of (a) normalized perturbed electron density (n_1) profile and (b) longitudinal electric field profile (c) analytically obtained blowout curve for a bi-Gaussian beam of peak density (n_{b0})=7, beam velocity (v_b)=0.9999, $\sigma_x = \sqrt{2}$ and $\sigma_y = 1$ at $\omega_{pe}t = 2.8$.

drops down after the wave breaking as shown in Fig. (5.11). This happens because wave breaking results in transfer of energy to high wave number which can not be resolved by the grid. The fluid description does not remain valid after breaking. However, in fluid simulation, it is observed that for a beam density $n_{b0} \leq 5$, the blowout can survive several plasma periods without any significant deformation.

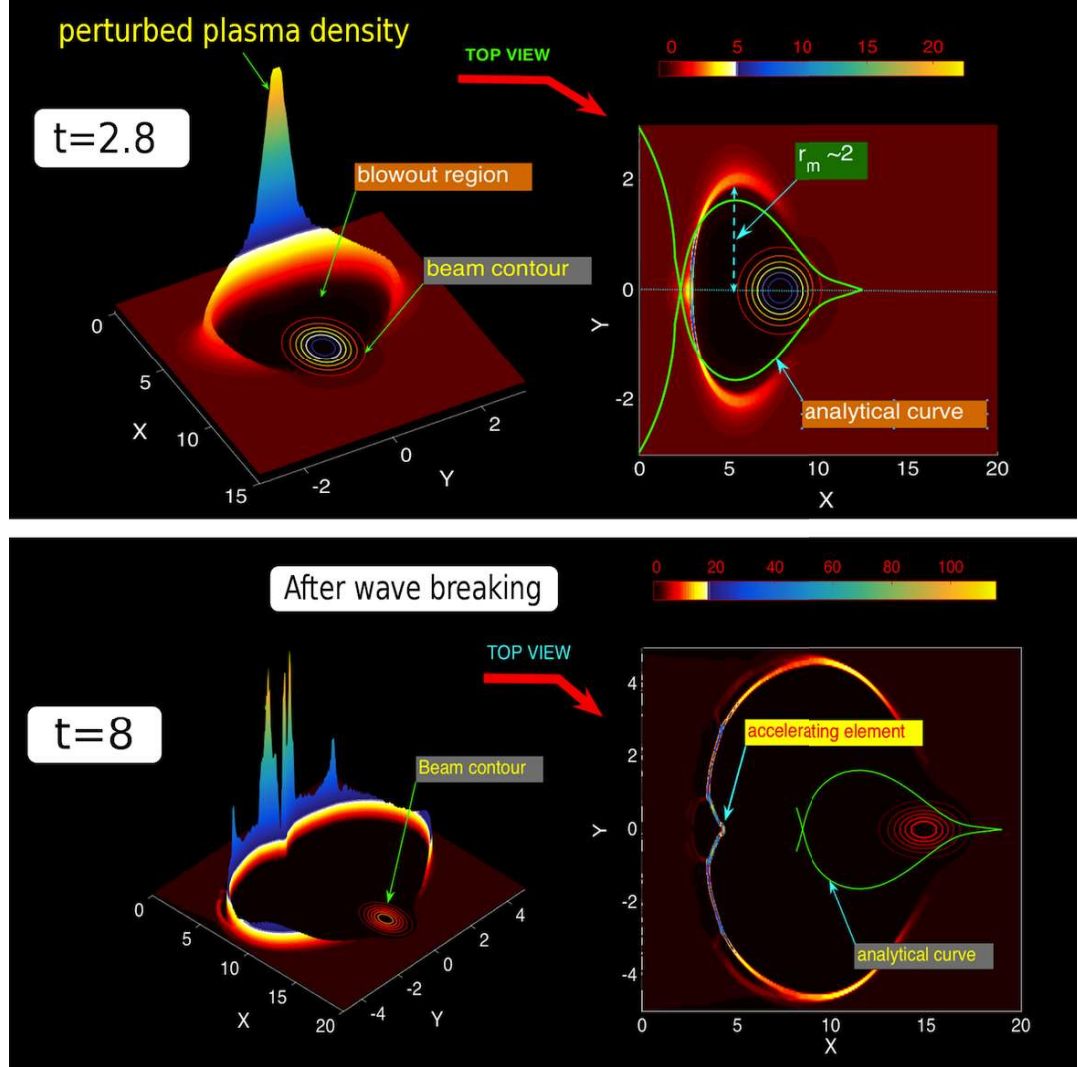


Figure 5.10: Plot of normalized perturbed electron density (n_1) profile and analytical obtained blowout curve (solid green line) for a bi-Gaussian beam having peak density (n_{b0})=7, beam velocity (v_b)=0.9999, $\sigma_x = \sqrt{2}$ and $\sigma_y = 1$ at different times $\omega_{pe}t = 2.8$ and $\omega_{pe}t = 8$.

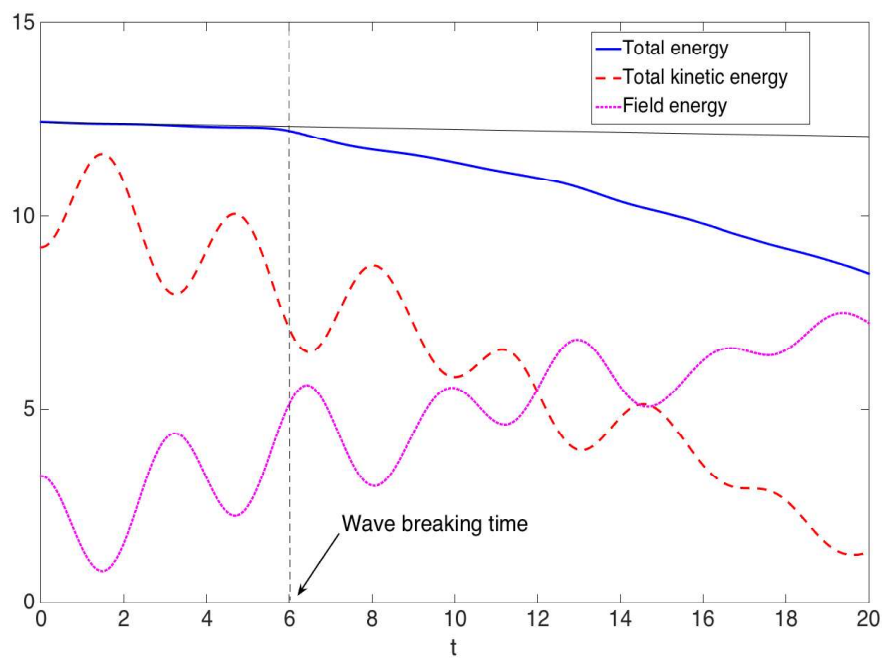


Figure 5.11: Plot of normalized values of total energy, kinetic energy and field energy vs. time for the normalized beam density $(n_b)=7.0$, $\sigma_x = \sqrt{2}$ and $\sigma_y = 1$.

Test particle simulation

In this section, we have performed the test particle (electron) simulation to study the energy gain in the process of acceleration. Test electrons are introduced into the fluid simulation and studied their distribution of energy at different times. The dynamics of the test electron are determined by the equation of motion, $\frac{d\vec{p}_i}{dt} = -\vec{E} - (\vec{v}_i \times \vec{B})$; where $p_i = v_i(1 - v_i^2)^{-1/2}$ is the momentum of i -th electron having velocity v_i . The basic principle for advancing the position and velocity of the test particle in time is based on the Boris pusher algorithm [114]. The self-consistent effect of test electrons on the wakefield has been ignored. The detail of the simulation techniques is presented in the appendix (A.5).

In our first numerical experiment (shown in (5.12)), we have randomly distributed 10000 electrons having initial velocity $\vec{v}_0(t = 0) = 0$ (extremely cold electrons) in all over the simulation box. The beam having $n_{b0} = 3$, $\sigma_x = \sqrt{2}$, $\sigma_y = 1$, and $v_b = 0.99999999$ propagates from one end to other end and creates the wakefield in the plasma. The potential of the wake exhibiting the blowout structure traps the nearby test electrons which get thereby accelerated to high energies. The trapped electrons gain energy by the electric field in the blowout and propagate near the speed of light. We have plotted the velocity distribution function of these particles at $t = 0$ and 50. It is observed that the test electrons can gain maximum 40 MeV energy in a length of 50 ($\frac{c}{\omega_{pe}}$).

Next, we have simulated the experimental results given in ref. [?] where an electron beam having total number of electrons $N = 1.8 \times 10^{10}$, $\sigma_x = 20\mu m$, $\sigma_y =$

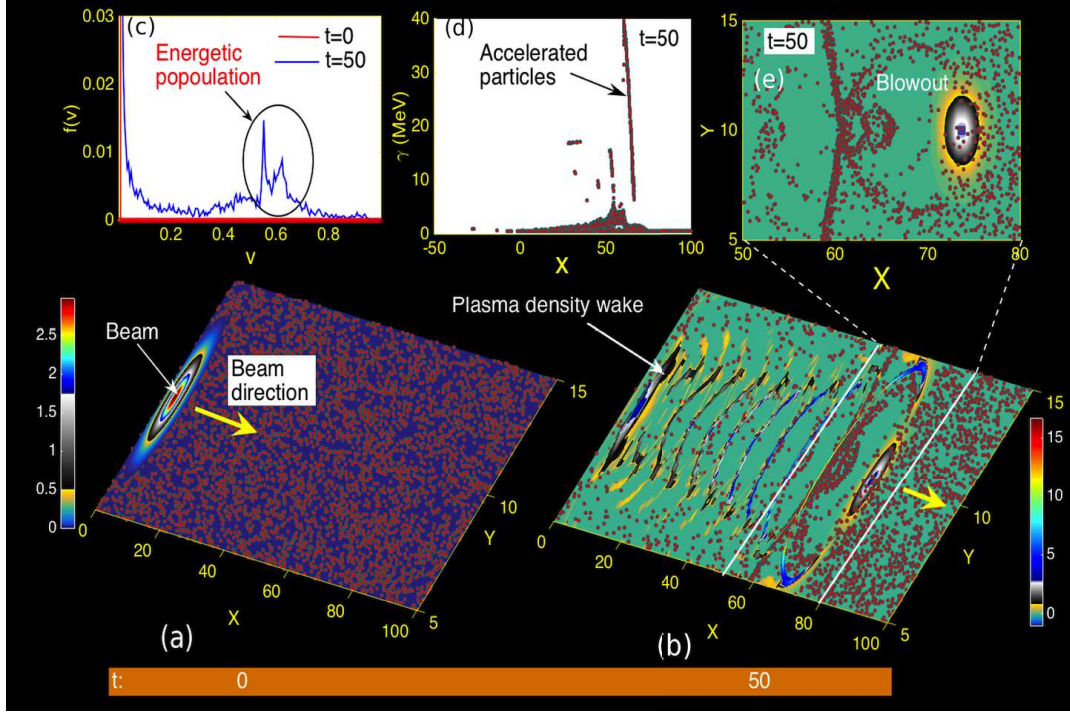


Figure 5.12: Plot of (a) normalized values of perturbed plasma density (n_1), electron beam density ($n_{b0} = 3$, $\sigma_x = \sqrt{2}$, $\sigma_y = 1$, $v_b = 0.99999999$), and distribution of test electrons at $t = 0$, (b) normalized values of perturbed plasma density (n_1), electron beam density (n_b), and distribution of test electrons at $t = 50$, (c) the speed distribution function ($f(v)$) of test electrons at $t = 0$ and $t = 50$, (d) the energy (γ) distribution of test electrons at $t = 0$ and $t = 50$, (e) the distribution of test electrons at the blowout structure.

$10\mu m$ and energy 28.5 GeV is injected in a plasma of density $n_0 = 2.8 \times 10^{17} cm^{-3}$. Therefore, we have, $n_{b0} = N / \left[(2\pi)^{\frac{3}{2}} \sigma_y^2 \sigma_x n_0 \right] = 2$, $\sigma_x \omega_{pe} / c = 2$, $\sigma_y \omega_{pe} / c = 1$, $v_b = 0.999999998461c$. Using these normalized values and also with 10000 test electrons having the initial energy of 28.5 GeV suspended just under the beam, we have performed our simulation. It is observed that the electrons from the front of the test beam lose their energy and the electrons from the back of the beam gain the maximum energy of $200 MeV$ in a length of $77 \left(\frac{c}{\omega_{pe}} \right)$ (see fig. 5.13). Therefore, the electrons can gain maximum energy up to $\sim 2.6 GeV$ in a 10 cm long

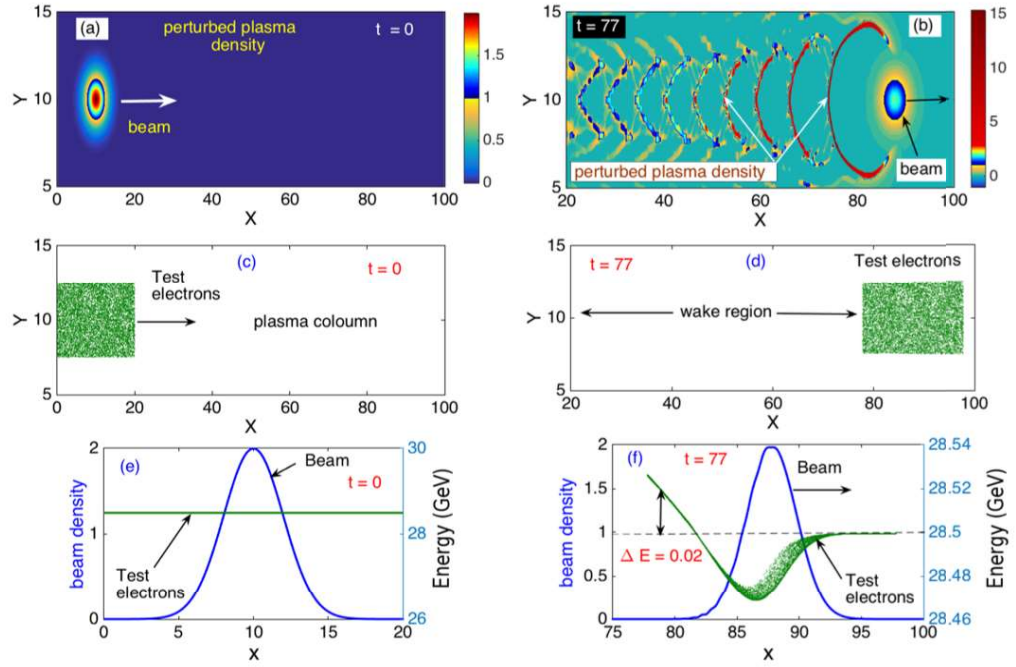


Figure 5.13: Plot of (a) normalized values of perturbed plasma density (n_1) and electron beam density (n_b) at $t = 0$, (b) normalized values of perturbed plasma density (n_1) and electron beam density (n_b) at $t = 77$, (c) the speed distribution function ($f(v)$) of test electrons at $t = 0$, (d) the distribution of test electrons at $t = 77$ (e) the energy distribution of test electrons at $t = 0$, (f) the energy distribution of test electrons at $t = 77$.

plasma. These results show a good conformity with the experimental results given in ref. [69]. Further, using same beam parameters, we inject the test electrons near the axial edge of the first blowout structure, where the amplitude of the longitudinal electric field is maximum (shown in fig. (5.14)). It is observed that the electrons can gain the maximum energy of 400 MeV in a length of $77 \left(\frac{c}{\omega_{pe}} \right)$. Therefore, the max. energy gained by these test electrons placed near the blowout can be doubled ~ 5.2 GeV after passing 10 cm long plasma. This shows that the energy gain can be doubled when the witness beam is placed near the axial edge of blowout instead of accelerating the electrons from the back of the driver beam.

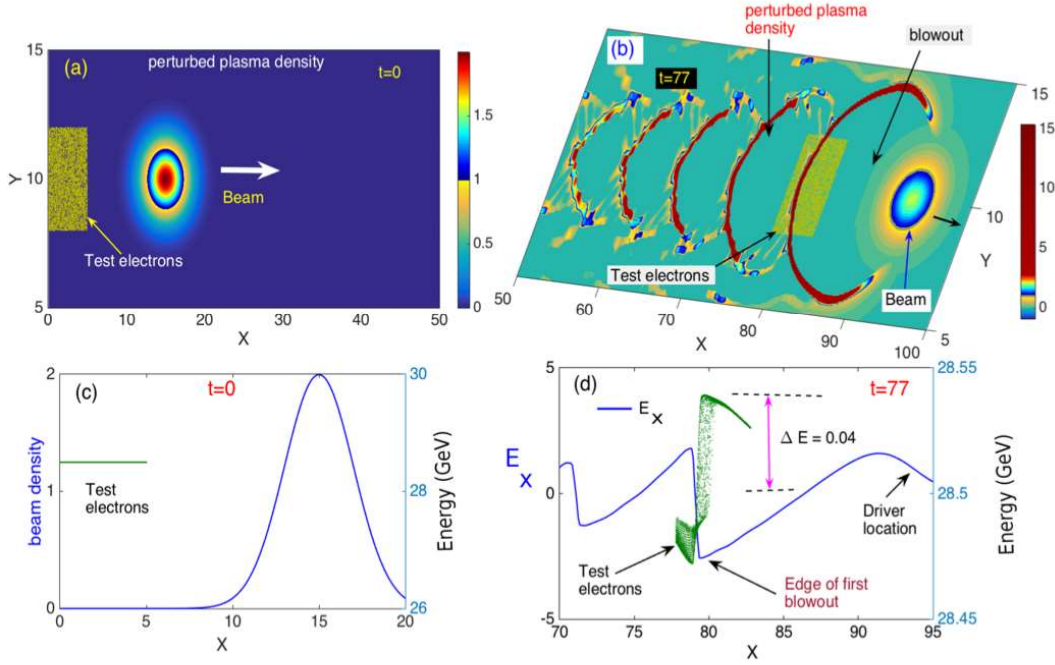


Figure 5.14: Plot of (a) normalized values of perturbed plasma density (n_1), electron beam density (n_b), and the distribution of test electrons at $t = 0$, (b) normalized values of perturbed plasma density (n_1), electron beam density (n_b), and the distribution of test electrons at $t = 77$, (c) the energy distribution and the driver beam profile at $t = 0$, (d) the energy distribution and the driver beam profile at $t = 77$

Summary

The 2-D excitation of relativistic electron beam driven wakefield in a cold plasma is studied using fluid simulation techniques. The simulation results show a good agreement with 1-D results [101] for a beam having larger transverse extension compared to the longitudinal extension. It is also shown that, for short and over dense beam, the structure of the excited wake field exhibits blowout structure which also matches with the analytically modeled results given in ref. [25]. Further, injecting the test particles in the simulation, we show that the maximum energy

gains 2.6 GeV by an electron from the back of the beam of energy 28.5 in a 10 cm long plasma, matches with the earlier experimental observation presented in ref. [69]. Using a discrete trailing beam instead of accelerating electrons from the back of the driver, which is placed near the axial edge of the first blowout, the maximum energy gain is found to be doubled ~ 5.2 GeV.

6

Conclusion and Future Scope

Salient features of this thesis

In this thesis, we have carried out detailed linear and non-linear studies of relativistic electron beam driven wakefield excitation in a cold plasma, both in 1-D and 2-D using two electron fluid description. The wakefields excited using an ultra-relativistic beam form the foundation in Plasma Wakefield Accelerators (PWFA) which are capable of producing energetic electrons in almost thousand times shorter distance compared to conventional accelerators. The success of PWFA has been experimentally demonstrated by accelerating electrons to $\sim 85\text{GeV}$ in a meter long plasma channel [72]. Theoretical studies on wakefield description have, however, relied on quasi-static approximation where the self-consistent evolution of the beam is ignored [31, 80, 94–96, 98]. An electron beam would typically evolve on a length scale of the betatron wavelength, which is $\sqrt{2\gamma_b}\lambda_p$ for a beam particle in an

ion channel. Here γ_b and λ_p are the Lorentz factor associated with the beam electrons and plasma wavelength respectively. Therefore, theoretical treatment which ignore beam evolution would be valid for a beam which is sufficiently energetic. In 1-D, linear and non-linear theories have been put forth for under-dense beam parameters [31, 78–80, 101]. The 2-D analytical studies in the linear regime have been carried out for special profiles of driver beam [94, 95]. The structure of wakefields driven by a relativistic electron beam in the non-linear regime has been provided by the analytical model of Lu et al. [96]. In the recent PWFA experiments, the driver beam is tightly focused to achieve “blow-out” structure, a highly non-linear regime (“blow-out”), for better acceleration. The experimental designs and results would have all these features (viz., multidimensionality, non-linear regime, evolution of the driver). So far PIC simulations have been carried out extensively with OSIRIS, QUICKPIC, EPOCH etc [25, 72, 73, 84, 96–98] to provide guidance to the experiments. The PIC simulations involve computation of trajectories of billions of particles for hundreds of plasma periods. Clearly, these simulations are computationally expensive and hence require powerful computational facilities [99].

This thesis investigates the excitation of wakefield driven by a relativistic electron beam over a wide range of beam parameters (both under-dense and over-dense) by employing fluid description for beam and plasma electrons. The fluid description is not only simple to implement numerically, but also provides ease in physics comprehension. Our investigations in this thesis on electron beam driven wakefield in a cold plasma reveal a number of important features in this field. For example, study of the structure and dynamics of the wakefield over a wide range of beam parameters, characterization of transformer ratio which determines the

energy gain in the process of acceleration for different beam densities, the characterization of wake wave breaking both in 1-D and 2-D, role of ion motion on the excitation, effect of finite transverse beam size on the excitation of wakefield etc. have been examined. These have been detailed in the various chapters of the thesis. Here we summarize important observations made in the thesis.

In chapter 2, we have studied the excitation of relativistic electron beam driven wakefield in a cold plasma in 1-D both analytically and numerically. The analytical structure of the wakefield in 1-D has been given by Rosenzweig et al. [31] for a rigid beam having density less than or equal to half the equilibrium background plasma density. In rigid beam limit, the self-consistent evolution of the beam gets ignored. The beam is assumed to penetrate infinite length inside the plasma without deformation. We have extended the analytical work of Rosenzweig et al. [31] for arbitrary beam to plasma electron density. The numerical simulations have been performed using two fluid description for both rigid and non-rigid driver. For a non-rigid beam, the self-consistent evolution is taken into account. Our simulations show good agreement with the analytical results for the case of rigid beam, thereby testifying the correctness of the numerical technique. Moreover, for evolving non-rigid beam, many interesting features have been observed in the simulation. We have observed that the beam gets compressed for $l_b < \lambda_p$, and gets split into different beam-lets for $l_b > \lambda_p$; where l_b is the length of the beam. It is also seen that beam can propagate a long distance without any significant deformation if the velocity of the beam is larger than $0.99c$. Thus the energy limit for the rigid beam approximation to be valid gets established.

In chapter 3, the space-time evolution of relativistic electron beam driven wake wave in a cold plasma has been investigated using 1-D fluid simulation techniques. It is observed that the wake wave gradually modifies with time and eventually breaks, exhibiting sharp spikes in the density profile and sawtooth-like features in the electric field profile after several plasma periods. This is a clear indication of wake wave breaking in a cold, homogeneous plasma [85–87, 100, 105]. The simulation has been performed for a long enough time for the excited wave to break. The wave breaking process is a crucial mechanism in plasma-based acceleration which helps to self-inject the plasma electrons in an appropriate phase [?] for acceleration. Therefore, a complete knowledge of the wake wave breaking is required for controlling and stabilizing the acceleration process. In this chapter, a complete characterization of the longitudinal wake wave breaking has been investigated. It has been found here that the excited wakefield before it breaks is identical to longitudinal Akhiezer-Polovin (AP) mode [81] excited using the same value of β_{ph} (phase velocity) and u_m (maximum fluid velocity) of the wake wave [88]. The steepening (breaking) of this wake has been understood in terms of phase mixing process of the AP mode. The wake wave breaking time has been studied as a function of beam density and beam velocity. Interestingly, it is found that the wake wave breaking time follows the well-known scaling presented in ref. [88]

In chapter 4, we have addressed the role of ion motion on the relativistic electron beam driven wakefield in a cold plasma. With the help of the 1-D fluid simulation techniques, the excitation of relativistic electron beam driven wakefield is studied where the effect of the ion motion is included. Rosenzweig et al. [80] have presented a semi-analytical form of the electron beam driven wakefield in the presence of

ions and estimated the approximate value of transformer ratio (for mass ratio $\mu = m_e/m_i \ll 1$). However, this has been done only for beam density equal to half the plasma density, where m_e and m_i are the mass of electron and ion respectively. In this thesis Rosenzweig's work [80] has been extended to arbitrary mass ratio and beam density. Simulation using three fluid description of the problem for a rigid beam with a rectangular spatial profile. As mentioned in chapter 2, the beam can be treated rigid if its velocity exceeds $0.99c$. It is shown that simulation results match with the semi-analytical results given by Rosenzweig et al. [30] in the appropriate limits. The transformer ratio, which determines the gain in the acceleration process, is also studied as a function of mass ratio and beam density. For over-dense beam, the transformer ratio saturates at unity for both $\mu = 1$ and $\mu = 1/1836$. We have also seen that the excited wave breaks via the gradual process of phase mixing after several plasma periods, exhibiting sharp spikes in the density profile. The corresponding electric field profile turns into the sawtooth form which is a clear signature of wave breaking. This particular feature observed in the present simulation has been found to be absent in the analytical calculations given in ref. [80]. However, it is shown that the wake wave, before it breaks, is identical to the Khachatryan mode [82] obtained for same parameters values of the wake wave (i.e. mass ratio, phase velocity and maximum value of the electric field). The physical mechanism behind the wave breaking has been understood in terms of phase mixing process of the Khachatryan mode. It is seen here that the numerically obtained wave breaking limit lies much below the analytically estimated value given in ref. [82] due to the possibility of phase mixing.

In numerical (via PIC simulations) and experimental PWFA studies, the wake-

field excitations for a short, intense beam has been considered. The nonlinear structure in this case has been termed as “blowout” structure. This is essentially an ion cavity totally free from cold plasma electrons [?, 64, 72, 73, 89, 90, 96]. Keeping this in view we have employed fluid simulations in chapter 5, to study the excitation of 2-D wakefield structures. In our 2-D simulations, we have shown that the 1-D limit is recovered when the transverse size of the beam is much larger than the longitudinal extension. The 2-D effects start showing up when the transverse extension is chosen to be finite. We choose a few specific spatial forms of the beam profile such as bi-Gaussian and bi-parabolic for our studies. The beam has been treated as rigid. The observations are shown to agree with linear 2-D analysis when the beam density is much smaller than the plasma electron density. At higher beam density the blow-out regime has been observed. The radius of the blowout structure as well as the longitudinal electric field profile matches with the analytical form given by Lu et al. [96]. However, we observe that in this case too the blow-out structure ultimately shows the tendency to break. The fluid description is no longer valid beyond this limit. Using the expression for the analytical excursion length of the electrons we have been able to show that it exceeds the curvature of the blow-out structure just before the onset of wave breaking process [111]. We have added and studied the evolution of test particles in the blow-out structure. This provides for an estimate of the energy gained by the particles in these structures. In fact a quantitative comparison with one of the recent experiments has been made (Hogan et al. [70]). We have shown in the simulation that maximum energy gain of 2.6 GeV is possible in a 10 cm long plasma. This is in conformity with the experiments where the electrons at the back of a driver beam of energy 28.5 GeV gain around 2.7 GeV in a 10 cm long plasma. We have also shown that

the test particles can gain more energy if they are placed appropriately in the wake structure. In fact when they are placed near the axial edge of the first blow out structure the energy gain has been observed to get doubled.

This thesis focuses on the fluid simulation of relativistic electron beam driven wakefield excitation in a cold plasma. We show that the fluid simulations which are much simpler and faster than any sophisticated PIC simulations are pretty adequate at representing the wakefield structure both in 1-D and 2-D. These simulations are also found to be good enough for describing the basic physics involved in PWFA settings including the structure of wakefields, breaking of wake wave, role of ion motion, effect of the transverse beam dimensions, and the acceleration of witness beams etc. The results presented in this thesis show a good agreement with the PIC results and experimental findings or analytical results, only before wave-breaking occurs. This is because the results obtained from our fluid simulations, which solve coupled fluid-Maxwell equations, subsequent to the breaking become irrelevant. In our simulations, the wave breaking has been identified in terms of spiky features in the density profile which is accompanied by sawtooth-like structures in the corresponding electric field profile. It is well known that the peak of the electron density theoretically goes to infinity and coherent electrostatic energy starts to convert into the random kinetic energy of the system at the onset of this critical amplitude (wave-breaking amplitude). In kinetic simulations which compute the microscopic properties of the system including the particle velocity distributions and randomness, it can be seen that, subsequently, all the electrostatic energy would get converted into random kinetic energy of the particles once the coherent oscillations are broken. Therefore, at the onset of the breaking,

the fluid behavior of the plasma's completely breaks and the kinetic description dominates. Therefore, the particle-based simulations (PIC simulations or kinetic simulations) would be more relevant to describe the phenomena after breaking in the plasmas. As we observed in our fluid simulation, the total energy of the system drops down after the wave breaking due to the formation of the fine (smaller than the size of the grid) structure. Whereas, in the kinetic simulation, the particles get heated up simultaneously as the wave exceeds the critical amplitude and then form new structures. Due to the absence of wave-particle interaction, the fluid simulation fails to predict the correct structure after the wave breaking. Recently, we have reported comparing the results of 1-D fluid with 1-D PIC simulations even after wave breaking [104]. It was shown that the amount of energy dropped in the fluid simulation after breaking matches with the amount of thermal energy carried by the particles in the in PIC simulation.

Future scope

The beam plasma interaction is an important topic of investigation with applications not merely in the context of particle acceleration but also in areas as diverse as fast ignition, astrophysical electron jets etc. We provide some scope of future possible studies in the area of beam plasma interaction.

- The extension of 2-D fluid code to 3-D would help investigate a more realistic scenario for the understanding of beam plasma interaction. This will help understand the implication on the wake structure that permitting variations along the third dimension would provide.
- One of the recent proposed plan at CERN is to have a proton-driven wake-

fields (PDPWFA) for acceleration. It would be interesting to study such a possibility with our fluid description.

- However, it would mimic more realistic scenario of PWFA if one can include the ion dynamics in 2-D geometry rather than that considered in 1-D settings. Typically, the ion motions become more important for the studies which include the relativistic dynamics of the electron. Due to relativistic motion of the electrons, the electron-plasma frequency can be comparable to the ion-plasma frequency. Hence both the electrons and ions can play important role in the plasma dynamics. Including the ion dynamics in our 1-D fluid simulation, we have shown that the effect of ion motion can be ignored for hydrogen plasma even for beam velocity close to $0.9999c$; where c is the speed of light. It was also shown that the efficiency of the acceleration (measured by transformer ratio) settles down to unity in the over-dense regime for both the electron-positron and hydrogen plasmas. We, therefore, believe that the study including the effect of ion dynamics in 2-D could be important for studying many problems in plasma wakefield acceleration scheme. It could be more relevant for investigating self-modulation instability in proton-driven plasma wakefield acceleration (PDPWFA) which has been recently proposed by AWAKE, CERN for the acceleration of electrons to meet the criteria of LHC regime.
- In the fast ignition (FI) fusion scheme, one relies on energetic electrons for the creation of ignition spark in the compressed core where lasers cannot penetrate. Thus the propagation and stopping of electron beam in compressed over-dense plasma are important to understand. This includes a proper understanding of instabilities associated with the beam propagation in plasma

medium, the possibility of magnetic field generation and turbulence excitations which may lead to anomalous transport of electrons. In fact as an aside we would like to mention that we have already made progress in identifying a novel finite beam instability in the beam plasma system in addition to Weibel and Kelvin Helmholtz which gets excited when the electron beam is of a finite size [112]. This work is in progress and not the part of this thesis

- Furthermore, in the FI scenario the compressed core is inhomogeneous and highly dense. It is likely that the dense cool plasma in such a case be in strongly coupled regime. Thus effect of plasma density inhomogeneity and the role of strongly coupled background plasma on beam propagation needs to be looked at carefully.
- In the recent impressive developments of ultra-short lasers (femtosecond and, more recently, attosecond), it is possible that the de-Broglie wavelength of the charge carriers becomes equal to or greater than the dimension of the quantum plasma system. In such cases, the quantum effects become important in the behavior of the charged particles in plasmas. For example, the interaction of ultra-fast lasers with metallic nano-structures constitute an ideal arena to study the dynamical properties of quantum plasmas. Therefore, including the quantum effects to the fluid equations would be important and fruitful to study.
- The fluid code can also be used to study the interaction of laser pulse with the plasma. we have recently demonstrated it in the context of studying the evolution of the exact nonlinear solutions of the laser plasma coupled system (see refs. [41, 104] which again is not the part of this thesis) in 2-

D. Further studies in this direction incorporating inhomogeneous plasmas, quantum effects, strongly coupled behavior is desirable.

A

Appendix

2-D fully relativistic electromagnetic fluid simulation techniques

In this section, we present the 2-D fluid simulation techniques used for the excitation of relativistic electron beam driven wakefield in a cold plasma. The basic equations governing the excitation of 2-D relativistic electron beam driven wakefield in a cold plasma are the relativistic fluid-Maxwell equations. The equations contain the equation of continuity and the equation of momentum for both plasma electrons and beam electrons. We have used Maxwell's equations for the evolution of electro-magnetic fields. The dynamics of ion have been ignored because of their heavy mass. They only provide a neutralizing background. Therefore, the basic governing equations for the excitation of two-dimensional relativistic electron beam

driven wakefield in a cold plasma are,

$$\frac{\partial n}{\partial t} + \vec{\nabla} \cdot (n\vec{v}) = 0 \quad (\text{A.1})$$

$$\frac{\partial \vec{p}}{\partial t} + (\vec{v} \cdot \vec{\nabla}) \vec{p} = -e\vec{E} - \frac{e}{c}(\vec{v} \times \vec{B}) \quad (\text{A.2})$$

$$\frac{\partial n_b}{\partial t} + \vec{\nabla} \cdot (n_b \vec{v}_b) = 0 \quad (\text{A.3})$$

$$\frac{\partial \vec{p}_b}{\partial t} + (\vec{v}_b \cdot \vec{\nabla}) \vec{p}_b = -e\vec{E} - \frac{e}{c}(\vec{v}_b \times \vec{B}) \quad (\text{A.4})$$

$$(\vec{\nabla} \times \vec{B}) = -\frac{4\pi e}{c}(n\vec{v} + n_b \vec{v}_b) + \frac{1}{c} \frac{\partial \vec{E}}{\partial t} \quad (\text{A.5})$$

$$(\vec{\nabla} \times \vec{E}) = -\frac{1}{c} \frac{\partial \vec{B}}{\partial t} \quad (\text{A.6})$$

$$\vec{\nabla} \cdot \vec{E} = 4\pi e(n_0 - n - n_b) \quad (\text{A.7})$$

$$\vec{\nabla} \cdot \vec{B} = 0 \quad (\text{A.8})$$

where $\vec{p} = m_e \gamma \vec{v}$ and $\vec{p}_b = m_e \gamma \vec{v}_b$ is the momentum of plasma electron and beam electron having density n and n_b respectively. Here $\gamma = \left(1 - \frac{v^2}{c^2}\right)^{-1/2}$ and $\gamma_b = \left(1 - \frac{v_b^2}{c^2}\right)^{-1/2}$ is the relativistic factor associated with the plasma electron and beam electron having velocity \vec{v} and \vec{v}_b respectively. In the above equations, \vec{E} and \vec{B} represents the electric and magnetic field respectively. The equations are solved in 2-D geometry (“x-y” plane) and the electron beam is propagating along x -direction. Now, we have made the following replacements in the physical quantities, $t \rightarrow \omega_{pe} t$, $(x, y) \rightarrow \frac{\omega_{pe}(x, y)}{c}$, $\vec{E} \rightarrow \frac{e\vec{E}}{m_e c \omega_{pe}}$, $\vec{B} \rightarrow \frac{e\vec{B}}{m_e c \omega_{pe}}$, $\vec{v} \rightarrow \frac{v}{c}$, $\vec{v}_b \rightarrow \frac{v_b}{c}$, $\vec{p} \rightarrow \frac{\vec{p}}{m_e c}$, $\vec{p}_b \rightarrow \frac{\vec{p}_b}{m_e c}$, $n \rightarrow \frac{n}{n_0}$, and $n_b \rightarrow \frac{n_b}{n_0}$. Using these normalizations in the above equations (A.1-

A.8), we have,

$$\frac{\partial n}{\partial t} + \vec{\nabla} \cdot (n\vec{v}) = 0 \quad (\text{A.9})$$

$$\frac{\partial \vec{p}}{\partial t} + (\vec{v} \cdot \vec{\nabla})\vec{p} = -\vec{E} - (\vec{v} \times \vec{B}) \quad (\text{A.10})$$

$$\frac{\partial n_b}{\partial t} + \vec{\nabla} \cdot (n_b \vec{v}_b) = 0 \quad (\text{A.11})$$

$$\frac{\partial \vec{p}_b}{\partial t} + (\vec{v}_b \cdot \vec{\nabla})\vec{p}_b = \vec{E} - (\vec{v}_b \times \vec{B}) \quad (\text{A.12})$$

$$\frac{\partial \vec{E}}{\partial t} = (n\vec{v} + n_b \vec{v}_b) + (\vec{\nabla} \times \vec{B}) \quad (\text{A.13})$$

$$\frac{\partial \vec{B}}{\partial t} = -(\vec{\nabla} \times \vec{E}) \quad (\text{A.14})$$

$$\vec{\nabla} \cdot \vec{E} = (1 - n - n_b) \quad (\text{A.15})$$

$$\vec{\nabla} \cdot \vec{B} = 0 \quad (\text{A.16})$$

Equations (A.9-A.16) are the key equations to study the 2-D excitation of relativistic electron beam driven wakefield in a cold plasma. These normalized set of equations (A.9-A.16) are solved using two-dimensional fluid simulation techniques. Therefore, a fully relativistic electromagnetic fluid code has been developed using LCPFCT suite of subroutines based on flux-corrected transport scheme [102]. The basic principle of this scheme is based on the generalization of two-step Lax-Wendroff method [103]. As the observations are made in (“x-y”)-plane, therefore, we have written the above equations in Cartesian geometries ($x - y$) as,

$$\frac{\partial n}{\partial t} + \frac{\partial}{\partial x}(nv_x) + \frac{\partial}{\partial y}(nv_y) = 0 \quad (\text{A.17})$$

$$\frac{\partial p_x}{\partial t} + (v_x \frac{\partial}{\partial x} + v_y \frac{\partial}{\partial y}) p_x = -E_x - (v_y B_z - B_y v_z) \quad (\text{A.18})$$

$$\frac{\partial p_y}{\partial t} + (v_x \frac{\partial}{\partial x} + v_y \frac{\partial}{\partial y}) p_y = -E_y - (v_z B_x - B_z v_x) \quad (\text{A.19})$$

$$\frac{\partial p_z}{\partial t} + (v_x \frac{\partial}{\partial x} + v_y \frac{\partial}{\partial y}) p_z = -E_z - (v_x B_y - B_x v_y) \quad (\text{A.20})$$

$$\frac{\partial n_b}{\partial t} + \frac{\partial}{\partial x} (n_b v_{bx}) + \frac{\partial}{\partial y} (n_b v_{by}) = 0 \quad (\text{A.21})$$

$$\frac{\partial p_{bx}}{\partial t} + (v_{bx} \frac{\partial}{\partial x} + v_{by} \frac{\partial}{\partial y}) p_{bx} = -E_x - (v_{by} B_z - B_y v_{bz}) \quad (\text{A.22})$$

$$\frac{\partial p_{by}}{\partial t} + (v_{bx} \frac{\partial}{\partial x} + v_{by} \frac{\partial}{\partial y}) p_{by} = -E_y - (v_{bz} B_x - B_z v_{bx}) \quad (\text{A.23})$$

$$\frac{\partial p_{bz}}{\partial t} + (v_{bx} \frac{\partial}{\partial x} + v_{by} \frac{\partial}{\partial y}) p_{bz} = -E_z - (v_{bx} B_y - B_x v_{by}) \quad (\text{A.24})$$

$$\frac{\partial E_x}{\partial t} = (n v_x + n_b v_{bx}) + \frac{\partial B_z}{\partial y} \quad (\text{A.25})$$

$$\frac{\partial E_y}{\partial t} = (n v_y + n_b v_{by}) - \frac{\partial B_z}{\partial x} \quad (\text{A.26})$$

$$\frac{\partial E_z}{\partial t} = (n v_z + n_b v_{bz}) + (\frac{\partial B_y}{\partial x} - \frac{\partial B_x}{\partial y}) \quad (\text{A.27})$$

$$\frac{\partial B_x}{\partial t} = -\frac{\partial E_z}{\partial y} \quad (\text{A.28})$$

$$\frac{\partial B_y}{\partial t} = \frac{\partial E_z}{\partial x} \quad (\text{A.29})$$

$$\frac{\partial B_z}{\partial t} = -\left(\frac{\partial E_y}{\partial x} - \frac{\partial E_x}{\partial y}\right) \quad (\text{A.30})$$

$$\frac{\partial E_x}{\partial x} + \frac{\partial E_y}{\partial y} = (1 - n - n_b) \quad (\text{A.31})$$

$$\frac{\partial B_x}{\partial x} + \frac{\partial B_y}{\partial y} = 0 \quad (\text{A.32})$$

The right sides of the above equations are separated into two parts, the x -direction terms and the y -direction terms. This arrangement in each of the equations separates the x -derivatives and the y -derivatives in the divergence and gradient terms into parts which can be treated sequentially by a general one-dimensional continuity equation solver (LCPFCT). Therefore, we split the above equations in two different directions and use LCPFCT techniques for solving the equations. Using the above methodology, the one-dimensional LCPFCT subroutines have been used repetitively to construct the 2-D fluid code by splitting the time steps in the different directions (x and y). First we solve the integration along x -direction and then, subsequently, along y -direction in the same time interval t to $t + \Delta t$. The method of integration using time-step splitting is discussed in detail in ref. [102]. The approach can also be extended to three dimensions and to fully general geometries. To use this split-step approach, the time step must be small enough that the distinct components of the fluxes do not change the cell-averaged values appreciably during the time steps t to $t + \delta t$. This approach is second-order accurate as long as the time step is small and changed slowly, but there is still a bias built in depending on which direction, x or y , is integrated first. To remove this bias,

the results from two calculations for each time step can be averaged to obtain an expensive but effective solution.

In our simulation, we have used non-periodic boundary conditions (open) to retain the form of wake wave at the boundary. Initially, we have introduced the beam at one end of the simulation window which propagates with a velocity along x -direction towards another end. The spatial resolution Δx or Δy has been chosen in such a way that the skin depth ($\frac{c}{\omega_{pe}}$) is adequately resolved in both the directions. The temporal resolution i.e. time step (Δt) is then calculated from Courant-Friedrichs-Lewy (CFL) condition $\Delta t = C_n(\Delta)/u_{max}$, where u_{max} and C_n , are the maximum fluid velocity and CFL number [102]. Here Δ is the minimum value between Δx and Δy . In our simulations, the maximum fluid velocity $u_{max} = 1$ as the maximum velocity of any fluid element can reach up to the speed of light and $C_n = 0.2$ for a good temporal resolution and stability. Therefore, the value of Δt has been fixed through out the simulation. The numerical observations have been also repeated by changing the grid size Δx or Δy , C_n and Δt and the results have been recorded at each time step in terms of n , n_b , \vec{v} , \vec{v}_b , \vec{E} , and \vec{B} with their components.

At each time step, it is checked that the results must satisfy the following equations,

$$\frac{\partial E_x}{\partial x} + \frac{\partial E_y}{\partial y} = (1 - n - n_b) \quad (\text{A.33})$$

$$\frac{\partial B_x}{\partial x} + \frac{\partial B_y}{\partial y} = 0 \quad (\text{A.34})$$

At each time step, we have also checked the conservation of energy principle in the simulation. It is seen that the total energy (T_{tot}) of the system is conserved at

each time steps. The total energy of the system is defined as,

$$T_{tot} = T_{kin} + T_{field} \quad (\text{A.35})$$

where T_{kin} and T_{field} are the kinetic and field energy of the system. The kinetic energy of the system is given by,

$$T_{kin} = \sum_{i=1}^{N_x} \sum_{j=1}^{N_y} [n(i, j)(\gamma(i, j) - 1)] \Delta x \Delta y + \sum_{i=1}^{N_x} \sum_{j=1}^{N_y} [n_b(i, j)(\gamma_b(i, j) - 1)] \Delta x \Delta y \quad (\text{A.36})$$

The field energy of the system can be written as,

$$T_{field} = \sum_{i=1}^{N_x} \sum_{j=1}^{N_y} \left[\frac{E^2(i, j) + B^2(i, j)}{2} \right] \Delta x \Delta y \quad (\text{A.37})$$

where $E^2 = E_x^2 + E_y^2 + E_z^2$ and $B^2 = B_x^2 + B_y^2 + B_z^2$ are the square of the magnitude of the electric and magnetic field respectively. here i and j represents the index corresponding to the grid numbers along x and y -directions respectively. N_x and N_y are the total number of grid points along x and y - directions respectively.

Derivation of wave breaking limit for a relativistic electron-ion mode (Khachtryan) in a cold plasma

In this section we present a detailed derivation of an relativistic electron ion mode excited in a cold homogeneous plasma. This derivation has already presented by Khachtryan et al. briefly earlier [82]. Here we have re-derived the expression for

wave breaking limit of an Khachatryan mode [82] in detail. The basic normalized equations governing the electron and ion in a plasma in 1-D (z -direction) can be written as (see chapter 4),

$$\frac{\partial n_e}{\partial t} + \frac{\partial(n_e v_e)}{\partial z} = 0 \quad (\text{A.38})$$

$$\frac{\partial p_e}{\partial t} + v_e \frac{\partial p_e}{\partial z} = -E \quad (\text{A.39})$$

$$\frac{\partial n_i}{\partial t} + \frac{\partial(n_i v_i)}{\partial z} = 0 \quad (\text{A.40})$$

$$\frac{\partial p_i}{\partial t} + v_i \frac{\partial p_i}{\partial z} = \mu E \quad (\text{A.41})$$

$$\frac{\partial E}{\partial z} = (n_i - n_e) \quad (\text{A.42})$$

where $p_e = \gamma_e v_e$ and $p_i = \gamma_i v_i$ are the z -components of momentum of plasma electron and plasma ion having z -component of velocity v_e and v_i respectively. Here, $\gamma_e = (1 - v_e^2)^{-1/2}$ and $\gamma_i = (1 - v_i^2)^{-1/2}$ are the relativistic factors associated with plasma electron and plasma ion respectively. In the above equations, n and n_i represents the density of plasma electron and plasma ion respectively. E and μ represents the z -component of the electric field and mass ratio (ratio of electron to ion mass) respectively. We have used the normalization factors as, $t \rightarrow \omega_{pe} t$, $z \rightarrow \frac{\omega_{pe} z}{c}$, $E \rightarrow \frac{eE}{m_e c \omega_{pe}}$, $v_e \rightarrow \frac{v_e}{c}$, $v_i \rightarrow \frac{v_i}{c}$, $p_e \rightarrow \frac{p_e}{m_e c}$, $p_i \rightarrow \frac{p_i}{m_e c}$, $n_e \rightarrow \frac{n_e}{n_0}$, $n_i \rightarrow \frac{n_i}{n_0}$.

Using the frame $\xi = (z - v_{ph} t)$ transformation, the operators can be written as,

$$\frac{\partial}{\partial t} \equiv -v_{ph} \frac{d}{d\xi}$$

$$\frac{\partial}{\partial z} \equiv \frac{d}{d\xi}$$

where v_{ph} is the phase velocity of the wave which is normalized to speed of the light c . Using the above operator transformations, equations (A.38-A.42) can be expressed as,

$$v_{ph} \frac{dn_e}{d\xi} - \frac{d(n_e v_e)}{d\xi} = 0 \quad (\text{A.43})$$

$$(v_e - v_{ph}) \frac{d(\gamma_e v_e)}{d\xi} = -E \quad (\text{A.44})$$

$$v_{ph} \frac{dn_i}{d\xi} - \frac{d(n_i v_i)}{d\xi} = 0 \quad (\text{A.45})$$

$$(v_i - v_{ph}) \frac{d(\gamma_i v_i)}{d\xi} = \mu E \quad (\text{A.46})$$

$$\frac{dE}{d\xi} = (n_i - n_e) \quad (\text{A.47})$$

The electric field can also be written as, $E = -\frac{\partial \phi}{\partial z}$, where ϕ is the electrostatic potential normalized to $m_e c^2 / e$. We now define, $\Phi = \Phi_- = 1 + \phi$ and $\Phi_+ = 1 - \mu \phi = 1 + \mu(1 - \Phi_-)$. Using the frame transformation, the electric field thus can be written as,

$$E = -\frac{\partial \Phi}{\partial \xi} = -\frac{\partial \Phi_-}{\partial \xi} = \frac{1}{\mu} \frac{\partial \Phi_+}{\partial \xi} \quad (\text{A.48})$$

Substituting the form of electric field in equation (A.44), we have,

$$(v_e - v_{ph}) \frac{d(\gamma_e v_e)}{d\xi} = \frac{1}{v_{ph}^2} \frac{\partial \Phi_-}{\partial \xi} \quad (\text{A.49})$$

This equation can also be written as,

$$v_e \frac{d(\gamma_e v_e)}{d\xi} - v_{ph} \frac{d(\gamma_e v_e)}{d\xi} = \frac{\partial \Phi_-}{\partial \xi} \quad (\text{A.50})$$

We know the following relation,

$$v_e \frac{d(\gamma_e v_e)}{d\xi} = \frac{d\gamma_e}{d\xi}$$

Therefore using the above expression, the equation (A.51) can be written as,

$$\frac{d}{d\xi} (\gamma_e (1 - v_e v_{ph})) = \frac{\partial \Phi_-}{\partial \xi} \quad (\text{A.51})$$

We have then integrated the above equation using the boundary condition $v_e = 0$ and $\phi = 0$ at $\xi = 0$. Therefore, we have,

$$\gamma_e (1 - v_e v_{ph}) = \Phi_- \quad (\text{A.52})$$

Substituting the value of $\gamma_e = 1/\sqrt{1 - v_e^2}$, the above equation can be written as,

$$(1 - v_e v_{ph})^2 = (1 - v_e^2) \Phi_-^2 \quad (\text{A.53})$$

Re-arranging the terms of the above equation, we have,

$$(v_{ph}^2 + \Phi_-^2) v_e^2 - 2v_{ph} v_e + (1 - \phi_-^2) = 0 \quad (\text{A.54})$$

The solutions of the quadratic equation of v_e can be written as,

$$v_e = \frac{2v_{ph} \pm \sqrt{4v_{ph}^2 - 4(1 - \Phi_-^2)(v_{ph}^2 + \Phi_-^2)}}{2(v_{ph}^2 + \Phi_-^2)} \quad (\text{A.55})$$

The maximum phase velocity (v_{ph}) of the wave can reach up to the speed of light. The maximum velocity of the electron v_e can not exceed the speed of light. Therefore we only consider “-” sign in the above equation. Thus the solution of the equation (A.54) is,

$$v_e = \frac{2v_{ph} \pm \sqrt{4v_{ph}^2 - 4(1 - \Phi_-^2)(v_{ph}^2 + \Phi_-^2)}}{2(v_{ph}^2 + \Phi_-^2)} \quad (\text{A.56})$$

The solution again can be re-arranged as,

$$v_e = \frac{v_{ph} \pm (\Phi_- \sqrt{\Phi_-^2 - \gamma_{ph}^{-2}})}{(v_{ph}^2 + \Phi_-^2)} \quad (\text{A.57})$$

It is to be noted that for a real solution of v_e , $\Phi_- \geq 1/\gamma_{ph}$. Similarly, the velocity of the ion v_i can be written as,

$$v_i = \frac{v_{ph} \pm (\Phi_+ \sqrt{\Phi_+^2 - \gamma_{ph}^{-2}})}{(v_{ph}^2 + \Phi_-^2)} \quad (\text{A.58})$$

Now, integrating the the continuity equation (A.43) for electron we get,

$$n_e = \frac{v_{ph}}{v_{ph} - v_e} \quad (\text{A.59})$$

Substituting the form of v_e from equation (A.57), we get,

$$n_e = \frac{v_{ph}(F^2 + 1)}{(v_{ph}F^2 + F\Phi_-)} \quad (\text{A.60})$$

where $F^2 = \Phi_-^2 - \gamma_{ph}^{-2}$ and $v_{ph}^2 + \Phi_-^2 = F^2 + 1$. We can also re-arrange the equation in following form,

$$n_e = \frac{v_{ph}(F^2 + 1)(v_{ph}F - \Phi_-)}{F(v_{ph}^2F^2 - \Phi_-^2)} \quad (\text{A.61})$$

Substituting $\Phi_-^2 = F^2 + \gamma_{ph}^{-2}$ and rearranging the above equation, we get,

$$n_e = -\frac{v_{ph}\gamma_{ph}^2(F^2 + 1)(v_{ph}F - \Phi_-)}{F(F^2 + 1)} \quad (\text{A.62})$$

The final form of the equation for density n_e therefore can be written as,

$$n_e = v_{ph}\gamma_{ph}^2 \left[\frac{\Phi_-}{(\Phi_-^2 - \gamma_{ph}^{-2})^{-1/2}} - v_{ph} \right] \quad (\text{A.63})$$

The density of ion similarly can be derived as,

$$n_i = v_{ph}\gamma_{ph}^2 \left[\frac{\Phi_+}{(\Phi_+^2 - \gamma_{ph}^{-2})^{-1/2}} - v_{ph} \right] \quad (\text{A.64})$$

Substituting the form of n_e and n_i in equation (A.47) and using equation (A.48), we have the following differential equation,

$$\frac{d^2\Phi}{d\xi^2} = -v_{ph}\gamma_{ph}^2 \left[\frac{\Phi_+}{(\Phi_+^2 - \gamma_{ph}^{-2})^{-1/2}} - \frac{\Phi_-}{(\Phi_-^2 - \gamma_{ph}^{-2})^{-1/2}} \right] \quad (\text{A.65})$$

Using the expression, $U = v_{ph}\gamma_{ph}^2 ((v_{ph} - (\Phi_+^2 - \gamma_{ph}^{-2})^{1/2})/\mu - (v_{ph} - (\Phi_-^2 - \gamma_{ph}^{-2})^{1/2}))$,

the differential equation can be written as,

$$\frac{d^2\Phi}{d\xi^2} + \frac{dU}{d\Phi} = 0 \quad (\text{A.66})$$

The above equation describes the one-dimensional motion of a particle in a field with potential $U(\Phi)$; the values Φ and E correspond to the coordinate and velocity of this fictitious particle respectively. Now we choose $U(\Phi) = 0$ at $\Phi = 1$. We also integrate both side of the above equation (A.66) w. r. t. ξ . We finally get,

$$\frac{d\Phi}{d\xi} = -E = \pm [2(U_{max} - U)]^{1/2} \quad (\text{A.67})$$

where U_{max} defines the maximum value of U . The value of U_{max} defines the wave breaking amplitude in electric field. The wave breaking limit can be written as, $E_{WB} = \sqrt{2U_{max}}$; where $E - WB$ is the maximum electric field supported by an electron-ion mode. It can be shown that, the value of U_{max} can be obtained at $\Phi = 1/\gamma_{ph}$. Substituting the value of $\Phi = 1/\gamma_{ph}$ in the expression of U , we can write the maximum amplitude of electric field which is wave breaking limit as a function of μ and γ_{phas} ,

$$E_{WB} = \sqrt{2}\gamma_{ph}(1 + (1 - \sqrt{\nu_1\nu_2})/\mu) \quad (\text{A.68})$$

Where $\nu_1 = 1 + \mu$ and $\nu_2 = 1 + [\mu(\gamma_{ph} - 1)/(\gamma_{ph} + 1)]$. Clearly, the above expression for $\mu \ll 1$ can be reduced to the following form,

$$E_{WB} = \sqrt{2(\gamma_{ph} - 1)} \quad (\text{A.69})$$

This is the well known expression of wave breaking limit for an Akhiezer-Polovin

mode (immobile ions) [87].

Analytical formalism for 2-D linear relativistic electron beam wakefields

Here we present an analytical forms of relativistic electron beam driven wakefields in the linear regime. Clearly, the linear calculations are valid for a low amplitude excitations which have been excited for a beam having density $n_b \ll 1$. In this derivation, we have ignored the evolution of the beam in the self-consistent electric and magnetic field. In the time scale of excitation, the perturbation in the beam is negligibly small. This approximation is valid for a sufficiently energetic beam (discussed in chapter (5) in detail). As the beam velocity is equal to the speed of light which implies the beam is infinitely massive. Therefore, the plasma parameters can be expressed as,

$$n = n_0 + n_1$$

$$\vec{v} = \vec{v}_0 + \vec{v}_1$$

$$\vec{E} = \vec{E}_0 + \vec{E}_1$$

$$\vec{B} = \vec{B}_0 + \vec{B}_1$$

It is assumed that the unperturbed plasma velocity \vec{v}_0 be zero and the perturbed plasma density n_1 be much smaller than its unperturbed density $n_0 = 1$. The unperturbed electric field (\vec{E}_0) and magnetic field (\vec{B}_0) is zero. Therefore, the final

expression of these quantities are,

$$n = 1 + n_1$$

$$\vec{v} = \vec{v}_1$$

$$\vec{E} = \vec{E}_1$$

$$\vec{B} = \vec{B}_1$$

Applying the above linearizations, the normalized equations (A.9) and (A.10) can be written as,

$$\frac{\partial n_1}{\partial t} + \vec{\nabla} \cdot \vec{v}_1 = 0 \quad (\text{A.70})$$

$$\frac{\partial \vec{v}_1}{\partial t} = -\vec{E}_1 \quad (\text{A.71})$$

In the frame transformation ($\xi = x - v_b t$, y , z) and $v_b = 1$, we have, $\partial/\partial x = \partial/\partial \xi$ and $\partial/\partial t = -\partial/\partial \xi$. A schematic diagram of the beam dynamics in this frame is shown in figure (5.4). Using these transformations, the above equations (A.70) and (A.71) can be written as,

$$\frac{\partial n_1}{\partial \xi} - \vec{\nabla} \cdot \vec{v}_1 = 0 \quad (\text{A.72})$$

$$\frac{\partial \vec{v}_1}{\partial \xi} = \vec{E}_1 \quad (\text{A.73})$$

Operating $\partial/\partial \xi$ both side in equation (A.72) and using equations (A.73) and (A.13), we have,

$$\frac{\partial^2 n_1(\xi, r)}{\partial \xi^2} + n_1(\xi, r) = -n_b(\xi, r) \quad (\text{A.74})$$

$$\vec{E} = -\vec{\nabla}\phi - \partial\vec{A}/\partial t \quad (\text{A.75})$$

where \vec{A} and ϕ is the vector potential and scalar potential respectively. Therefore the equation (A.13) in the Coulomb gauge $\vec{\nabla} \cdot \vec{A} = 0$ takes the following form.

$$\nabla^2 \phi = -(n_1 + n_b) \quad (\text{A.76})$$

Similarly the equation (A.13) can be written as,

$$(\vec{\nabla} \times \vec{\nabla} \times \vec{A}) = -(n\vec{v} + n_b\vec{v}_b) + \frac{\partial \vec{E}}{\partial t}$$

Using the Coulomb gauge $\vec{\nabla} \cdot \vec{A} = 0$ and equation (A.75), the above equation can be expressed as,

$$-\nabla^2 \vec{A} = -(n\vec{v} + n_b\vec{v}_b) + \frac{\partial}{\partial t}(-\vec{\nabla}\phi - \partial\vec{A}/\partial t)$$

Now, we have, $\nabla^2 = \partial^2/\partial x^2 + \nabla_\perp^2$. Therefore, we have the following form,

$$-\nabla_\perp^2 \vec{A} = -(n\vec{v} + n_b\vec{v}_b) - \frac{\partial}{\partial t}(\vec{\nabla}\phi) + \left(\frac{\partial^2 \vec{A}}{\partial x^2} + \frac{\partial^2 \vec{A}}{\partial t^2}\right)$$

In the (ξ, r) frame, we have the following form of the above equation,

$$\nabla_\perp^2 \vec{A} = (n\vec{v} + n_b\vec{v}_b) - \frac{\partial}{\partial \xi}(\vec{\nabla}\phi)$$

Operating $\partial/\partial\xi$ both the sides and using linearized forms of the quantities in the above equation, we get,

$$\nabla_{\perp}^2 \frac{\partial \vec{A}_1}{\partial \xi} = \frac{\partial}{\partial \xi} (\vec{v}_1 + n_b \vec{v}_b) - \frac{\partial^2}{\partial \xi^2} (\vec{\nabla} \phi_1)$$

Substituting $\partial \vec{v}_1 / \partial \xi$ from equation (A.73), we have,

$$\nabla_{\perp}^2 \frac{\partial \vec{A}_1}{\partial \xi} = \vec{E}_1 + \frac{\partial}{\partial \xi} (n_b \vec{v}_b) - \frac{\partial^2}{\partial \xi^2} (\vec{\nabla} \phi_1)$$

Therefore, the above equation can be re-written as,

$$\nabla_{\perp}^2 \frac{\partial \vec{A}_1}{\partial \xi} = -\vec{\nabla} \phi_1 + \frac{\partial \vec{A}_1}{\partial \xi} + \frac{\partial}{\partial \xi} (n_b \vec{v}_b) - \frac{\partial^2}{\partial \xi^2} (\vec{\nabla} \phi_1)$$

Taking the x -component of the equation, we have,

$$\nabla_{\perp}^2 \frac{\partial A_{1x}}{\partial \xi} = -\frac{\partial}{\partial \xi} \phi_1 + \frac{\partial A_{1x}}{\partial \xi} + \frac{\partial}{\partial \xi} (n_b v_{bx}) - \frac{\partial^3}{\partial \xi^3} (\phi_1)$$

Integrating over ξ with the boundary conditions that $\vec{A}_1 = 0$, $\phi_1 = 0$, $n_b = 0$ at $\xi = 0$ (head of the beam), we have,

$$\nabla_{\perp}^2 A_{1x} = -\phi_1 + A_{1x} + (n_b v_{bx}) - \frac{\partial^2}{\partial \xi^2} (\phi_1)$$

In the other way, this equation can be written as,

$$\nabla_{\perp}^2 A_{1x} = -\phi_1 + A_{1x} + (n_b v_{bx}) - \nabla^2 \phi_1 + \nabla_{\perp}^2 \phi_1$$

Therefore, using equation (A.76), the above equation can be written as,

$$\nabla_{\perp}^2 A_{1x} = -\phi_1 + A_{1x} + (n_b v_{bx}) - n_1 - n_b + \nabla_{\perp}^2 \phi_1$$

Using $v_{bx} = 1$, the above equation finally can be written as,

$$(\nabla_{\perp}^2 - 1)(A_{1x} - \phi_1) = -n_1 \quad (\text{A.77})$$

The expression of longitudinal electric field can also be obtained from following equation from equation (A.75).

$$E_{1x} = \frac{\partial}{\partial \xi}(A_{1x} - \phi_1) \quad (\text{A.78})$$

The equations (A.74) and (A.77) are the key equations to obtain the analytical solution of electron beam driven wakefield in the linear regime for a given form of n_b .

Method of Green's function for solving ODE's

Solution of forced SHO like equation

Let us look for solution to the equation,

$$\frac{d^2 x}{dt^2} + \omega_0^2 x = f(t) \quad (\text{A.79})$$

Here ω_0 and $f(t)$ represents the natural frequency of the oscillator and the driving term respectively. The solution of the above equation can be written in terms of

Green's function $G(x, x')$ as,

$$x(t) = \int_{t_i}^{t_f} dt' G(t, t') f(t') \quad (\text{A.80})$$

Here t_i and t_f are the initial and final time of the integration. Notice that t_i can be $-\infty$ and t_f can be ∞ if the solution at all times is desired. The solution of Green's function can be obtained by solving the following equation with appropriate boundary conditions.

$$\frac{d^2}{dt^2} G(t, t') + \omega_0^2 G(t, t') = \delta(t - t') \quad (\text{A.81})$$

If we are thinking about the differential equations in time, there will often be a different boundary condition, which is set by the fact of causality. This suggests that any physical system can not respond before it is hit. The response of the system at any time t can be obtained by integrating the equation (A.80) from t_i (initial time) to t . One can expect a boundary condition for such system as,

$$G(t, t') = 0; \quad t' > t$$

This choice of the condition will give us a Green's function that will be called the 'retarded Green's function', which says that any effects of force appear only after the force is applied. The causal Green's function is particularly easy to find because we only need to think about the behavior at $t' < t$. For the differential equations in space, we have to integrate over all space. Now, for $t' < t$, the equation (A.81) can be written as,

$$\frac{d^2}{dt^2} G(t, t') + \omega_0^2 G(t, t') = 0 \quad (\text{A.82})$$

Therefore, the solution of $G(t, t')$ is,

$$G(t, t') = A(t')\sin(\omega_0 t) + B(t')\cos(\omega_0 t); \quad t' < t \quad (\text{A.83})$$

Integrating equation (A.81) both the sides over a small interval $t' - \epsilon$ to $t' + \epsilon$ containing the origin at t' , where $\epsilon \rightarrow 0$, we get,

$$\int_{t'-\epsilon}^{t'+\epsilon} \frac{d^2 G(t, t')}{dt^2} dt + \omega_0^2 \int_{t'-\epsilon}^{t'+\epsilon} G(t, t') dt = \int_{t'-\epsilon}^{t'+\epsilon} \delta(t - t') dt \quad (\text{A.84})$$

The second term in LHS of the equation (A.84) will be negligibly small because,

$$\left| \int_{t'-\epsilon}^{t'+\epsilon} G(t, t') dt \right| \leq \max |G(t, t')| 2\epsilon \rightarrow 0$$

In the limit $\epsilon \rightarrow 0$, we therefore get,

$$\frac{d}{dt} G(t, t') \big|_{t=t'+\epsilon} - \frac{d}{dt} G(t, t') \big|_{t=t'-\epsilon} = 1 \quad (\text{A.85})$$

Since $\frac{d}{dt} G(t, t') = 0$ for $t = t' - \epsilon$, we find the following expression for $\epsilon \rightarrow 0$,

$$\frac{d}{dt} G(t, t') \big|_{t=t'+\epsilon} = 1 \quad (\text{A.86})$$

Now, we can write,

$$\int_{t'-\epsilon}^{t'+\epsilon} \frac{d}{dt} G(t, t') dt = G(t, t') \big|_{t=t'+\epsilon} - G(t, t') \big|_{t=t'-\epsilon}$$

The LHS of the above equation goes to zero in the limit $\epsilon \rightarrow 0$ since

$$\left| \int_{t'-\epsilon}^{t'+\epsilon} \frac{d}{dt} G(t, t') dt \right| \leq \max \left| \frac{d}{dt} G(t, t') \right| 2\epsilon$$

Thus we can write,

$$G(t, t')|_{t=t'+\epsilon} = G(t, t')|_{t=t'-\epsilon} = 0 \quad (\text{A.87})$$

The continuity of $G(t, t')$ at $t = t' + \epsilon (\rightarrow 0)$ implies,

$$A(t')\sin(\omega_0 t') + B(t')\cos(\omega_0 t') = 0 \quad (\text{A.88})$$

Using equation (A.86), we can write in the limit $\epsilon \rightarrow 0$,

$$A(t')\omega_0\cos(\omega_0 t') - B(t')\omega_0\sin(\omega_0 t') = 1 \quad (\text{A.89})$$

Solving equation (A.88) and (A.89), we have,

$$A = \frac{1}{\omega_0}\cos(\omega_0 t'), B = -\frac{1}{\omega_0}\sin(\omega_0 t')$$

Using equation (A.83), the solution for Green's function can be written as,

$$G(t, t') = \frac{1}{\omega_0}\sin(\omega_0[t - t']) \quad (\text{A.90})$$

Therefore the motion of SHO can be determined by solving the following equation,

$$x(t) = \frac{1}{\omega_0} \int_{t_i}^t dt' \sin(\omega_0[t - t']) f(t') \quad (\text{A.91})$$

Solution of Poisson like equation in cylindrical geometry

Let us look for solution to the equation,

$$(\nabla_r^2 - 1)\phi(r) = f(r) \quad (\text{A.92})$$

In cylindrical geometry, equation (A.92) can be written as,

$$\left(\frac{\partial^2}{\partial r^2} + \frac{1}{r} \frac{\partial}{\partial r} - 1\right)\phi(r) = f(r) \quad (\text{A.93})$$

The solution of the equation (A.93) can be written as,

$$\phi(r) = \int_0^\infty r' dr' f(r') R(r, r') \quad (\text{A.94})$$

where $R(r, r')$ is the Green's function corresponding to the equation (A.93) which satisfies the following equation,

$$\left(\frac{\partial^2}{\partial r^2} + \frac{1}{r} \frac{\partial}{\partial r} - 1\right)R(r, r') = \delta(r, r') \quad (\text{A.95})$$

The differential equation for $r \neq r'$ looks exactly similar to the ODE of modified Bessel function [?]. The solution of the above equation can be written as,

$$R(r, r') = I_0(r_<)K_0(r_>) \quad (\text{A.96})$$

Here $r_<$ defines $r < r'$ and $r_>$ defines $r > r'$. $I_0(r)$ and $K_0(r)$ represents the modified Bessel function of first and second kind respectively. The detail derivation is given in ref. [115] (see Eq. (9.196)). The solution of equation (A.92) therefore takes the following form,

$$\phi(r) = \int_0^r r' dr' f(r') I_0(r') K_0(r) + \int_r^\infty r' dr' f(r') I_0(r) K_0(r') \quad (\text{A.97})$$

Test particle simulation techniques

In this section, we present the test particle simulation techniques which have been used to estimate the energy gain in the process of acceleration. Test-particle simulations provide a useful complement to the kinetic simulations of many-body systems (plasma) and their approximate treatment with multiple moments. In a kinetic approach, systems are described at a microscopic level in terms of a large number of degrees of freedom. Fluid or multiple moment approaches provide a description at the macroscopic level, in terms of relatively few physical parameters involving averages or moments of particle distribution functions. Ideally, fully kinetic descriptions are the more appropriate description for describing the physical phenomena in a system. But, due to their complexity, the use of these approaches is often impractical in many cases of interest. In comparison, the fluid approximation is much simpler to implement and solve. It can be used to describe complex phenomena in multi-dimensional geometry with realistic boundary conditions. The main drawback of fluid descriptions that they are inadequate for describing the phenomena taking place on fine space or time-scales (individual particle level), or phenomena involving nonlocal transport or heating. With the test-particle method, particle trajectories are calculated using approximated fields obtained from a low-level approach (fluid or macroscopic description). Assuming that these fields are representative of actual systems, various kinetic and statistical properties of the system can then be calculated, such as particle distribution functions and moments etc.

The fluid simulations which are extensively used for the excitation of relativistic

electron beam driven wakefields provide the structure of the electric and magnetic fields in the system by defining the values at each cell center and interfaces in the computation domain (see the section (A.1)). These fields are then used for determining the motion of the test particles injected in the fluid simulations. The motion of these test electrons is completely guided by the fields obtained from our fluid simulation. Therefore, the study including test particles in the fluid simulation provides a complete characterization for estimating the energy gain in the process of acceleration in plasma wakefield acceleration. The equation which determines the dynamics of the test electrons is the equation of motion in a normalized form, $\frac{d\vec{p}_i}{dt} = -\vec{E} - (\vec{v}_i \times \vec{B})$; where $\vec{p}_i = \gamma_i \vec{v}_i = v_i(1 - v_i^2)^{-1/2}$ and γ_i is the momentum and relativistic factor of i -th test electron having velocity \vec{v}_i . E and B are the electric and magnetic field acting on i -th particle which are obtained from fluid simulation. The contribution of the mutual interactions between the test electrons are ignored here. However, the test electrons do not react back to the system. It is to be noted that the fields obtained from the fluid simulation are defined at the cell interfaces. Therefore, we have calculated the fields at the position of the particle by the method of interpolation using the values in the corresponding nearest grids at each time step for each individual test particles. After distributing the fields to the location of the particle, the test particles are then pushed according to the equation of motion.

The basic principle for advancing the position and velocity of the test particle in time is based on the Boris pusher algorithm [114]. In Fig. (A.1), a schematic diagram of simulation techniques in 2-D simulation domain for a single test electron is shown. Initially at $t = 0$, we distribute the test particles in the simulation pro-

viding their initial positions $(x_{p0}(i), y_{p0}(i))$ and velocities $(v_{px0}(i), v_{py0}(i))$; where $x_{p0}(i)$ and $y_{p0}(i)$, are the position of the i -th test electrons having velocities $v_{px0}(i)$ and $v_{py0}(i)$ in x and y -directions respectively.

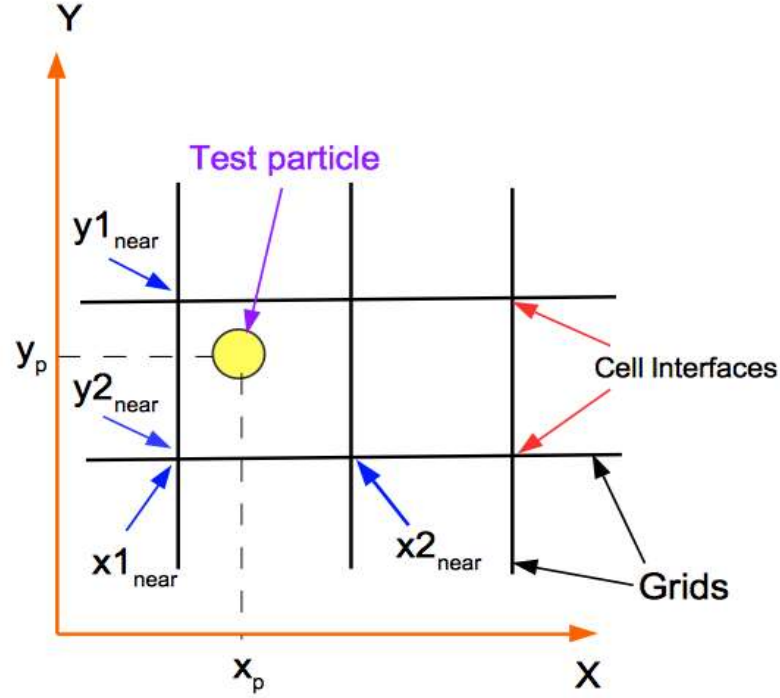


Figure A.1: A schematic diagram of test particle simulation techniques.

Next, we identify the nearest grid interfaces and cell centres to the test particles where the fields are known from the fluid simulation. Therefore, we first start to find out the nearest grid interfaces to the i -th electron in x -direction by calculating Δx_{pmin} which is the minimum value of Δx_p defined as, $\Delta x_p(ii) = |(x_{p0}(i) - x_{int}(ii))|$; where $x_{int}(ii)$ defines the position of the ii -th grid interfaces in the fluid simulation. Therefore the most nearest grid interface in x -direction to the i -th test electron is, $x1_{near}(i) = x_{p0}(i) - \Delta x_{pmin}$. Again we define, $\Delta(i) = x1_{near}(i) - x_{p0}(i)$. It is clear that the nearest interface lies at the left side of the test electrons if $\Delta(i) < 0$. Otherwise, the nearest grid interface lies at the

right to the test electron. Therefore the i -th test electron lies in x -axis between, $x1_{near}(i)$ and $x2_{near}(i)$; where $x2_{near}(i) = x1_{near}(i) + \Delta x$, for $\Delta < 0$, and $x2_{near}(i) = x1_{near}(i) - \Delta x$ for $\Delta > 0$. Following this method of calculating nearest grid interfaces, we also calculate the nearest grid interfaces in y -direction $y1_{near}(i)$ and $y2_{near}$. Once these interfaces in x and y are calculated properly, we then define the fields at the location of the particle by averaging the fields defined at the nearest grid interfaces and cell centres as,

$$\begin{aligned} \vec{E}(i) = \frac{1}{4}[\vec{E}(x1_{near}(i), y1_{near}(i)) + \vec{E}(x1_{near}(i), y2_{near}(i)) \\ + \vec{E}(x2_{near}(i), y1_{near}(i)) + \vec{E}(x2_{near}(i), y2_{near}(i))] \end{aligned} \quad (\text{A.98})$$

$$\begin{aligned} \vec{B}(i) = \frac{1}{4}[\vec{B}(x1_{near}(i), y1_{near}(i)) + \vec{B}(x1_{near}(i), y2_{near}(i)) \\ + \vec{B}(x2_{near}(i), y1_{near}(i)) + \vec{B}(x2_{near}(i), y2_{near}(i))] \end{aligned} \quad (\text{A.99})$$

Following the Boris pusher algorithm (see ref. ()), the momentum of the i -th test electrons from time t to $t + \Delta t$ is advanced by following equation,

$$\vec{p}_i(t + \frac{\Delta t}{2}) = \vec{p}_i(t - \frac{\Delta t}{2}) - \Delta t \left[\vec{E}^t(i) + (\vec{v}^t(i) \times \vec{B}^t(i)) \right] \quad (\text{A.100})$$

The velocity of the test electrons can then be obtained from, $\vec{v}_p(i) = \frac{\vec{p}_i}{\gamma_i}$; where $\gamma_i = \sqrt{1 + p_i^2}$. Therefore, the position (x_p, y_p) of the i -th test electrons from time t to $t + \Delta t$ is advanced by following equations,

$$x_p^{(t+\Delta t)}(i) = x_p^t(i) + \Delta t v_{px}^{(t+\frac{\Delta t}{2})} \quad (\text{A.101})$$

$$y_p^{(t+\Delta t)}(i) = y_p^t(i) + \Delta t v_{py}^{(t+\frac{\Delta t}{2})} \quad (\text{A.102})$$

The flow-chart of the above techniques is shown in Fig. (A.2). The above

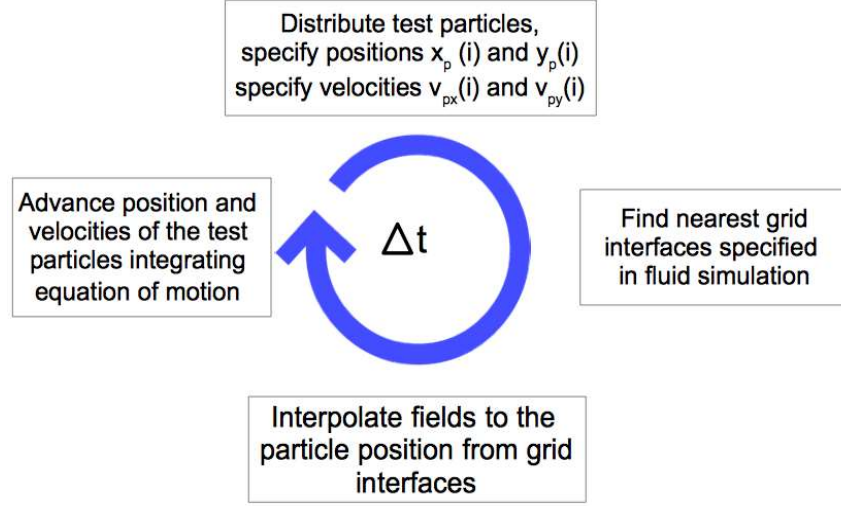


Figure A.2: Flow chart of test particle simulation techniques.

technique and its stability has been verified by reproducing the dynamics of a charge particle in several known configurations (see ref. [12]).

Bibliography

- [1] D. A. Edwards and M. J. Syphers. An introduction to the physics of high energy accelerators. *Wiley Series in Beam Physics and Accelerator Technology*, 2004.
- [2] C. et al. DesRosiers. 150-250 mev electron beams in radiation therapy. *Phys.Med. Biol.*, 45:1781–1805, 2000.
- [3] J. D. Kmetec, C. L. Gordon, J. J. Macklin, B. E. Lemoff, G. S. Brown, and S. E. Harris. Mev x-ray generation with a femtosecond laser. *Phys. Rev. Lett.*, 68:1527–1530, Mar 1992.
- [4] G. Aad et al. Observation of a new particle in the search for the standard model higgs boson with the atlas detector at the lhc. *Physics Letters B*, 716:1–29, 2012.
- [5] Beringer et al. Review of particle physics. *Phys. Rev. D*, 86:010001, Jul 2012.
- [6] Arthur Beiser. Concepts of modern physics, 5th edition. *McGraw-Hill*, 1995.
- [7] A. Ratti C. Turner R. Miyamoto H.S. Mattis, P. Humphreys and J. Stiller. Simulations of the lhc high luminosity monitors at beam energies 3.5 tev to 7.0 tev. *BNL-94204-2011-CP*, April, 2011.
- [8] Adrian Cho. The large hadron collider redux: Hoping for a long, hard slog. *Science*, 325(5944):1067–1069, 2009.
- [9] James William Rohlf. Introduction to modern physics. *John Wiley and Sons, Inc*, 1994.

- [10] Oliver Morton. The final tally leaves lep a probable loser. *Science*, 290(5495):1274–1274, 2000.
- [11] A. Debus F. Budde O. JÄdckel S. Pfotenhauer H. Schworer E. Rohwer J. G. Gallacher E. Brunetti R. P. Shanks S. M. Wiggins H. P. Schlenvoigt, K. Haupt and D. A. Jaroszynski. A compact synchrotron radiation source driven by a laser-plasma wakefield accelerator. *Nat Physics*, 4:130–133, 2008.
- [12] Francis F Chen. Introduction to plasma physics and controlled fusion. *PLENUM PRESS NEW YORK AND LONDON*, 1974.
- [13] C. B. Schroeder E. Esarey and W. P. Leemans. Physics of laser-driven plasma-based electron accelerators. *Rev. Mod. Phys.*, 81:1229, 2009.
- [14] V. Malka, S. Fritzler, E. Lefebvre, M.-M. Aeonard, F. Burgy, J.-P. Chambaret, J.-F. Chemin, K. Krushelnick, G. Malka, S. P. D. Mangles, Z. Najmudin, M. Pittman, J.-P. Rousseau, J.-N. Scheurer, B. Walton, and A. E. Dangor. Electron acceleration by a wake field forced by an intense ultrashort laser pulse. *Science*, 298(5598):1596–1600, 2002.
- [15] V. Malka et al. Principles and applications of compact laser-plasma accelerators. *Nat. Phys.*, 4, 2008.
- [16] P. Muggli and M. J. Hogan. Review of high-energy plasma wakefield experiments. *Comptes Rendus Physique*, 10:116–129, 2009.
- [17] C. Joshi. The development of laser- and beam-driven plasma accelerators as an experimental field. *Physics of Plasmas*, 14(5):055501, 2007.
- [18] Chandrashekhhar Joshi. Plasma wake field accelerator. *Scientific American*, 294:40, 2006.

- [19] Chan Joshi and Victor Malka. Focus on laser- and beam-driven plasma accelerators. *New. J. Physics*, 12:045003, 2010.
- [20] V. Malka. Laser plasma accelerators. *Physics of Plasmas*, 19(5):055501, 2012.
- [21] T. Tajima and J.M. Dawson. Laser electron accelerator. *Phys. Rev. Lett.*, 43, 1979.
- [22] H.Nakanishi A. Ogata Y. Kitagawa R. Kodama K. Mima H. Shiraga K. Suzuki K. Yamakawa T. Zhang Y. Kato D. Fisher M. Downer T. Tajima Y. Sakawa T. Shoji N. Yugami K. Nakajima, T. Kawakubo and Y. Nishida. Proof-of-principle experiments of laser wakefield acceleration using a 1 ps 10 tw nd:glass laser. *Proc. AIP Conf. Advanced Accelerator Concept*;, P. Schoessow, Ed. New York: Amer. Inst. Phys, 335, 1995.
- [23] P. Sprangle, E. Esarey, and A. Ting. Nonlinear interaction of intense laser pulses in plasmas. *Phys. Rev. A*, 41:4463–4469, Apr 1990.
- [24] S. Lee, T. Katsouleas, P. Muggli, W. B. Mori, C. Joshi, R. Hemker, E. S. Dodd, C. E. Clayton, K. A. Marsh, B. Blue, S. Wang, R. Assmann, F. J. Decker, M. Hogan, R. Iverson, and D. Walz. Energy doubler for a linear collider. *Phys. Rev. ST Accel. Beams*, 5:011001, Jan 2002.
- [25] W. Lu, C. Huang, M. Zhou, M. Tzoufras, F. S. Tsung, W. B. Mori, and T. Katsouleas. A nonlinear theory for multidimensional relativistic plasma wave wakefields. *Physics of Plasmas*, 13(5):056709, 2006.

- [26] Pisin Chen, J. M. Dawson, Robert W. Huff, and T. Katsouleas. Acceleration of electrons by the interaction of a bunched electron beam with a plasma. *Phys. Rev. Lett.*, 54:693–696, Feb 1985.
- [27] Han Sup Uhm and Glenn Joyce. Theory of wakefield effects of a relativistic electron beam propagating in a plasma. *Physics of Fluids B: Plasma Physics*, 3(7):1587–1598, 1991.
- [28] Rhon Keinigs and Michael E. Jones. Two-dimensional dynamics of the plasma wakefield accelerator. *The Physics of Fluids*, 30(1):252–263, 1987.
- [29] N. Barov and J. B. Rosenzweig. Propagation of short electron pulses in underdense plasmas. *Phys. Rev. E*, 49:4407–4416, May 1994.
- [30] T. Katsouleas. Physical mechanisms in the plasma wake-field accelerator. *Phys. Rev. A*, 33:2056–2064, Mar 1986.
- [31] J. B. Rosenzweig. Nonlinear plasma dynamics in the plasma wake-field accelerator. *Phys. Rev. Lett.*, 58:555–558, Feb 1987.
- [32] Mike Downer and Rafal Zgadzaj. Accelerator physics: Surf’s up at slac. *Nature*, 515:40, 2014.
- [33] Johanna L. Miller. Plasma wakefield acceleration shows promise. *Physics Today*, 68(1):11, 2015.
- [34] P. Sprangle, E. Esarey, A. Ting, and G. Joyce. Laser wakefield acceleration and relativistic optical guiding. *Applied Physics Letters*, 53(22):2146–2148, 1988.

- [35] V I Berezhiani and I G Murusidze. Interaction of highly relativistic short laser pulses with plasmas and nonlinear wake-field generation. *Physica Scripta*, 45(2):87, 1992.
- [36] Wim Leemans and Eric Esarey. Laser-driven plasma-wave electron accelerators. *Physics Today*, 62(3):44–49, 2009.
- [37] Y. Kitagawa, T. Matsumoto, T. Minamihata, K. Sawai, K. Matsuo, K. Mima, K. Nishihara, H. Azechi, K. A. Tanaka, H. Takabe, and S. Nakai. Beat-wave excitation of plasma wave and observation of accelerated electrons. *Phys. Rev. Lett.*, 68:48–51, Jan 1992.
- [38] P. Gibbon and A. R. Bell. Cascade focusing in the beat-wave accelerator. *Phys. Rev. Lett.*, 61:1599–1602, Oct 1988.
- [39] M. N. Rosenbluth and C. S. Liu. Excitation of plasma waves by two laser beams. *Phys. Rev. Lett.*, 29:701–705, Sep 1972.
- [40] A. S. Sakharov and V. I. Kirsanov. Theory of raman scattering for a short ultrastrong laser pulse in a rarefied plasma. *Phys. Rev. E*, 49:3274–3282, Apr 1994.
- [41] Deepa Verma, Ratan Kumar Bera, Amita Das, and Predhiman Kaw. The stability of 1-d soliton in transverse direction. *Physics of Plasmas*, 23(12):123102, 2016.
- [42] K. Krushelnick, A. Ting, C. I. Moore, H. R. Burris, E. Esarey, P. Sprangle, and M. Baine. Plasma channel formation and guiding during high intensity short pulse laser plasma experiments. *Phys. Rev. Lett.*, 78:4047–4050, May 1997.

- [43] Z. Najmudin, K. Krushelnick, E. L. Clark, S. P. D. Mangles, B. Walton, A. E. Dangor, S. Fritzler, V. Malka, E. Lefebvre, D. Gordon, F. S. Tsung, and C. Joshi. Self-modulated wakefield and forced laser wakefield acceleration of electrons. *Physics of Plasmas*, 10(5):2071–2077, 2003.
- [44] A. Ting, C. I. Moore, K. Krushelnick, C. Manka, E. Esarey, P. Sprangle, R. Hubbard, H. R. Burris, R. Fischer, and M. Baine. Plasma wakefield generation and electron acceleration in a self-modulated laser wakefield accelerator experiment. *Physics of Plasmas*, 4(5):1889–1899, 1997.
- [45] C. A. Coverdale, C. B. Darrow, C. D. Decker, W. B. Mori, K-C. Tzeng, K. A. Marsh, C. E. Clayton, and C. Joshi. Propagation of intense subpicosecond laser pulses through underdense plasmas. *Phys. Rev. Lett.*, 74:4659–4662, Jun 1995.
- [46] A. Ting, E. Esarey, and P. Sprangle. Nonlinear wakefield generation and relativistic focusing of intense laser pulses in plasmas. *Physics of Fluids B: Plasma Physics*, 2(6):1390–1394, 1990.
- [47] P. Sprangle, E. Esarey, J. Krall, and G. Joyce. Propagation and guiding of intense laser pulses in plasmas. *Phys. Rev. Lett.*, 69:2200–2203, Oct 1992.
- [48] I. Kostyukov, A. Pukhov, and S. Kiselev. Phenomenological theory of laser-plasma interaction in “bubble” regime. *Physics of Plasmas*, 11(11):5256–5264, 2004.
- [49] A. Pukhov and J. Meyer-ter Vehn. Laser wake field acceleration: the highly non-linear broken-wave regime. *Applied Physics B*, 74(4):355–361, Apr 2002.

-
- [50] S. Y. Kalmykov, A. Beck, S. A. Yi, V. N. Khudik, M. C. Downer, E. Lefebvre, B. A. Shadwick, and D. P. Umstadter. Electron self-injection into an evolving plasma bubble: Quasi-monoenergetic laser-plasma acceleration in the blowout regime. *Physics of Plasmas*, 18(5):056704, 2011.
- [51] S. M. Hooker. Developments in laser-driven plasma accelerators. *Nat Photon*, 7:775–782, 2013.
- [52] J. Faure et al. A laser-plasma accelerator producing monoenergetic electron beams. *Nature*, 431:541–544, Sep2004.
- [53] S. P. D. Mangles et al. Monoenergetic beams of relativistic electrons from intense laser-plasma interactions. *Nature*, 431:535–538, Sep2004.
- [54] C. G. R. Geddes et al. High-quality electron beams from a laser wakefield accelerator using plasma-channel guiding. *Nature*, 431:538–541, Sep2004.
- [55] A. Norlin A. Lifschitz Y. Glinec J. Faure, C. Rechatin and V. Malka. Controlled injection and acceleration of electrons in plasma wakefields by colliding laser pulses. *Nature*, 444:737, 2006.
- [56] C. E. Clayton, C. Joshi, C. Darrow, and D. Umstadter. Relativistic plasma-wave excitation by collinear optical mixing. *Phys. Rev. Lett.*, 54:2343–2346, May 1985.
- [57] A. J. Gonsalves Cs. TÃşth K. Nakamura C. G. R. Geddes E. Esarey C. B. Schroeder W. P. Leemans, B. Nagler and S. M. Hooker. GeV electron beams from a centimetre-scale accelerator. *Nat Physics*, 2:696–699, 2006.
- [58] G. Golovin, S. Chen, N. Powers, C. Liu, S. Banerjee, J. Zhang, M. Zeng, Z. Sheng, and D. Umstadter. Tunable monoenergetic electron beams from

independently controllable laser-wakefield acceleration and injection. *Phys. Rev. ST Accel. Beams*, 18:011301, Jan 2015.

- [59] W. Lu, M. Tzoufras, C. Joshi, F. S. Tsung, W. B. Mori, J. Vieira, R. A. Fonseca, and L. O. Silva. Generating multi-gev electron bunches using single stage laser wakefield acceleration in a 3d nonlinear regime. *Phys. Rev. ST Accel. Beams*, 10:061301, Jun 2007.
- [60] H. S. Mao K. Nakamura C. Benedetti C. B. Schroeder Cs. Tth J. Daniels D. E. Mittelberger S. S. Bulanov J. L. Vay C. G.R. Geddes W. P. Leemans, A. J. Gonsalves and E. Esarey. Multi-gev electron beams from capillary-discharge-guided subpetawatt laser pulses in the self-trapping regime. *Phys. Rev. Lett*, 113:245002, 2014.
- [61] S. Kneip, S. R. Nagel, S. F. Martins, S. P. D. Mangles, C. Bellei, O. Chekhlov, R. J. Clarke, N. Delerue, E. J. Divall, G. Doucas, K. Ertel, F. Fiuza, R. Fonseca, P. Foster, S. J. Hawkes, C. J. Hooker, K. Krushelnick, W. B. Mori, C. A. J. Palmer, K. Ta Phuoc, P. P. Rajeev, J. Schreiber, M. J. V. Streeter, D. Urner, J. Vieira, L. O. Silva, and Z. Najmudin. Near-gev acceleration of electrons by a nonlinear plasma wave driven by a self-guided laser pulse. *Phys. Rev. Lett.*, 103:049901, Jul 2009.
- [62] J. E. Ralph, K. A. Marsh, A. E. Pak, W. Lu, C. E. Clayton, F. Fang, W. B. Mori, and C. Joshi. Self-guiding of ultrashort, relativistically intense laser pulses through underdense plasmas in the blowout regime. *Phys. Rev. Lett.*, 102:175003, Apr 2009.

- [63] J. B. Rosenzweig, D. B. Cline, B. Cole, H. Figueroa, W. Gai, R. Konecny, J. Norem, P. Schoessow, and J. Simpson. Experimental observation of plasma wake-field acceleration. *Phys. Rev. Lett.*, 61:98–101, Jul 1988.
- [64] K. V. Lotov, A. P. Sosedkin, A. V. Petrenko, L. D. Amorim, J. Vieira, R. A. Fonseca, L. O. Silva, E. Gschwendtner, and P. Muggli. Electron trapping and acceleration by the plasma wakefield of a self-modulating proton beam. *Physics of Plasmas*, 21(12):123116, 2014.
- [65] W. P. Leemans and Eric Esarey. Laser-driven plasma-wave electron accelerators. *Physics Today*, 62:44, 2009.
- [66] C. E. Clayton, B. E. Blue, E. S. Dodd, C. Joshi, K. A. Marsh, W. B. Mori, S. Wang, P. Catravas, S. Chattopadhyay, E. Esarey, W. P. Leemans, R. Assmann, F. J. Decker, M. J. Hogan, R. Iverson, P. Raimondi, R. H. Siemann, D. Walz, T. Katsouleas, S. Lee, and P. Muggli. Transverse envelope dynamics of a 28.5-gev electron beam in a long plasma. *Phys. Rev. Lett.*, 88:154801, Apr 2002.
- [67] J. B. Rosenzweig, D. B. Cline, B. Cole, H. Figueroa, W. Gai, R. Konecny, J. Norem, P. Schoessow, and J. Simpson. Experimental observation of plasma wake-field acceleration. *Phys. Rev. Lett.*, 61:98–101, Jul 1988.
- [68] P. Muggli, B. E. Blue, C. E. Clayton, S. Deng, F.-J. Decker, M. J. Hogan, C. Huang, R. Iverson, C. Joshi, T. C. Katsouleas, S. Lee, W. Lu, K. A. Marsh, W. B. Mori, C. L. O’Connell, P. Raimondi, R. Siemann, and D. Walz. Meter-scale plasma-wakefield accelerator driven by a matched electron beam. *Phys. Rev. Lett.*, 93:014802, Jun 2004.

- [69] M. J. Hogan, C. D. Barnes, C. E. Clayton, F. J. Decker, S. Deng, P. Emma, C. Huang, R. H. Iverson, D. K. Johnson, C. Joshi, T. Katsouleas, P. Krejcik, W. Lu, K. A. Marsh, W. B. Mori, P. Muggli, C. L. O'Connell, E. Oz, R. H. Siemann, and D. Walz. Multi-gev energy gain in a plasma-wakefield accelerator. *Phys. Rev. Lett.*, 95:054802, Jul 2005.
- [70] M. J. Hogan, R. Assmann, F.-J. Decker, R. Iverson, P. Raimondi, S. Rokni, R. H. Siemann, D. Walz, D. Whittum, B. Blue, C. E. Clayton, E. Dodd, R. Hemker, C. Joshi, K. A. Marsh, W. B. Mori, S. Wang, T. Katsouleas, S. Lee, P. Muggli, P. Catravas, S. Chattopadhyay, E. Esarey, and W. P. Leemans. E-157: A 1.4-m-long plasma wake field acceleration experiment using a 30 gev electron beam from the stanford linear accelerator center linac. *Physics of Plasmas*, 7(5):2241–2248, 2000.
- [71] N. Barov, J. B. Rosenzweig, M. C. Thompson, and R. B. Yoder. Energy loss of a high-charge bunched electron beam in plasma: Analysis. *Phys. Rev. ST Accel. Beams*, 7:061301, Jun 2004.
- [72] Ian Blumenfeld, Christopher E. Clayton, Franz-Josef Decker, Mark J. Hogan, Chengkun Huang, Rasmus Ischebeck, Richard Iverson, Chandrashekhar Joshi, Thomas Katsouleas, Neil Kirby, Wei Lu, Kenneth A. Marsh, Warren B. Mori, Patric Muggli, Erdem Oz, Robert H. Siemann, Dieter Walz, and Miaomiao Zhou. Energy doubling of 42 gev electrons in a metre-scale plasma wakefield accelerator. *Nature*, 445:741–744, 2007.
- [73] M. Litos, E. Adli, W. An, C. I. Clarke, C. E. Clayton, S. Corde, J. P. Delahaye, R. J. England, A. S. Fisher, J. Frederico, S. Gessner, S. Z. Green, M. J. Hogan, C. Joshi, W. Lu, K. A. Marsh, W. B. Mori, P. Muggli, N. Vafaei-

- Najafabadi, D. Walz, G. White, Z. Wu, V. Yakimenko, and G. Yocky. High-efficiency acceleration of an electron beam in a plasma wakefield accelerator. *Nature*, 515:92–95, 2014.
- [74] N. Vafaei-Najafabadi, K. A. Marsh, C. E. Clayton, W. An, W. B. Mori, C. Joshi, W. Lu, E. Adli, S. Corde, C. I. Clarke, M. Litos, S. Z. Green, S. Gessner, J. Frederico, A. S. Fisher, Z. Wu, D. Walz, and M. J. Hogan. Limitation on the accelerating gradient of a wakefield excited by an ultra-relativistic electron beam in rubidium plasma. *Phys. Rev. Accel. Beams*, 19:101303, Oct 2016.
- [75] E. S. Dodd, R. G. Hemker, C.-K. Huang, S. Wang, C. Ren, W. B. Mori, S. Lee, and T. Katsouleas. Hosing and sloshing of short-pulse gev-class wakefield drivers. *Phys. Rev. Lett.*, 88:125001, Mar 2002.
- [76] C. Huang, W. Lu, M. Zhou, C. E. Clayton, C. Joshi, W. B. Mori, P. Muggli, S. Deng, E. Oz, T. Katsouleas, M. J. Hogan, I. Blumenfeld, F. J. Decker, R. Ischebeck, R. H. Iverson, N. A. Kirby, and D. Walz. Hosing instability in the blow-out regime for plasma-wakefield acceleration. *Phys. Rev. Lett.*, 99:255001, Dec 2007.
- [77] David H. Whittum, William M. Sharp, Simon S. Yu, Martin Lampe, and Glenn Joyce. Electron-hose instability in the ion-focused regime. *Phys. Rev. Lett.*, 67:991–994, Aug 1991.
- [78] P. L. Morton R. D. Ruth, A. Chao and P. B. Wilson. *Particle Accelerator*, 17:171, 1985.

- [79] S. Elbakram A. Ts. Amatuni and E. V. Sekhpeesian. *Yerevan Physics Institute Report*, 85:832, 1985.
- [80] J. B. Rosenzweig. Multiple-fluid models for plasma wake-field phenomena. *Phys. Rev. A*, 40:5249–5255, Nov 1989.
- [81] A. I. Akhiezer and R. V. Polovin. Theory of wave motion of an electron plasma. *Sov. Phys. JETP*, 3:696, 1956.
- [82] A. G. Khachatryan. Ion motion and finite temperature effect on relativistic strong plasma waves. *Physical Rev. E*, 58:6, 1998.
- [83] J. B. Rosenzweig, A. M. Cook, A. Scott, M. C. Thompson, and R. B. Yoder. Effects of ion motion in intense beam-driven plasma wakefield accelerators. *Phys. Rev. Lett.*, 95:195002, Oct 2005.
- [84] J. Vieira, R. A. Fonseca, W. B. Mori, and L. O. Silva. Ion motion in self-modulated plasma wakefield accelerators. *Phys. Rev. Lett.*, 109:145005, Oct 2012.
- [85] Sudip Sengupta, Vikrant Saxena, Predhiman K. Kaw, Abhijit Sen, and Amita Das. Phase mixing of relativistically intense waves in a cold homogeneous plasma. *Phys. Rev. E*, 79:026404, Feb 2009.
- [86] Sudip Sengupta, Predhiman Kaw, Vikrant Saxena, Abhijit Sen, and Amita Das. Phase mixing/wave breaking studies of large amplitude oscillations in a cold homogeneous unmagnetized plasma. *Plasma Physics and Controlled Fusion*, 53(7):074014, 2011.
- [87] Prabal Singh Verma, Sudip Sengupta, and Predhiman Kaw. Breaking of longitudinal akhiezer-polovin waves. *Phys. Rev. Lett.*, 108:125005, Mar 2012.

- [88] Arghya Mukherjee and Sudip Sengupta. Analytical estimate of phase mixing time of longitudinal akhiezer-polovin waves. *Physics of Plasmas*, 21(11):112104, 2014.
- [89] K. V. Lotov. Blowout regimes of plasma wakefield acceleration. *Phys. Rev. E*, 69:046405, Apr 2004.
- [90] J. B. Rosenzweig, B. Breizman, T. Katsouleas, and J. J. Su. Acceleration and focusing of electrons in two-dimensional nonlinear plasma wake fields. *Phys. Rev. A*, 44:R6189–R6192, Nov 1991.
- [91] Y. C. Lee Guo-Zheng Sun, Edward Ott and Parvez Guzdar . Self-focusing of short intense pulses in plasmas. *Phys. Fluids*, 30:526, 1987.
- [92] F. S. Tsung, Ritesh Narang, W. B. Mori, C. Joshi, R. A. Fonseca, and L. O. Silva. Near-gev-energy laser-wakefield acceleration of self-injected electrons in a centimeter-scale plasma channel. *Phys. Rev. Lett.*, 93:185002, Oct 2004.
- [93] A. Modena. Electron acceleration from the breaking of relativistic plasma waves. *Nature*, 377, 1995.
- [94] J. M. Dawson S. Wilks, T. Katsouleas and J. J. Su. Beam loading efficiency in plasma accelerators. *Proceedings of the 1987 IEEE Particle Accelerator Conference: Accelerator Engineering and Technology*, 1:100–102, 1987.
- [95] Pisin Chen. Beam loading efficiency in plasma accelerators. *SLAC-PUB-3823 (Rev.)*, SLAC/AP-46, (A/AP):46, November 1985.
- [96] W. Lu, C. Huang, M. Zhou, W. B. Mori, and T. Katsouleas. Nonlinear theory for relativistic plasma wakefields in the blowout regime. *Phys. Rev. Lett.*, 96:165002, Apr 2006.

- [97] David Tsiklauri. Electron plasma wake field acceleration in solar coronal and chromospheric plasmas. *Physics of Plasmas*, 24(7):072902, 2017.
- [98] Neeraj Jain, John Palastro, T. M. Antonsen Jr., Warren B. Mori, and Weiming An. Plasma wakefield acceleration studies using the quasi-static code wake. *Physics of Plasmas*, 22(2):023103, 2015.
- [99] R. Fonseca et al. *Lecture Notes in Computer Science (Springer, Heidelberg)*, 2329:III–342, 2002.
- [100] E. Infeld and G. Rowlands. Relativistic bursts. *Phys. Rev. Lett.*, 62:1122–1125, Mar 1989.
- [101] Sudip Sengupta Ratan Kumar Bera and Amita Das. Fluid simulation of relativistic electron beam driven wakefield in a cold plasma. *Physics of Plasmas*, 22(7):073109, 2015.
- [102] J.P. Boris, A.M. Landsberg, E.S. Oran, and J.H. Gardner. Lcpfct - a flux-corrected transport algorithm for solving generalized continuity equations. Technical Report NRL Memorandum Report 93-7192., Navel Research Laboratory, 1993.
- [103] W. Press et al. Numerical recipes: The art of scientific computing. *Cambridge University Press*, 1992.
- [104] Deepa Verma, Ratan Kumar Bera, Atul Kumar, Bhavesh Patel, and Amita Das. Observation of 1-d time dependent non-propagating laser plasma structures using fluid and pic codes. *Physics of Plasmas*, 24(12):123111, 2017.
- [105] John M. Dawson. Nonlinear electron oscillations in a cold plasma. *Phys. Rev.*, 113:383–387, Jan 1959.

-
- [106] L. A. Cottrill, A. B. Langdon, B. F. Lasinski, S. M. Lund, K. Molvig, M. Tabak, R. P. J. Town, and E. A. Williams. Kinetic and collisional effects on the linear evolution of fast ignition relevant beam instabilities. *Physics of Plasmas*, 15(8):082108, 2008.
- [107] Prabal Singh Verma, Sudip Sengupta, and Predhiman Kaw. Bernstein-greene-kruskal waves in relativistic cold plasma. *Physics of Plasmas*, 19(3):032110, 2012.
- [108] I. S. Gradshteyn and I. M. Ryzhik. Table of integrals, series, and products. *Academic Press, Inc., 1980*, ISBN: 0-12-294760-6.
- [109] Ratan Kumar Bera, Arghya Mukherjee, Sudip Sengupta, and Amita Das. Relativistic electron beam driven longitudinal wake-wave breaking in a cold plasma. *Physics of Plasmas*, 23(8):083113, 2016.
- [110] J. Krall and G. Joyce. Transverse equilibrium and stability of the primary beam in the plasma wakefield accelerator. *Physics of Plasmas*, 2(4):1326–1331, 1995.
- [111] S. V. Bulanov, F. Pegoraro, A. M. Pukhov, and A. S. Sakharov. Transverse-wake wave breaking. *Phys. Rev. Lett.*, 78:4205–4208, Jun 1997.
- [112] Chandrasekhar Shukla Ratan Kumar Bera Deepa Verma Bhavesh Patel Y. Hayashi K. A. Tanaka Amit D. Lad G. R. Kumar Amita Das, Atul Kumar and Predhiman Kaw. Evidence of new finite beam plasma instability for magnetic field generation. *arXiv:1712.03099*, 2017.
- [113] S. Kato, B. Bhattacharyya, A. Nishiguchi, and K. Mima. Wave breaking and absorption efficiency for short pulse p-polarized laser light in a very

steep density gradient. *Physics of Fluids B: Plasma Physics*, 5(2):564–570, 1993.

[114] C.K. Birdsall and A.B Langdon. Plasma physics via computer simulation. *McGraw-Hill*, 1985.

[115] George B. Arfken and Hans J. Weber. Mathematical methods for physicists (sixth edition). *Elsevier Academic Press, 30 Corporate Drive, Suite 400, Burlington, MA 01803, USA*, 2005.